INVESTIGATION OF GEOSYNTHETIC REINFORCED TIERED RETAINING WALLS USING FINITE ELEMENT ANALYSIS

by

Tolga Yardımcı

B.S., Civil Engineering, Çukurova University, 2009

Submitted to the Institute for Graduate Studies in
Science and Engineering in partial fulfillment of
the requirements for the degree of
Master of Science

Graduate Program in Civil Engineering

Boğaziçi University

2013

INVESTIGATION OF GEOSYNTHETIC REINFORCED TIERED RETAINING WALLS USING FINITE ELEMENT ANALYSIS

APPROVED BY:

Prof. Erol Güler (Thesis Supervisor)	.....
Assoc. Prof. İsmail Hakkı Aksoy	.....
Assoc. Prof. Özer Çinicioğlu	.....

DATE OF APPROVAL: 09.07.2013

ACKNOWLEDGEMENTS

I would like to express my sincere gratitude to my thesis supervisor, Prof. Erol Güler, for his helpful suggestions, guidance, and understanding that he provided throughout the preparation of this thesis.

I would like to thank the members of my thesis committee, for their kind and supportive attitude to me and showing high interests and valuable advices to my thesis.

I would also like to thank my friends, Cihan Cengiz, Emrah Kılıç, Anıl Yıldız and Haluk Laman for their generous academical help and enjoyable times we have spent together. I have to express my deep gratitude to my boss and mentor, Görkem İçöz for his understanding and support. I would also like to thank Nisa Talay for her patience.

I will give special thanks to my beloved family for always standing by my side, and their endless support. I could not be the one who I am right now without my mother's sincere love and my father's infinite wisdom.

I owe heartfelt gratitude to TÜBİTAK, because of the scholarship I got during my master period.

ABSTRACT

INVESTIGATION OF GEOSYNTHETIC REINFORCED TIERED RETAINING WALLS USING FINITE ELEMENT ANALYSIS

Tiered reinforced soil retaining (RSR) walls can be used to take advantage of both the aesthetics and the economics of RSR walls while considering high heights. In such walls, an offset between each pair of adjacent tiers is introduced, thus reducing the displacements and increasing the factor of safety. This study was divided into two parts and in both of the parts a commercial computer program Plaxis 8.2 which is based on finite element method is used to conduct totally 58 analyses. In the first part of the study; effects of reinforcement length (L), type of reinforced soil and offset distance between tiers (S) on the behaviour of two tiered reinforced soil retaining wall was investigated using numerical analyses.Increasing reinforcement length causes increase in factor of safety and decrease in the horizontal displacements. However; when offset distance exceeds 1.5 times the tier height, effect of reinforcement length on factor of safety and displacements decreases significantly. Increasing the offset distance increases the factor of safety and reduces the permanent horizontal displacements as expected. For the chosen soil types; when cohesive fill used instead of non cohesive fill, lower safety factors and higher displacements in magnitude were obtained. Second part of the study was conducted to determine the critical offset distance beyond which two tiered wall behaves like two independent walls. For non cohesive fill, critical offset distance was found as 2 times of the tier height (2H). When cohesive fill was used, this value was 2.25 times the tier height (2.25H).

ÖZET

SONLU ELEMANLAR ANALİZİ KULLANILARAK GEOSENTETİK DONATILI KATLI İSTİNAT DUVARLARININ İNCELENMESİ

Yüksek duvar tasarımında; estetik ve ekonomik avantajlarından dolayı donatılan dırılmış katlı zemin istinat duvarları kullanılabilir. Bu tür duvarlarda, deplasmanların azalması ve güvenlik katsayısının artması için komşu iki duvar arasında belirli bir mesafe bulunur. Bu çalışma iki bölüme ayrılmıştır ve her iki bölümde de sonlu elemanlar yöntemini kullanan Plaxis 8.2 adlı ticari bir bilgisayar programı yardımıyla toplam 58 adet analiz yapılmıştır. Çalışmanın birinci bölümünde; donatı uzunluğunun (L), duvar dolgu tipinin ve duvarlar arası mesafenin (S) donatılandırılmış iki katlı zemin istinat yapısının davranışına olan etkisi sayısal analizler kullanılarak incelenmiştir. Artan donatı uzunluğu güvenlik katsayısında artışa ve yatay deplasmanlarda azalmaya sebep olmuştur. Fakat, duvarlar arası mesafenin duvar yüksekliğinin 1.5 katını geçtiği durumlarda donatı etkisinin önemli ölçüde azaldığı gözlenmiştir. Duvarlar arası mesafenin arttırılmasıyla güvenlik katsayısı artmıştır ve kalıcı yatay deplasmanlar azalmıştır. Kohezyonsuz dolgu yerine kohezyonlu dolgu kullanıldığı durumlarda, güvenlik katsayısının azaldığı ve deplasmanların arttığı gözlenmiştir Çalışmanın ikinci bölümü, katlı istinat duvarının iki bağımsız duvar olarak çalışmaya başladığı öteleme mesafesini tayin etmek için yapılmıştır. Kohezyonsuz dolgularda; kritik öteleme mesafesi kat yüksekliğinin 2 katı (2H) olarak bulunmuştur. Kohezyonlu dolgu kullanıldığında bu değer duvar katının 2.25 katı (2.25H) olarak gözlenmiştir.

TABLE OF CONTENTS

LIST OF FIGURES

LIST OF TABLES

LIST OF SYMBOLS

a_h	Horizontal acceleration
a_{max}	Peak ground acceleration
a_v	Vertical acceleration
a_y	Yield acceleration
$\acute{B_f}$	Equivalent bearing area for the retaining wall
c	Cohesive strength of the soil
C_{ds}	Coefficient of direct sliding
D_d	Pseudo-static driving force
d_{max}	Upper bound to the permanent displacements
d_{perm}	Permanent displacement
D_s	Static driving force
FS_{sl}	Factor of safety against sliding
FS_{ot}	Factor of safety against overturning
FS_{bc}	Factor of safety against bearing capacity
FS_{os}	Factor of safety against over-stressing of reinforcement
FS_{po}	Factor of safety against pull-out
FS_{sli}	Factor of safety against internal sliding
FS_{sc}	Factor of safety against interface shear
FS_{cs}	Factor of safety against connection failure
FS_{otl}	Factor of safety against local overturning
FS_{otc}	Factor of safety against crest overturning
F_{stai}	Static component of reinforcement load
F_{dyni}	Dynamic component of reinforcement load
g	Acceleration due to gravity
H_t	Total height of the wall
K_0	Coefficient of lateral earth pressure at rest
K_A	Coefficient of active earth pressure
K_{AE}	Coefficient of dynamic active earth pressure
K_P	Coefficient of passive earth pressure

K_{PE}	Coefficient of dynamic passive earth pressure
k_h	Horizontal seismic coefficient
k_v	Vertical seismic coefficient
k_y	Yield seismic coefficient
L_{min}	Minimum reinforcement length
L_w	Facing width
M_r	Resisting moment
M_o	Driving moment
m_a	Mass of thin element for active case
m_p	Mass of thin element for pasive case
N_c	Bearing capacity coefficient
N_g	Bearing capacity coefficient
N_q	Bearing capacity coefficient
P_A	The active earth pressure resultant
p_A	Active earth pressure
p_P	Passive earth pressure
P_P	Passive earth pressure
P_{AE}	Dynamic active earth pressure resultant
P_{PE}	Dynamic passive earth pressure resultant
P_{IR}	Horizontal inertial force due to the reinforced mass
P_{AEH}	Horizontal component of dynamic earth force
Q_h	Total horizontal inertial force
Q_{hp}	Horizontal seismic inertia force in passive case
Q_h	Horizontal seismic inertia force in active case
q_{ult}	Ultimate bearing capacity of the foundation soil
q_a	Applied bearing stress at the base of the reinforced soil mass and facing column (composite mass)
R_s	Available static resisting force
R_d	Available pseudo-static resisting force
s_v	Vertical spacing of reinforcements
t	Time
T_a	Allowable tensile load for the reinforcement

T_{pulli}	The anchorage capacity corresponding to reinforcement layer
v_{max}	Peak ground velocity
W_a	Weight of the failure wedge in active case
V_s	Shear wave velocity
W_a	Weight of the failure wedge in active case
W_p	Weight of the failure wedge in passive case
W_i	Total weight of the reinforced zone
W_β	Weight of the wedge of soil in the slope above the crest of the wall
W_w	Total weight of the facing column
W_r	Total weight of the reinforced soil zone (coposite mass)
X_w	Horizontal distance from the toe of the wall to the center of gravity of the entire facing column
X_i	Moment arm quantity
X_β	Moment arm quantity
z	Depth from the top of the wall
δ	Soil-wall interface friction angle
θ	Wall batter angle
α_A	Angle of critical failure surface to the horizontal for active case
α_P	Angle of critical failure surface to the horizontal for pasive case
α_{AE}	Angle of critical failure surface to the horizontal for dynamic active case
α_{PE}	Angle of critical failure surface to the horizontal for dynamic pasive case
$\acute{\sigma_v}$	Vertical effective stress at a certain depth behind the wall
γ	Unit weight of soil
ϕ	Angle of internal friction of the soil
β	Degree of backfill inclination
ψ	Dilatancy angle
v	Poisson's ratio

ω	Angular frequency of base shaking
ΔP_{dynH}	Dynamic increment of backfill soil force

LIST OF ACRONYMS/ABBREVIATIONS

E	Young's modulus
F	Soil reaction acting at an angle of ϕ (angle of internal friction of the soil) to the normal to the inclined failure wedge
FS	Factor of safety
G	Shear modulus
H	Height of the wall
L	Reinforcement length
S	Offset distance between walls

1. INTRODUCTION

The simple thought to add "inclusions" in the soil, in such a way to improve its technical properties dates back to ancient times. Through the centuries the concept of reinforced soil has been developed and the concept is still used all over the world. Reinforced soil retaining wall, as the name suggests, is a retaining wall reinforced with discrete steel strips, metallic grid reinforcement and geosynthetic reinforcements. Combination of geosynthetic and soil is a similar concept with reinforced concrete. Reinforcements have high tensile strength while they have very low compressive strength. Contrary to reinforcements, compressive strength of soil material is higher when compared with its tensile strength. On the other hand, soil material can be found cheaply and in large amounts while reinforcements are relatively expensive materials. Thus, combination of these two materials compensates weakness of each other and improves the global characteristics of this composite material like the relationship of concrete and steel in reinforced concrete.

Nowadays, implementation of Geosynthetics-Reinforced Soil (GRS) retaining structures is growing rapidly. It is more used worldwide compared to conventional concrete retaining walls, mainly due to its benefits such as aesthetics and vegetation, cost, time-consuming of construction, and sound performance. The first application of the reinforced walls was introduced by Henri Vidal in the early 1960s. More than 20 years, reinforced soil has been applied all over the world.

There are many situations where reinforced walls are constructed in a multi tiered configuration. One of the reasons is cost issue. The stresses in a reinforced wall increase rapidly with increasing wall height. To alleviate tensile stresses in the reinforcement, the reinforcement may be placed at the increasingly closer spacing. This leads to increased costs for reinforcement and construction. Alternatively, a wall having the desired overall height is constructed by using several tiers with some offset distance between the wall faces, which is referred to as multi tiered reinforced wall. The interaction mechanism between upper and lower tiers is quite complicated, depends on the

offset distance, S, which is the setback distance between two tiers. Two tiers interact through the extension of failure surface from lower to upper tier and and the equivalent surcharge from upper to lower tier. Therefore, design of multi tiered wall addressed in the Federal Highway Administration (FHWA, 2009) design guidelines is function of the offset distance. For small offset distance, the structure is designed as a single wall. For intermediate offset distance, designed as a compound wall, for large offset distance, design as independent wall, assuming there is no interaction between two tiers.

In order to gain better insight into mechanism affecting the behavior of such structures, engineers are turning to numerical experimental (simulation) analysis. For both under the static loading conditions and dynamic loading conditions, currently the most popular numerical analysis technique in use is the finite element method. This powerful analytical tool holds much promise for simulating the behavior of reinforced soil retaining structures, especially under dynamic stress conditions which are accepted as a very sophistical manner.

This study was carried out to investigate the behaviour of tiered reinforced soil retaining walls in static conditions, by using finite element analysis. Plaxis 8.2, a commercial computer program was used to conduct the analyses. The Plaxis program which was used in the analysis of reinforced soil walls, is a finite element package specifically intended for analysis of deformation and stability in geotechnical engineering projects. Geotechnical applications require advanced constitutive models for the simulation of the nonlinear and time dependent behaviour of soils. The modeling of the soil itself is an important issue; many geotechnical engineering projects involve the modeling of the structures and the interaction between the structures and the soil. In this finite element program a two-dimensional plain strain model is used for structures with a (more or less) uniform cross-sections and corresponding stress-state and loading scheme over a certain length perpendicular to the cross section.

This research study consists of seven main sections. Chapter 1 is an Introduction. The background, history of this study, a general statement of the scope is given in this section as well as the order of the study. Chapter 2 contains summarized informations

about Polymers and Geosynthetics. Introductional datas such as background, history, definitions and types are given Chapter 2. In third section, Reinforced Soil Retaining Walls are described. Chapter 4 consists of Literature Review in which calculation methods for reinforced soil retaining walls, failure modes of the wall and previous studies are discussed. The fifth section is the Methodology in which the finite element method, the computer program Plaxis and modeling works are illuminated. Sixth chapter is the Results and Discussions, in this section result of the Plaxis analyses and discussions on these results are presented. The seventh section is the final section. Conclusions of the study are explained in this section.

2. POLYMERS AND GEOSYNTHETICS

2.1. Polymers

2.1.1. Background

Within the last hundred years there has been an evolution from naturally occurring polymers to creation and use of synthetic polymers. The majority of the synthetic polymers used today include, polyethylene, nylon, polypropylene and polyester. These materials are created from low molecular weight materials such as oil (Filshill, 2010).

Synthetic polymers are used in various fields which range from packaging to everyday building materials. Recently, traditional materials are being substituted by synthetic polymers. Steel parts in cars such as car fenders (bumpers) have been replaced with ones made from Polypropylene (PP) and glass bottles of carbonated drinks have been replaced with polyethylene terephthalate (PET) bottles. In civil engineering, steel reinforcements used in soil have been replaced geosynthetics that are composed of synthetic polymers. Synthetic polymers are used in many industries due to their increased durability, increased design flexibility, light weight, low temperature impact resistance and efficient manufacturability.

2.1.2. History

The first human-made plastic was invented by Alexander Parkes in 1855; he called this plastic Parkesine (latercalled celluloid). It was unveiled at the 1862 Great International Exhibition (Fenichell, 1996). The development of plastics has come from the use of natural plastic materials (e.g., chewing gum, shellac) to the use of chemically modified natural materials (e.g., rubber, nitrocellulose, collagen, galalite) and finally to completely synthetic molecules (e.g., bakelite, epoxy, polyvinyl chloride, polyethylene).

Bakelite, a phenol-formaldehyde polymer, was the first completely synthetic plas-

tic, first made by Leo Baekeland in 1907. The independent chemist and inventor Leo Baekeland and an assistant started their research in 1904 looking for a synthetic substitute for shellac. Bakelite was commercially introduced in 1909. Bakelite was first used to make billiard balls, but, later, was used to make molded insulation, valve parts, knobs, buttons, knife handles, many types of molded plastic containers for radios and electronic instruments, and more (Katz, 1998).

By the invention of Bakelite and other fully synthetic materials, which aren't derived from living matter, a much more stable raw material became available in civil engineering applications. Lifetimes of centuries can be predicted even for harsh environmental conditions for properly formulated and produced synthetic polymeric materials.

2.1.3. Definition and Properties

The word *polymer* comes from the Greek word poly meaning "many" and *meros* meaning "parts" (Koerner, 2005). Thus a large number of minor, similar units (parts) are used to produce the polymer. Each part which is used to produce polymer, is called monomer. Polymers are made by linking *monomer* molecules together using chemical reactions. The process by which monomers are linked each other and build up polymers is known as *polymerisation*.

Alignment of the polymer chains, bonding between polymer molecules and their chains determines polymers' individual characteristics. According to types of bonding between polymer molecules and their chains, synthetic polymers can be subdivided into 3 main groups, namely thermoplastics, elastomers and thermosets. In addition, thermoplastics, which are the most common materials used in geosynthetics, are subdivided into 2 main groups in terms of alignment of the polymer chains (Figure 2.1).

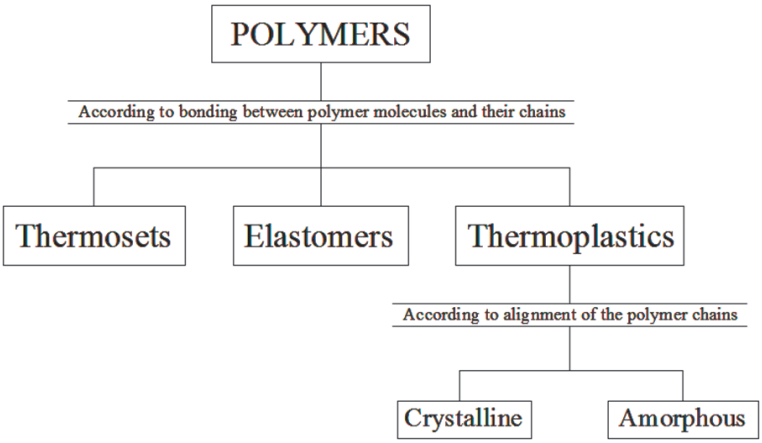

Figure 2.1. Types of Synthetic Polymers.

Thermoset polymers are rarely used polymers in geosynthetics. They are prepared by a reaction between monomers, at least one which is three or poly functional. Their closed three dimensional molecular net structure and chemical bonding (cross-linking) between polymer molecules and their chains causes a rigid behaviour. Also, their shape is retained by chemical bonding. Even though thermosets can be softened by heating, they retain their form. In order to shape them, cross-links should be broken by applying higher temperatures. Thermosets are stiff materials.

Elastomers' preparation method is same with the thermosets. Also, their shape is retained by cross-linking, so high temperatures should be applied to break cross-links and shape them. Elastomers have comparatively open three dimensional molecular structure and they are highly extensible materials. (Zanten, 1986) Elastomers are very sensitive to stress. When they subjected to stress, they can have high elongations of up to ten times their original size. Subsequent to release of stress, they recover their original shape.

Thermoplastics are the most commonly used polymers in the manufacture of geosynthetics. Thermoplastic polymer is prepared by a reaction between bi-functional monomers. They can be shaped above a specific temperature, and retain their shape after they have cooled down. Therefore, they are also known as thermosoftening plastics. Thermoplastics owe this property to bonding mechanism between polymer molecules

and their chains. There are no cross linked (chemically bonded) sites or chains to fix the polymer chain in position, so their shape retained by physical strength. Thermoplastics are stiff to relatively stiff materials when compared with thermosets. Thermoplastics can be divided into two groups in terms of crystallinity, namely crystalline and amorphous.

One can define crystallinity as the degree of aligned portions of the polymer chains. Crystallinitiy exists in every polymeric material but its degree varies but no polymer is completely crystalline. Decreasing degree of crystallinity makes material close to the amorphous form. In other words, nonaligned regions of the polymer chains are called amorphous.

Vast majority of the geosynthetics are made from amorphous or semi crystalline (there isn't any completely crystalline polymer) thermoplastics. For this reason, crystallinity is significant in the properties of polymeric geosynthetics. With the increase in crystallinitiy; stiffness/hardness, heat resistance, tensile strength and chemical resistance increases, however flexibility, impact strength diffusive permeability and stress crack resistance decreases.

Most commonly used polymers used in geosynthetics industry are polyethylene (PE), polypropylene (PP), polyvinyl chloride (PVC), polyester (PET), polyamide (PA) (nylon6/6) and polystrene (PS).

2.1.3.1. Polyethylene (PE). Polyethylene is one of the most common thermoplastic polymer, that is used in bottles, plastic bags, geomembranes and more. Polyethylenes can be produced in a highly crystalline form. Molecular weight (melt-index), molecular weight distribution, degree of crsytallinity (density) and degree of stabilization are four main parameters control the processibility and performance of polyethylene. In terms of process of production, polyethylene can be divided into three main groups, namely:

- Low density polyethylene (LDPE) (920-930 kg/m^3)

- Linear low density polyethylene (LLDPE) (925-945 kg/m^3)
- High density polyethylene (940-960 kg/m^3)

These three types of polyethylene polymers have different production processes, especially applied pressure during production determines their properties. LDPE is the one which was developed first. Very high pressures (up to 300 MPa) are applied during the production of LDPE, which enables to control flexibility and permeability properties of the production.

Contrary to LDPE, HDPE is produced at relatively low pressures and temperatures by using chromium/silica catalysts, Ziegler-Natta catalysts or metallocene catalysts. This different production process makes HDPE stronger, more rigid, tougher and also makes HDPE has a better chemical resistance than the LDPE.

Third main group of polyethylene is LLDPE, which is also made a low pressure process. However, LLDPE is manufactured by co-polymerizing ethylene with a small amount of alpha-olefins (for example, 1-butene, 1-hexene and 1-octene), which lowers the density by forming short chain side branches on the linear polymer chain (Zanten, 1986).

2.1.3.2. Polypropylene (PP). Polypropylene is another important thermoplastic polymer used in manufacture of geosynthetics. Polypropylene is also a crystalline polymer that is formed by polymerization of propylene monomers. Polypropylene is the lightest plastic which has a low density about 900-910 kg/m^3.

In order to define properties of PP; melt-index, degree of crystallinity/isotacticity, molecular weight distribution, degree of stabilization and copolymerization with other monomers (especially ethylene) should be investigated well.

2.1.3.3. Polyvinyl Chloride (PVC). Polyvinyl chloride (commonly abbreviated as PVC) is made from vinyl chloride (VC), that is the product of the reaction between ethylene

and chlorine. Also, reaction of ethylene, air and hydrochloric acid provides vinyl chloride. Polyvinyl chloride (as abbreviated as PVC) is one of the most widely produced plastic materials with polyethylene and polypropylene. PVC can be manufactured by two methods. In first method, it can be produced by heating pure vinyl chloride under pressure to about 60^oC. Alternatively, VC can be polymerized as an emulsion in water which includes certain catalysts.

2.1.3.4. Polyester (PET). Polyester is made by polymerization of petroleum derivatives such as, ethylene glycol with dimethyl terephthalate or with terephthalic acid. Even though the most common polyesters are thermoplastic, thermoset polyesters can be produced by changing their chemical structure. Shape of polyesters as thermoplastics might be changed by applying heat. When they are faced with flame, they extinguish themselves by shrinking away from flames.

2.1.3.5. Polyamide (PA) (nylon 6.6). Polyamide (nylon) 6.6 is an aliphatic polymer, which means it is composed of chains which don't contain ring-shaped rigid structure. PA 6.6 is obtained by the polymerization of petroleum derivatives such as a salt of adipic acid and hexamethylenediamine. Generally, autoclaves are used to produce PA 6.6 in a discontinuous process. However, a continuous process can be conducted to make polyamide 6.6. (Zanten, 1986).

2.1.3.6. Polystyrene (PS). Polystyrene is manufactured by polymerization of styrene, which is a petroleum derived monomer. Short-range van der Waals bondings between polymer chains are the main factor that determines the polystyrene's properties. Either rigid or foamed po lystyrenes can be encountered. The most important property of polystyrene is its unit weight. Polystyrenes are light-weight materials (about 95% air), and they have very good insulation properties. In room temperature; polystyrene is solid, but it starts to flow when it is heated above 100^oC. After cooling, it becomes rigid again. This feature enables manufacturers to mold it with fine detail. Repeating molecular units of these polymers and geosynthetics they are used in are shown in Table 2.1.

Table 2.1. Repeating Molecular Units of Polymers Used in the Manufacture of Geosynthetics (Koerner, 2005).

Polymer	**Repeating Unit**	**Types of Geosynthetics**
Polyethylene (PE)	$\left[\begin{array}{cc} H & H \\ \vert & \vert \\ C & -C \\ \vert & \vert \\ H & H \end{array}\right]_n$	Geotextiles, geomembranes, geogrids, geopipe, geonets, geocomposites
Polypropylene (PP)	$\left[\begin{array}{cc} H & CH_3 \\ \vert & \vert \\ C & -C \\ \vert & \vert \\ H & H \end{array}\right]_n$	Geotextiles, geomembranes, geogrids, geocomposites
Polyvinyl chloride (PVC)	$\left[\begin{array}{cc} H & Cl \\ \vert & \vert \\ C & -C \\ \vert & \vert \\ H & H \end{array}\right]_n$	Geomembranes, geopipe, geocomposites
Polyester (polyetyhlene terephthalate) (PET)	$\left[\begin{array}{cccccc} & & & O & & O \\ & & & \vert & & \vert \\ O- & R- & O- & C- & R- & C \end{array}\right]_n$	Geotextiles, geogrids
Polyamide (PA)	$\left[\begin{array}{cccccc} H & & H & O & & O \\ \vert & & \vert & \vert & & \vert \\ N- & (CH_2)_6- & N- & C- & (CH_2)_6- & C \end{array}\right]_n$	Geotextiles, geogrids, geocomposites
Polystyrene (PS)	$\left[\begin{array}{cccc} & H & H & \\ & \vert & \vert & \\ & H & C & \\ & // & & \\ H- & C & C & -H \\ \vert & & & \parallel \\ H- & C & C & -H \\ & & & \\ & / & & \\ & C & & \\ & \vert & & \\ & H & & \end{array}\right]_n$	Geocomposites, geofoam

2.2. Geosynthetics

2.2.1. Background

In only a very few years, geosynthetics have joined the list of traditional civil engineering construction materials. Often the use of a geosynthetic can significantly increase the safety factor, improve performance, and reduce costs in comparison with conventional construction alternatives. (Chen and Liew, 2003).

Geosynthetics are used in various disciplines such as civil, geotechnical, transportational, geoenvironmental and hydraulic engineering. In addition, they're used in private development applications including roads, airfields, railroads, embankments, retaining structures, reservoirs, canals, dams, erosion control, sediment control, landfill liners, landfill covers, mining, aquaculture and agriculture.

The vast majority of the geosynthetics used today include, geogrids, geotextiles, geomembranes, geocompozites, geosynthetic clay liners, geofoams, geopipes and geonets. Geosynthetics are available in a wide range of forms and materials, each to suit a slightly different end use. They are used for separation, reinforcement, filtration, drainage and insulation.

2.2.2. History

Inclusions of different sorts mixed with soil have been used for thousands of years. Thus, one can say that industry of geosynthetics is as old as civilization itself. The Babylonians used palm fronds and hemp to constructed soil-reinforced "ziggurats" more than 3000 years ago, and the Chinese have used reeds to construct a type of corduroy road since prehistoric times (Holtz, 1988). In Roman days, inclusions mixed with soil were used to stabilize roadways and their edges. In Egypt, they were also used to build steep slopes as with several pyramids and walls as well. These all early applications were made by using natural fibers, fabrics or vegetation mixed with soil. The main problem with using natural materials (silk, vegetation, wood, cotton, etc.)

in a buried environment is the biodegradation that are caused by microorganisms in the soil. However, with the invention of synthetic polymers in the beginning of the 20th century a much more stable raw material became available. This new material inspired scientists and engineers to produce geosynthetics.

The first papers on geosynthetics in the 1960s were as filters in the U.S. and as reinforcement in Europe. In the mid-1970s, Bob Holtz studied on using geotextiles to replace steel reinforcements in soil, while the Dick Bell-J.E. Steward team studied the same in the Pacific Northwest. In 1977, many manufacturers and practitioners got together because of the conference in Paris. The International Geosynthetics Society (IGS), which was founded in 1982, has subsequently organized worldwide conference every four years. Geosynthetics are available worldwide and the activity is robust and steadily growing. Historical developments in the area of geosynthetics and their applications are shown in Table 2.2.

2.2.3. Definition and Properties

The term "Geosynthetic" has two parts: the prefix "geo", referring to an end use associated with improving the performance of civil engineering works involving earth/ground/soil and the suffix "synthetic", referring to the fact that the materials are almost exclusively from man-made products (Shukla and Jin, 2006). Rubber, plastics, fiberglass or other human-made synthetic materials may be used as raw material in geosynthetics. Geosynthetics are used for separation, filtration, drainage, reinforcing soil and moisture barrier.

According to their structure and technical properties, geosynthetics may be grouped into four main groups.

- Geotextiles
- Geogrids
- Geomembranes
- Geocomposites

Table 2.2. Historical developments in the area of geosynthetics and their applications (Shukla and Yin, 2005).

Decades	Developments
Early decades	The first use of fabrics in reinforcing roads was attempted by the South Carolina Highway Department in 1926 (Beckham and Mills, 1935). Polymers which form the bulk of geosynthetics did not come into commercial production until thirty years later starting with polyvinyl chloride (PVC) in 1933, low density polyethylene (LDPE) and polyamide (PA) (a.k.a. nylon) in 1939, expanded polystyrene (EPS) in 1950, poly- ester (PET) in 1953, and high density polyethylene (HDPE) and polypropylene (PP) in 1955 (Hall, 1981). The US Bureau of Reclamation has been using geomembranes in water conveyance canals since the 1950s (Staff, 1984).
Late 1950s	A range of fabrics was manufactured for use as separation and filter layers between granular fills and weak subsoils.Woven fabrics (nowadays called geotextiles) played critical filtration functions in coastal projects in The Netherlands and in the USA.
1960s	Rhone-Poulenc Textiles in France began working with nonwoven needle-punched geotextiles for quite different applications. Geotextiles found a role as beds for highway and railway track support systems. Chlorosulfonated polyethylene (CSPE) was developed around 1965.
1970s	The first geotextile used in a dam, in 1970, was a needle-punched nonwoven geotextile used as a filter for the aggregate downstream drain in the Valcross Dam (17 m high), France (Giroud, 1992). Geotextiles were incorporated as reinforcement in retaining walls, steep slopes, etc.The beginning of the ongoing process of standards development started with the formation of the ASTM D-13-18 joint committee on geosynthetics and the formation of industry task forces.The first samples of Tensar grid were made in the Blackburn laboratories of Netlon Ltd, UK, in July 1978.The first conference on geosynthetics was held in Paris in 1977. The geofoam was originally applied as a lightweight fill in Norway in 1972.
1980s	The beginning of the use of geosynthetics occurred in the construction of safe containment of environmentally hazardous wastes. Soil confinement systems based on cellular geotextile nets were first developed and evaluated in France during 1980. Netlon developed a similar concept, but on a larger scale, with the introduction of the Tensar Geocell Mattress in 1982. The first known environmental application of geonet was in 1984 for leak detection in a double-lined hazardous liquid-waste impoundment in Hopewell,Virginia. Koerner and Welsh wrote the first book on geosynthetics in 1980. The International Geosynthetics Society was established in 1983. The first volume of international journal entitled Geotextiles and Geomembranes was published in 1984.
1990s	Many standards on geosynthetics were published by the American Society of Testing Materials (ASTM), USA; the International Organization for Standardization (ISO), Switzerland; the British Standards Institution (BSI), UK; the Bureau of Indian Standards (BIS), India, etc.The second international journal entitled Geosynthetics International was first published in 1995.

2.2.3.1. Geotextiles. Geotextiles are indeed textiles in the traditional sense. In order to solve biodegredation and subsequent short lifetime problems, they consist of synthetic fibers rather than natural materials such as silk, cotton or wool. Synthetic fibers are made into geotextiles by standard weaving machinery or are matted together in a random or nonwoven manner. Also, some fibers are also knitted. Geotextiles are permeable materials across their manufactured planes and within their thickness, but degree of permeability widely varies. Geotextiles are one of the most all-purpose geosynthetics; however, it always performs at least one of the functions among :

- Separation

- Reinforcement
- Filtration
- Drainage
- Containment (barrier, when impregnated).

2.2.3.2. Geogrids. Instead of being a woven, nonwoven or knitted fabric, geogrids are formed into a grid-like configuration that has large apertures. These grid-like configured large apertures provides additional strength with interlocking mechanism when they are used in granular soils as reinforcement. Also, the apertures ensure vertical drainage of a reinforced free-draining soil. They can be manufactured by stretching in one (extruded uniaxial) or two directions (extruded biaxial) or made on weaving machinery by unique methods. Geogrids are mostly used as reinforcement in geotechnical engineering applications.

2.2.3.3. Geomembranes. Whereas geotextiles and geogrids are usually porous to allow water to filter through them, geomembranes are polymer sheets used to control fluid movement. Geomembranes are impervious materials which are made from thin, continuous polymeric sheets. They are used primarily for linings and for the covers of liquid or solid storage facilities as liquid or vapor barrier. This includes all types of landfills, reservoirs, canals, tunnels and other containment facilities. Geomembranes are used in various areas such as environmental, geotechnical, transportation and hydraulic engineering.

2.2.3.4. Geocomposites. The basic philosophy behind geocomposite materials is to combine the best features of different materials in such a way that specific applications are addressed in the optimal manner and at minimum cost. A geocomposite consists of a combination of geotextiles, geogrids, geonets and/or geomembranes in a factory fabricated unit. Also, any one of these four materials can be combined with another synthetic material (e.g., deformed plastic sheets or steel cables) or even with soil. The geocomposite category brings out the best creative efforts of the engineer and manufacturer. The application areas are numerous and constantly growing.

Geonets, geosynthetic clay liners (or GCLs), geopipes and geofoams are other important types of geosynthetics used in geotechnical engineering. Typical geosynthetic materials can be seen in Figure 2.2.

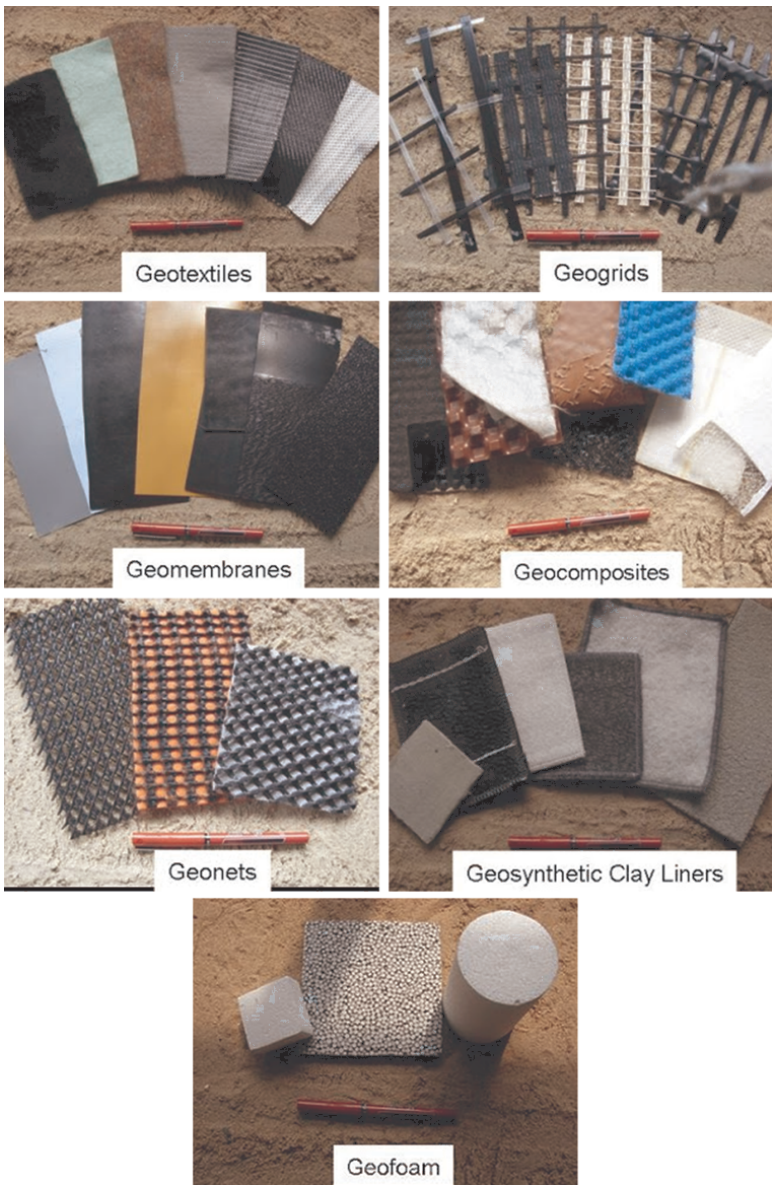

Figure 2.2. Typical Geosynthetic Materials.

3. GEOSYNTHETIC REINFORCED SOIL RETAINING WALLS

3.1. Description of Geosynthetic Reinforced Soil Retaining Walls

Geosynthetic reinforced soil retaining wall, as the name suggests, is a retaining wall reinforced with geosynthetics. Combination of geosynthetic and soil is a similar concept with reinforced concrete. Geosynthetic reinforcements have high tensile strength while they have very low compressive strength. Contrary to geosynthetic reinforcements, compressive strength of soil material is higher when compared with its tensile strength. On the other hand, soil material can be found cheaply and in large amounts while geosynthetic reinforcements are relatively expensive materials.

Thus, combination of these two materials compensates weakness of each other and improves the global characteristics of this composite material like the relationship of concrete and steel in reinforced concrete.

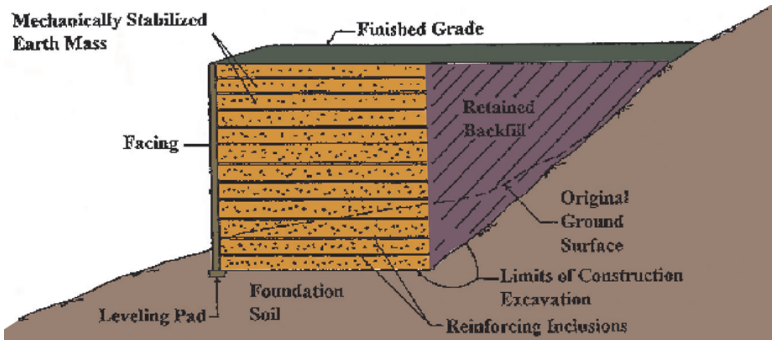

Figure 3.1. Generic cross-section of a MSE wall (Elias *et al.*, 2001).

Reinforcing soil with geosynthetics improves the strength of soil. However, in order to prevent soil raveling between reinforcement layers, reinforcements should be wrapped to provide a stable facing. Also, facing materials can be used to enable engineers build steeper geosynthetic reinforced soil walls. Therefore, very steep slopes and vertical walls can be constructed safely. A simple illustration of a geosynthetic reinforced soil wall can be seen in Figure 3.1 and an illustration of a geosynthetic

reinforced earth wall detail can be seen in Figure 3.2.

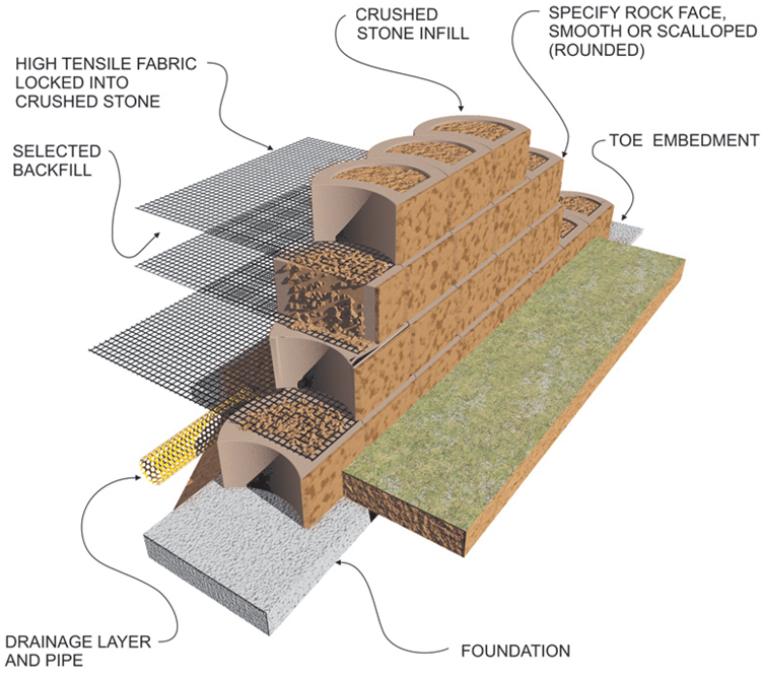

Figure 3.2. Schematic view of geosynthetic reinforced retaining wall (Terraforce, 2013).

All in all, geosynthetic reinforced soil retaining walls are considered to be typically more ductile, more tolerable to differential settlements, more adaptable to low quality backfill, easier to construct, and more economical when compared to other types of retaining structures (Enünlü, 2007).

3.2. Historical Development of Reinforced Soil Retaining Structures

The simple thought to add "inclusions" in the soil, in such a way to improve its technical properties dates back to ancient times. Through the centuries the concept of reinforced soil has been developed.

Reinforced soil concept is very ancient: 3000 years ago the Babylonians used intertwined palm branches to reinforce their "ziggurat". The Agar-Quf Ziggurat, in the actual Iraq, was made of clay bricks reinforced with woven mats of reed laid horizontally on a layer of sand and gravel at vertical spacing between 0.5 m and 2.0 m. This

structure was originally over 80 m high. The Romans used several types of soil reinforcement. An example is the use of timber baulks placed in the soil perpendicular to the face, for building retaining walls. The Great Wall of China, built more than 2000 years ago, contains some sections where clay and gravel were reinforced with tamarisk branches. More recently, in 1822 Colonel Pasley introduced in the British Army a form of reinforced soil, demonstrating by a series of trials that the lateral pressure on a retaining wall could be reduced if the backfill was reinforced by horizontal layers of brushwood, wooden plants or canvas (Tenax, 2006) However, using natural materials as inclusions has always been a problem, because of their limited durability and a very large uncontrollable variability in their engineering properties.

In the early 1960s, French architect and engineer Henri Vidal found the modern methods of soil reinforcement for retaining wall which was called Reinforced Earth®. Reinforced Earth® is a system in which steel strip reinforcement is used in soil. With the invention of Reinforced Earth®, using a more durable reinforcement for retaining walls became available.

The reinforced soil concept has got a huge momentum with the use of polymeric materials in soil. These plastic products, specifically engineered for soil reinforcement, provide civil engineers with factory controlled characteristics, uniform behaviour, very limited variability and very high durability (Tenax, 2006).

The use of geotextiles in MSE walls and RSS started after the beneficial effect of reinforcement with geotextiles was noticed in highway embankments over weak subgrades. The first geotextile reinforced wall was constructed in France in 1971, and the first structure of this type in the United States was constructed in 1974. Since about 1980, the use of geotextiles in reinforced soil has increased significantly. Geogrids for soil reinforcement were developed around 1980. The first use of geogrid in earth reinforcement was in 1981. Extensive use of geogrid products in the United States started in about 1983, and they now comprise a growing portion of the market (Elias *et al.*, 2001).

Due to their advantages, the use of reinforced soil slope structures has increased noticeably in early 1990s, and it is estimated that several hundred reinforced soil slope structures have been constructed all over the world. According to FHWA, 70 to 100 reinforced soil slope/wall projects are being constructed yearly in connection with transportation related projects in the United States, with an estimated projected vertical face area of 130,000 m^2/year. Also, it is estimated that since 1997, approximately 23,000 MSE walls have been constructed in the world.

3.3. Advantages and Disadvantages of Reinforced Soil Retaining Structures

3.3.1. Advantages of Reinforced Soil Retaining Structures

There are many advantages of MSE walls compared with conventional retaining structures such as reinforced concrete and concrete gravity retaining walls. Some advantages are:

- MSE wall construction is simple and rapid and doesnt have need of large construction equipment.
- Experienced craftsmen with special skills arent required for MSE wall construction.
- MSE walls require less site preparation than other alternatives.
- MSE walls need less space in front of the structure for construction operations.
- Right-of-way acquisition is reduced.
- MSE structures are tolerant to deformations, so they do not need rigid, unyielding foundation support. One of the greatest advantages of MSE walls is their flexibility and capability to absorb deformations due to poor subsoil conditions in the foundations. Also, based on observations in seismically active zones, these structures have demonstrated a higher resistance to seismic loading than have rigid concrete structures.
- MSE walls are cost effective. The relatively small quantities of manufactured materials required, rapid construction, and, competition among the developers

of different proprietary systems has resulted in a cost reduction relative to traditional types of retaining walls. MSE walls are likely to be more economical than other wall systems for walls higher than about 3 m (10 ft) or where special foundations would be required for a conventional wall.

- MSE walls can be constructed to heights in excess of 25m.
- Aesthetics. Precast concrete facing elements for MSE walls can be made with various shapes and textures (with little extra cost) for aesthetic considerations.
- MSE walls can be constructed in harmony with natural environment thanks to facing units. Masonry units, timber, and gabions also can be used with advantage to blend in the environment (Elias *et al.*, 2001).

3.3.2. Disadvantages of Reinforced Soil Retaining Structures

There is no material or method without disadvantages, and MSE walls also have some disadvantages like stated below. Actually, following disadvantages may be associated with all soil reinforced structures.

- A relatively large space behind the wall or outward face is required to obtain enough wall width to satisfy internal and external stability criteria.
- Select granular fill material is required especially for MSE walls. (At sites where there is a lack of granular soils, the cost of importing suitable fill material may render the system uneconomical).
- Specifications and contracting practices of such structures havent been completely standardized. Additionally, design and construction practice of all reinforced systems are still evolving.
- The design of soil-reinforced systems often requires a shared design responsibility between material suppliers and owners and greater input from agencies geotechnical specialists in a domain often dominated by structural engineers.
- In order to prevent the corrosion of steel reinforcing elements, suitable design criteria are required. They are also required to prevent deterioration of certain types of exposed facing elements such as geosynthetics by ultra violet rays, and potential degradation of polymer reinforcement in the ground.

3.4. The Elements of Reinforced Soil Walls

Geosynthetic reinforced soil retaining walls are composed of 5 elements, namely, reinforcement, mechanically stabilized soil mass, retained backfill, facing unit and foundation soil. Components of reinforced soil walls are shown in Figure 3.1.

3.4.1. Reinforcement

Reinforcements are inclusions, which are placed in horizontal layers throughout the height of the wall, used to provide tensile strength to hold soil mass together. These reinforcements are divided into two groups as inextensible an extensible reinforcements Steel strips (inextensible reinforcement) and geosynthetic sheets (extensible reinforcement) are the most common reinforcements used in soil walls.

- Inextensible reinforcements: Deformation of the inextensible reinforcement at failure is much less than the deformability of the soil. The most commonly used ones of this group are metallic reinforcements. Metallic reinforcements are typically made of mild steel. Metallic soil reinforcements may take the form of sheets, grids, meshes, strips, bars, rods, etc. The biggest problem of metallic reinforcements is corrosion. In order to prevent corrosion of the reinforcement, they can be galvanized or epoxy coated.
- Extensible reinforcements: The deformation of the reinforcement at failure is comparable to or even greater than the deformability of the soil (Elias et al., 2001). Polymeric materials such as geogrids and geotextiles are considered extensible reinforcement. Geosynthetic reinforcements are generally made from polyethylene, polyester and polypropylene.

Figure 3.3. Metal strip as an inextensible reinforcement.

Figure 3.4. Geogrid as an extensible reinforcement.

3.4.2. Mechanically Stabilized Soil Mass

Mechanically stabilized soil mass is a generic term used for reinforced part of the reinforced soil retaining wall. Stabilized soil mass is obtained by reinforcing soil in horizontal layers with either extensible or inextensible reinforcement. On the other hand, reinforcement makes soil behave like a coherent body.

According to FHWA; MSE walls require high quality backfill for durability, good drainage, constructability, and good soil reinforcement interaction which can be obtained from well graded, granular materials. Many MSE systems depend on friction between the reinforcing elements and the soil. In such cases, a material with high friction characteristics is specified and required. Some systems rely on passive pressure on reinforcing elements, and, in those cases, the quality of backfill is still critical. These performance requirements generally eliminate soils with high clay contents.

From a reinforcement capacity point of view, lower quality backfills could be used for MSEW structures; however, a high quality granular backfill has the advantages of being free draining, providing better durability for metallic reinforcement, and requiring less reinforcement. There are also significant handling, placement and compaction advantages in using granular soils. These include an increased rate of wall erection and improved maintenance of wall alignment tolerances (Elias *et al.*, 2001).

3.4.3. Retained Backfill

Retained backfill is the fill material located between the mechanically stabilized soil mass and the natural soil. Likewise the mechanically stabilized soil mass, the quality of retained backfill material is also has a crucial effect on geosynthetic reinforced soil retaining walls. For the reasons discussed previously for reinforced fill, use of soils containing shale, mica, gypsum, smectite, montmorillonite, organic materials or other soft particles of poor durability should be avoided.

On the other hand, the potential differential settlement or performance between the reinforced fill and retained backfill should be assessed. A transition wedge between reinforced fill and retained backfill should be taken into consideration. Upper two layers of soil reinforcement can be lengthened or reinforced zone can be extended beyond the reinforcement length to obtain a sufficient transition region. The maximum particle size in the retained backfill should be less or equal to the maximum particle size in reinforced fill, at least in this transition zone.

3.4.4. Facing Unit

In reinforced soil retaining walls, facing units are used to provide some form of barrier to contain the soil. Facing units can be either flexible or rigid to meet design criteria, but they have to be strong enough to back the local soil and to allow attachment of the reinforcement. Concrete panel is a good example for stiff facing units and modular block can be given as an example for flexible facing. The facing type is one of the major factors which influences settlement tolerances. In addition, the facing prevents sloughing and erosion of the backfill, and provides in certain cases drainage paths. Furthermore, facing units are the only visible part of the reinforced soil walls, so they affect the aesthetic of the wall directly. Major facing types are:

- Segmental precast concrete panel
- Welded wire grids
- Dry cast modular block wall (MBW) units
- Metallic facings
- Geosynthetic facings
- Gabion facing
- Postconstruction facing.

3.4.5. Foundation Soil

The soil below the mechanically stabilized soil mass and retained backfill is called foundation soil. Foundation soil can be considered the soil which carries the overall system of the retaining wall. Hence, foundation soil has to satisfy the design criteria specified in manuals. The bearing capacity, liquefaction potential, settlement potential and position of ground water level are some of the important factors that need to be investigated before the implementation of the reinforced earth structures.

To sum up, before the application, characteristics of foundation soil should be investigated properly. In case of necessity, foundation soil may be improved to satisfy the adequate bearing capacity and/or limiting total and/or differential settlements.

4. LITERATURE REVIEW

4.1. Static and Seismic Analysis Approaches

Likewise in all civil engineering applications, loads and pressures acting on retaining walls should be defined carefully in order to make a sufficient wall design. Total lateral earth pressures acting on retaining walls have a significant effect on the behaviour of the retaining walls. These total pressures mainly consist of the static pressures and the transient dynamic pressures induced by the earthquake. Since the response of a wall is influenced by both, the most commonly used lateral earth pressure approaches are presented.

Earth pressures acting on retaining structures are strongly influenced by wall and soil movements. There are three types of lateral earth pressures depending on wall movement such as active earth pressure, passive earth pressure and at rest pressure.

Active earth pressures develop as a retaining wall moves away from the soil behind it, inducing extensional lateral strain in the soil. When the wall movement is sufficient to fully mobilize the strength of the soil behind the wall, minimum active earth pressures act on the wall (Kramer, 1996). Active earth pressures develop by very little movements of the wall. Active earth pressures develop when a wall rotates about its base and away from the backfill an amount on the order of 0.001 to 0.003 radian (a top deflection of 0.001 to 0.003h, where h is the wall height) (Enünlü, 2007).

Passive earth pressures develop as a retaining wall moves toward the soil behind it, inducing compressive lateral strain in the soil. When the wall movement is sufficient to fully mobilize the strength of the soil behind the wall, maximum passive earth pressures act on the wall. In passive earth pressure conditions, higher horizontal stresses can be developed than for the active pressure conditions. Development of the maximum possible horizontal stress, or passive pressure, requires much larger wall rotations than for the active case, as much as 0.02 to 0.2 radians (Enünlü, 2007).

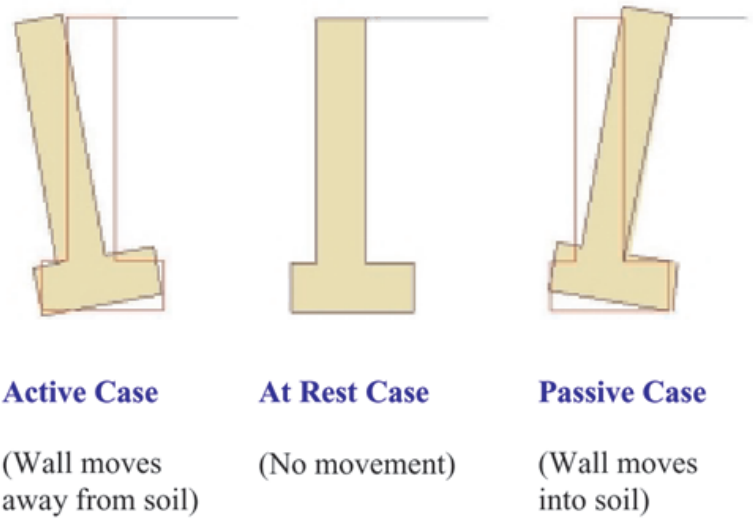

Figure 4.1. Wall movement and earth pressure types.

The at rest pressure develops when there is no lateral movement of the wall. At rest pressure classically occurs when the wall is restrained from movement.

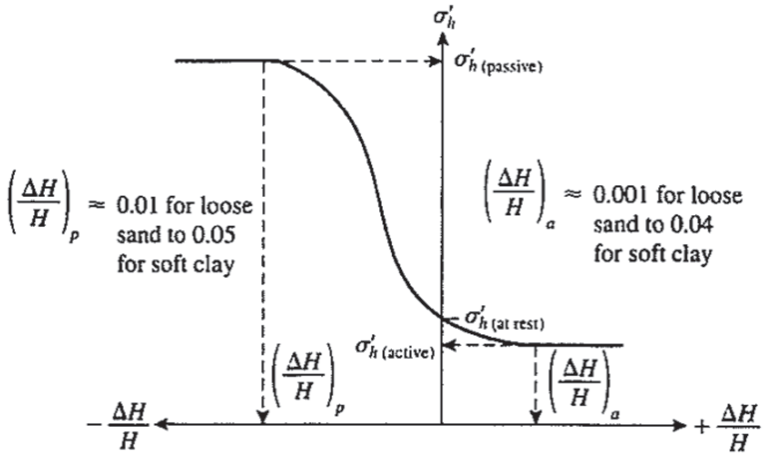

Figure 4.2. Nature of variation of lateral earth pressure at a certain depth (Das, 2007).

Prediction of actual retaining walls forces and deformations is a highly complicated problem. The typical approach is to estimate the forces acting on a wall and then to design the wall to resist those forces with a factor of safety high enough to produce acceptably small deformations. In many of these simplified approaches, deformations are rarely considered explicitly in design. On the other hand, nonlinear analyses are

capable of predicting permanent deformations as well as wall pressures. A number of software products are available for such analyses using finite-element analysis. The most common simplified earth pressure approaches, seismic displacement approaches and finite-element analyses which are used to design retaining walls are described in the following sections.

4.1.1. Static Earth Pressures Acting on Retaining Walls

There are two widely used earth pressure theories. Coulomb published the first precise analysis of the problem of lateral earth pressure in 1776. Almost a century later, Rankine (1857) proposed a different but simpler approach to the problem. These theories were proposed to estimate the magnitudes of active earth pressure and passive earth pressures.

4.1.1.1. Rankine Theory. After Coulomb (1776), Rankine proposed the simplest theory for estimating minimum active and maximum passive earth pressures in 1857. The Rankine theory assumes;

- There is no adhesion or friction between the wall and soil.
- Lateral pressure is limited to vertical walls.
- Failure (in the backfill) occurs as a sliding wedge along an assumed failure plane defined by ϕ(angle of internal friction).
- Lateral pressure varies linearly with depth and the resultant pressure is located one-third of the height (H) above the base of the wall.
- The resultant force is parallel to the backfill surface.

For active earth pressure conditions, the pressure "p_A" at a point on the back of a retaining wall can be determined as:

$$p_A = K_A \sigma'_v - 2c\sqrt{K_A} \tag{4.1}$$

where: K_A is the Coefficient of minimum active earth pressure, $\sigma'v$ is the Vertical effective stress at a certain depth behind the wall, c is the Cohesive strength of the soil.

In case of a smooth (no interface friction between wall and soil) wall and horizontal backfill, principal stress planes will be vertical and horizontal. In such a case, coefficient of active earth pressure can be formulated as

$$K_A = \frac{1 - sin\phi}{1 + sin\phi} = tan^2\left(45 - \frac{\phi}{2}\right) \tag{4.2}$$

When the cohesionless backfill inclined at an angle of β ($\beta \leq \phi$) with the horizontal, Terzaghi (1943) and Taylor (1948) proposed K_A as:

$$K_A = cos\beta \frac{cos\beta - \sqrt{cos^2\beta - cos^2\phi}}{cos\beta + \sqrt{cos^2\beta - cos^2\phi}} \tag{4.3}$$

When β=0, Equation 4.3 is equivalent to Equation 4.3. Angle of internal friction and cohesion of the soil influence the pressure distribution behind the wall which is indicated by Equation 4.1. Possible pressure distributions depending on shear strength components (ϕ and c) are shown in Figure 4.3. As it can be seen in Figure 4.3, in cohesive backfills, tensile stresses develop between the upper portion of the wall and backfill. However, use of cohesive backfills are avoided in the field due to their stress relaxation, creep and low permeability characteristics.

For dry homogeneous cohesionless backfills with unit weight γ, which are suggested and widely used instead of cohesive ones, a triangular active pressure distribution oriented parallel to the backfill surface is expected by Rankine. The active earth pressure resultant, P_A, acts at a point located H/3 above the base of a wall height, H (Figure 4.3) with magnitude:

$$P_A = \frac{1}{2} K_A \gamma H^2 \tag{4.4}$$

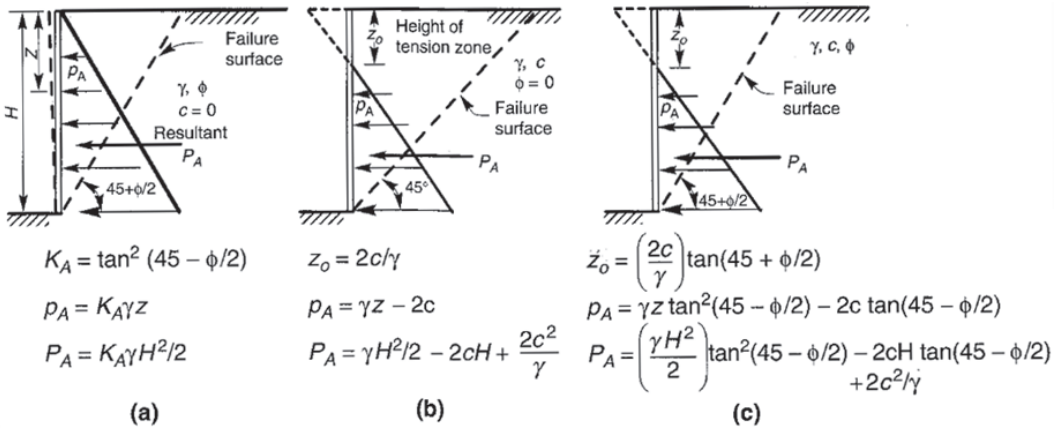

Figure 4.3. Minimum Rankine active earth pressure distributions for backfills with various combinations of frictional and cohesive strength: (a) frictional resistance, no cohesion; (b) cohesive soil, no frictional resistance; (c) combined cohesion and friction (Kramer, 1996).

For passive earth pressure conditions, the pressure "p_P" at a point on the back of a retaining wall can be determined as:

$$P_p = K_p \sigma'_v + 2c\sqrt{K_P} \tag{4.5}$$

where K_P is the coefficient of maximum passive earh pressure. In case of a smooth (no interface friction between wall and soil) wall and horizontal backfill, coefficient of passive earth pressure can be formulated as:

$$K_p = \frac{1 + sin\phi}{1 - sin\phi} = tan^2\left(45 + \frac{\phi}{2}\right) \tag{4.6}$$

When the cohesionless backfill inclined at an angle of β ($\beta \leq \phi$) with the horizontal, K_P can be determined as:

$$K_p = cos\beta \frac{cos\beta + \sqrt{cos^2\beta - cos^2\phi}}{cos\beta - \sqrt{cos^2\beta - cos^2\phi}} \tag{4.7}$$

When β=0, Equation 4.7 is equivalent to Equation 4.6. Angle of internal friction and cohesion of the soil influence the pressure distribution behind the wall which is

indicated by Equation 4.5. Possible pressure distributions depending on shear strength components (ϕ and c) are shown in Figure 4.4.

For dry homogeneous cohesionless backfills, which are suggested and widely used instead of cohesive ones, a triangular passive pressure distribution oriented parallel to the backfill surface is expected by Rankine. The passive earth pressure resultant, PP, acts at a point located H/3 above the base of a wall height, H (Figure 4.4) with magnitude:

$$P_P = \frac{1}{2} K_P \gamma H^2 \tag{4.8}$$

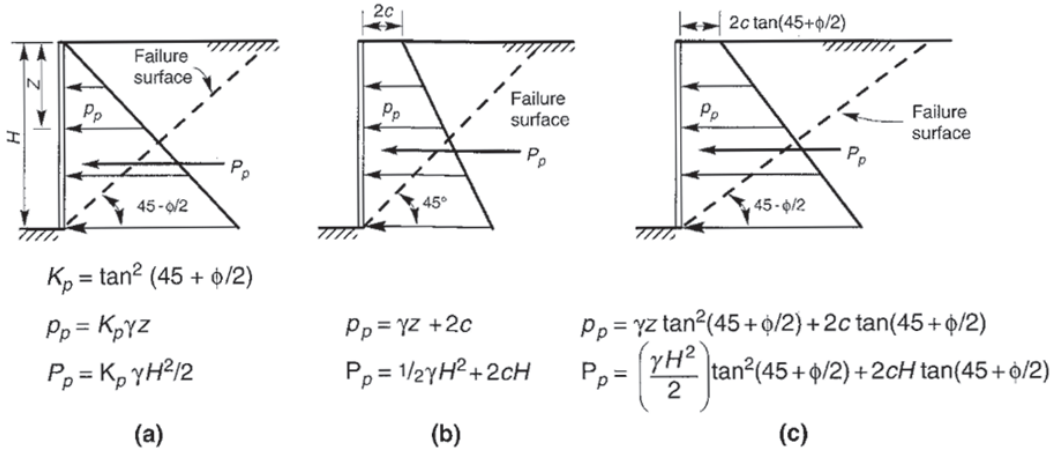

Figure 4.4. Maximum Rankine passsive earth pressure distributions for backfills with various combinations of frictional and cohesive strength: (a) frictional resistance, no cohesion; (b) cohesive soil, no frictional resistance; (c) combined cohesion and friction (Kramer, 1996).

Effective stresses are directly influenced by water in the backfill. In such a case, hydrostatic pressure that is caused by water must be added to the lateral earth pressure. Therefore, presence of water in the backfill behind a retaining wall increases total lateral thrust on a wall. Eventually, drainage of backfill must be provided to reduce the loads acting on a retaining wall.

4.1.1.2. Coulomb Theory. Coulomb developed the first theory for lateral earth pressures acting on retaining structures in 1776. Coulomb Theory is older than Rankine's, it is more sophisticated than Rankine Theory. The Coulomb Theory is generally similar to Rankine theory, but differences between Coulomb and Rankine Theory are:

- There is friction between the wall and soil and takes into account by using a soil-wall interface friction angle of ϕ. Soil-wall friction angle ϕ=2ϕ/3 is commonly used, but it ranges from ϕ/2 to 2ϕ/3 and.
- Lateral pressure is not limited to vertical walls.
- The resultant force is not necessarily parallel to the backfill surface because of the soil-wall friction δ.

Coulomb assumed a planar failure surface and obtained the force acting on the back of the retaining structure from the weight of the wedge of soil above failure surface. Wedges for active and passive pressures are given in Figure 4.5 and Figure 4.6. In Coulomb Theory, equilibrium of forces is used to calculate the magnitude of the soil thrust acting on the wall for both minimum active and maximum passive pressures. The failure surface that produces the greatest active thrust or the smallest passive thrust can be considered critical failure plane. In order to find the critical failure plane, various analysis should be made with different potential failure planes.

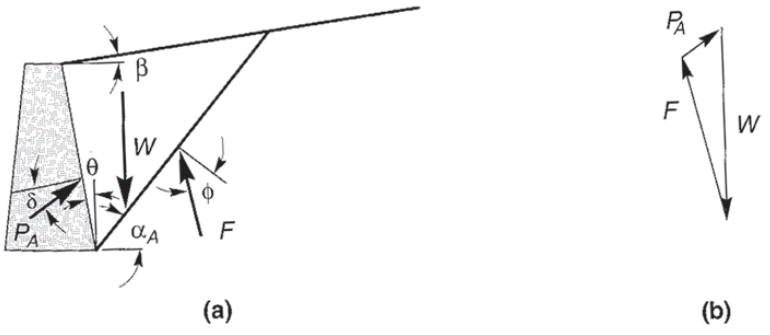

Figure 4.5. (a) Triangular active wedge bounded by planar backfill surface, failure surface and wall; (b) force polygon for active Coulomb wedge. The critical failure surface is that which gives the largest value of P_A (Kramer, 1996).

When minimum active earth pressure conditions develop, force equilibrium (Figure 4.5) is used to calculate the active thrust (Figure 4.5) on a wall. The distribution of active pressure cannot be predicted precisely. However, it can be presumed to be triangular for linear backfill surfaces without surcharge loads. Therefore, PA acts at a point located H/3 above the height of a wall of height H for the linear backfill without surcharge load.

For critical failure plane, Equation 4.9 can be used to calculate the active thrust acting on a wall retaining a cohesionless backfill.

$$P_A = \frac{1}{2} K_A \gamma H^2 \tag{4.9}$$

coefficient of active earth pressure K_A is formulated as;

$$K_A = \frac{cos^2(\phi - \theta)}{cos^2\theta cos(\delta + \theta)\left[1 + \sqrt{\frac{sin(\delta+\phi)sin(\phi-\beta)}{cos(\delta+\theta)cos(\beta-\theta)}}\right]^2} \tag{4.10}$$

The angles $\beta\theta$ and δ are shown in Figure 4.5. The angle of critical failure surface to the horizontal α_A is determined as:

$$\alpha_A = \phi + tan^{-1}\left[\frac{cos(\phi - \beta) + C_1}{C_2}\right] \tag{4.11}$$

where

$$C_1 = \sqrt{tan(\phi - \beta)[tan(\phi - \beta) + cot(\phi - \theta)][1 + tan(\delta + \theta)cot(\phi - \theta)]} \tag{4.12}$$

and

$$C_2 = 1 + tan(\delta + \theta)[tan(\phi - \beta) + cot(\phi - \theta)] \tag{4.13}$$

For maximum passive conditions shown in Figure 4.6, Equation 4.14 can be used to calculate the passive thrust acting on a wall retaining a cohesionless backfill.

$$P_P = \frac{1}{2} K_P \gamma H^2 \tag{4.14}$$

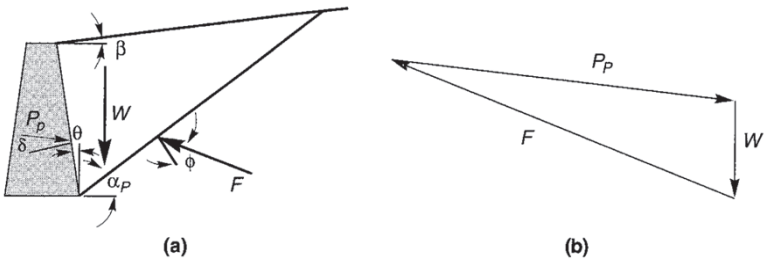

Figure 4.6. (a) Triangular passive wedge bounded by planar backfill surface, failure surface and wall; (b) force polygon for passive Coulomb wedge. The critical failure surface is that which gives the largest value of P_P (Kramer, 1996).

coefficient of passive earth pressure K_P is formulated as;

$$K_P = \frac{cos^2(\phi + \theta)}{cos^2\theta cos(\delta - \theta)\left[1 + \sqrt{\frac{sin(\delta+\phi)sin(\phi+\beta)}{cos(\delta-\theta)cos(\beta-\theta)}}\right]^2} \tag{4.15}$$

The angles β, θ and δ are shown in Figure 4.6. The angle of critical failure surface to the horizontal α_P is determined as:

$$\alpha_P = -\phi + tan^1\left[\frac{tan(\phi + \beta) + C_3}{C_4}\right] \tag{4.16}$$

where

$$C_3 = \sqrt{tan(\phi + \beta)[tan(\phi + \beta) + cot(\phi + \theta)][1 + tan(\delta - \theta)cot(\phi + \theta)]} \tag{4.17}$$

and

$$C_4 = 1 + tan(\delta - \theta)[tan(\phi + \beta) + (\phi + \theta)] \tag{4.18}$$

When Rankine Theory and Coulomb Theory compared, it can be seen that Coulomb Theory can be used to calculate soil thrusts on walls with irregular backfill slopes, concentrated loads on the backfill surface an seepage forces. By considering the soil above a potential failure plane as a free body and including forces due to concentrated loads, water pressures, and so on, the magnitude of the resultant thrust (P_A, P_P) can easily be computed (Kramer, 1996).

4.1.2. Pseudo-Static and Pseudo-Dynamic Methods for Seismic Pressures on Retaining Walls

Retaining walls are used throughout seismically active areas. Permanent deformation or collapse of retaining walls have seen due to earthquake loads in many historical cases. For this reason, behaviour of retaining walls under seismic loads should be taken into consideration while designing a retaining wall.

The response of even simplest type of retaining wall to dynamic loads is pretty difficult. Well-documented case histories involving field measurements, model tests and numerical analyses enabled researchers to develop various approaches to understand the behaviour of retaining walls under dynamic loads.

Pseudo-static and pseudo-dynamic approaches are the most simplified approaches to the seismic design for retaining walls. Such methods involve estimating the loads imposed on the wall during earthquake shaking and then ensuring that the wall resist those loads. Although the actual loading on retaining walls during earthquakes is extremely complicated, seismic pressures on retaining walls can be calculated approximately using simplified methods.

4.1.2.1. Mononobe-Okabes Pseudo-Static Method. Okabe (1926), Mononobe and Matsuo (1929), founded pseudo-static analysis to estimate the seismic earth pressures acting on retaining structures. The Mononobe-Okabe method is developed by modifying the static Coulomb theory. In Mononobe-Okabe method, pseudo-static accelerations are

used to obtain pseudo-static forces. The pseudo-static accelerations are applied to a Coulomb active or passive wedge. Consequently, force equilibrium of the wedge gives the pseudo-static soil thrust acting on a retaining structure. For active case of dry and cohesionless backfill, Figure 4.7 illustrates the situation in which M-O theory was developed. Horizontal and vertical pesudo-static forces, whose magnitudes are related to the mass of the wedge and pseudo-static accelerations, acting on the wall in addition to the forces that exist in static conditions.

$$a_h = k_h g \; and \; a_v = k_v g \tag{4.19}$$

It is known that the stability of a retaining structure is reduced by an increase in active pressure. Additionally, positive horizontal acceleration coefficient increases the total active thrust acting on retaining structure, so Mononobe-Okabe method produces seismic loads that are more critical than static loads.

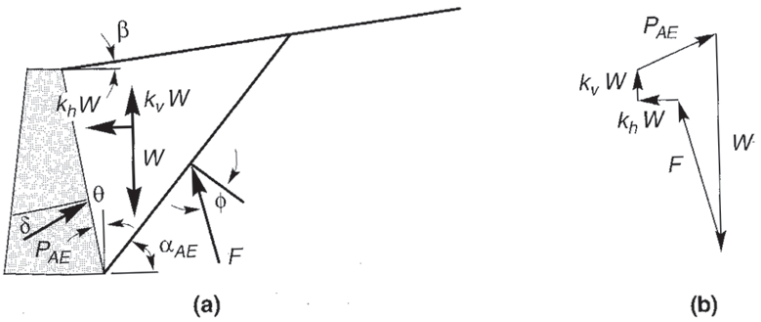

Figure 4.7. (a) Forces acting on passive wedge in Mononobe-Okabe analysis; (b) force polygon illustrating equilibrium of forces acting on passive wedge (Kramer, 1996).

According to M-O method, the total active thrust can be expressed as;

$$P_{AE} = \frac{1}{2} K_{AE} \gamma H^2 (1 - k_v) \tag{4.20}$$

coefficient of dynamic active earth pressure K_{AE} is formulated as;

$$K_{AE} = \frac{cos^2(\phi - \theta - \psi)}{cos\psi cos^2\theta cos(\delta + \theta + \psi)\left[1 + \sqrt{\frac{sin(\delta+\phi)sin(\phi-\beta-\psi)}{cos(\delta+\theta+\psi)cos(\beta-\theta)}}\right]^2} \tag{4.21}$$

where ϕ-$\beta \geq \psi$, $\gamma = \gamma_d$ and $\psi = \tan^{-1}$ [k_h/(1-k_v)]. The angle of critical failure surface to the horizontal α_{AE} is flatter than the critical failure surface for static conditions (Zarabi-Kashani, 1979). The angle of failure surface to horizontal is determined as:

$$\alpha_{AE} = \phi - \psi + tan^{-1}\Big[\frac{-tan(\phi - \psi - \beta) + C_{1E}}{C_{2E}}\Big] \tag{4.22}$$

where

$$\begin{aligned} C_{1E} &= \sqrt{tan(\phi - \psi - \beta)[tan(\phi - \psi - \beta) + cot(\phi - \psi - \theta)]} \\ &= \sqrt{[1 + tan(\delta + \psi + \theta)cot(\phi - \psi - \theta)]} \end{aligned} \tag{4.23}$$

and

$$C_{2E} = 1 + tan(\delta + \psi + \theta)[tan(\phi - \psi - \beta) + cot(\phi - \psi - \theta)] \tag{4.24}$$

According to M-O analysis, P_{AE} acts at a point H/3 above the base of a wall of height, H. On the other hand, it was seen in experimental results that P_{AE} actually acts at a higher point under dynamic loading conditions. The total active thrust P_{AE} (Equation 4.20) can be divided into a static component P_A from Coulomb's theory (Equation 4.9) and a dynamic component ΔP_{AE} (Kramer, 1996):

$$P_{AE} = P_{_A} + \Delta P_{AE} \tag{4.25}$$

It is already known that the static component acts at H/3 above the base of the wall. Seed and Whitman (1970) recommended that dynamic component be taken to act at approximately 0.6H. Therefore, acting point of the total active thrust above the base will be:

$$h = \frac{P_A(H/3) + \Delta P_{AE}(0.6H)}{P_{AE}} \tag{4.26}$$

Relative magnitudes of P_A and P_{AE} influence the value of h. M-O analyses show that

k_v, when taken as one-half to two-thirds the value of k_h, affects P_{AE} by less than 10%. Seed and Whitman (1970) concluded that vertical accelerations can be ignored when the M-O method is used to estimate P_{AE} for typical wall designs (Kramer, 1996).

For passive case of dry and cohesionless backfill, Figure 4.8 illustrates the situation in which M-O theory was developed. The parameters used in pseudo-static analysis of passive case can be determined similar to the active case. However, direction of the horizontal acceleration must be determined carefully, which influences the stability analysis of the wall. A positive horizontal acceleration coefficient causes the total passive thrust to be less than the static passive thrust, which makes the loading conditions more critical. Total passive thrust acting on a wall is calculated as:

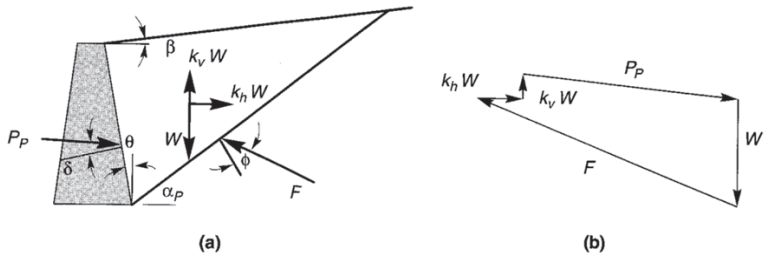

Figure 4.8. (a) Forces acting on passive wedge in Mononobe-Okabe analysis; (b) force polygon illustrating equilibrium of forces acting on passive wedge (Kramer, 1996).

$$P_{PE} = \frac{1}{2} K_{PE} \gamma H^2 (1 - k_v) \tag{4.27}$$

coefficient of dynamic active earth pressure K_{PE} is formulated as;

$$K_{PE} = \frac{cos^2(\phi - \theta - \psi)}{cos\psi cos^2\theta cos(\delta - \theta + \psi)\left[1 + \sqrt{\frac{sin(\delta+\phi)sin(\phi+\beta-\psi)}{cos(\delta-\theta+\psi)cos(\beta-\theta)}}\right]^2} \tag{4.28}$$

The angle of failure surface to horizontal is determined as:

$$\alpha_{PE} = \psi - \phi + tan^{-1}\left[\frac{tan(\phi + \psi + \beta) + C_{3E}}{C_{4E}}\right] \tag{4.29}$$

where

$$C_{3E} = \sqrt{tan(\phi+\beta+\psi)[tan(\phi+\beta-\psi)+cot(\phi+\theta-\psi)]} = \sqrt{[1+tan(\delta+\psi-\theta)cot(\phi+\theta-\psi)]} \tag{4.30}$$

and

$$C_{4E} = 1 + tan(\delta+\psi-\theta)[tan(\phi+\beta-\psi)+cot(\phi+\theta-\psi)] \tag{4.31}$$

Similar to active case, total passive thrust can be divided into its static and dynamic components:

$$P_{AE} = P_A + \Delta P_{AE} \tag{4.32}$$

Static and dynamic components of the total passive thrust are computed from Coulomb theory and M-O method, respectively. It must be taken into consideration that the directions of the dynamic component and static component are opposite which causes a reduction in available passive resistance.

The Mononobe-Okabe method, which is an pseudo-static extension of the Coulomb analysis, is used widely to make dynamic analysis. However, because of the shortcomings of the method listed below, M-O method should be used and interpreted carefully.

- All of the limitations that Coulomb theory is subjected are also valid for Mononobe-Okabe method.
- Mononobe Okabe analysis is subject to all of the limitations of pseudo-static analyses.
- Determination of the appropriate pseudo-static coefficient is difficult.
- The analysis is not appropriate for soils (e.g., liquefiable soils) that experience significant loss of strength during earthquakes.
- Mononobe-Okabe analysis overpredicts the actual total passive thrust, particu-

larly for $\delta > \phi/2$.

4.1.2.2. Steedman-Zengs Pseudo-Dynamic Method. The pseudo-static analysis gives the linear distribution of seismic earth pressure in a very approximate way. Determining seismic earth pressure in a simple and approximate way is possible. However, in order to account for phase difference and amplification effects within the backfill behind a retaining wall, Steedman and Zeng (1990) proposed another simple approach called pseudo-dynamic analysis can be used.

Steedman and Zeng (1990) considered in their analysis a vertical rigid retaining wall supporting a particular value of soil friction angle (ϕ) and a particular value of seismic horizontal acceleration ($k_h g$, where g is the acceleration due to gravity) only (Choudhury and Nimbalkar, 2006).

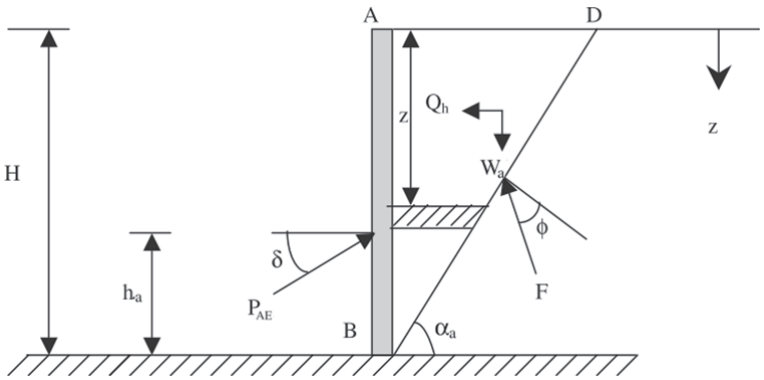

Figure 4.9. Model retaining wall considered for computation of pseudo dynamic active earth pressure (after Choudhury and Nimbalkar, 2006).

Consider the fixed base vertical rigid retaining wall AB of height H as shown in Figure 4.9. Where, is the Q_h Horizontal seismic inertia force in active case, is the W_a Weight of the failure wedge in active case, is the F Soil reaction acting at an angle of ϕ (angle of internal friction of the soil) to the normal to the inclined failure wedge, is the α_a Angle of failure plane to the horizontal in active case, is the P_{AE} Total active thrust of the soil, is the δ Wall friction angle.

The wall is supporting a cohesionless backfill material with horizontal ground.

If the base of the wall is subjected to harmonic horizontal seismic acceleration of amplitude a_hg (where g is the acceleration due to gravity) the acceleration at any depth z and time t, below the top of the wall can be expressed as:

$$a_h(z,t) = a_h sin\left(t - \frac{Hz}{V_s}\right) \tag{4.33}$$

where V_s is the Shear wave velocity. The mass of the thin element of wedge at depth z is:

$$m_a(z) = \frac{\gamma}{g}\frac{H-Z}{tan\alpha_a}dz \tag{4.34}$$

where γ is the Unit weight of backfill The weight of the whole wedge is,

$$W_a = \frac{1}{2}\frac{\gamma H^2}{2tan\alpha_a} \tag{4.35}$$

The total horizontal inertial force Q_h acting within the failure zone can be expressed as:

$$Q_h(t) = \int_0^H m_a(z)a_h(z,t)dz = \frac{\lambda H^2 a_h}{4\pi^2 g tan\alpha_a}[2\pi H cos\omega\xi + \lambda(sin\omega\xi - sin\omega t)] \tag{4.36}$$

where λ=2π V_s/ω is the wavelength of the vertically propagating shear wave and ξ=t-H/V_s. The special case of a rigid wedge is given, in the limit, as:

$$\lim_{v_s\to\infty}(Q_h)_{max} = \frac{\gamma H^2 a_h}{2g tan\alpha_a} = \frac{a_h}{g}W_a = k_h W_a \tag{4.37}$$

which is equivalent to the pseudo-static force assumed in the Mononobe-Okabe method. The total (static+dynamic) active thrust, P_{AE}(t) can be obtained by resolving forces on the wedge and considering the equilibrium of the forces and hence P_{AE}(t) can be expressed as follows:

$$P_{AE}(t) = \frac{W_a sin(\alpha_a - \phi) + Q_h(t)cos(\alpha_a - \phi)}{cos(\delta + \phi - \alpha_a)} \tag{4.38}$$

and the total earth pressure distribution by differentiating the total soil thrust:

$$p_{AE}(t) = \frac{\partial P_{AE}(t)}{\partial z} = \frac{\gamma z}{tan\alpha_a}\frac{sin(\alpha_a - \phi)}{cos(\delta + \phi - \alpha_a)} + \frac{k_h \gamma z}{tan\ \alpha_a cos(\delta + \phi - \alpha_a)} sin\left[\omega\left(t - \frac{z}{V_s}\right)\right] \tag{4.39}$$

where ω is the angular frequency of base shaking.

The first term in Equation 4.38, which increases linearly with depth and does not vary with time, represents the static earth pressure acting on wall. The resultant static thrust acts in accordance with static earth pressure theories at a point h_s=H/3 above the base of the wall. The second term represents the dynamic earth pressure. It increases as a nonlinear function of depth with a shape that depends on the ratio H/λ. A typical example of nonlinear dynamic pressure is shown in Figure 4.10. Since the dynamic pressure increases nonlinearly with depth, the position of the dynamic thrust varies with time according to the Equation 4.40 (Kramer, 1996).

$$h_d = H - \frac{2\pi^2 H^2 cos\omega\xi + 2\pi\lambda H sin\omega\xi - \lambda^2(cos\omega\xi - cos\omega t)}{2\pi H cos\omega\xi + \pi\lambda(sin\omega\xi - sin\omega t} \tag{4.40}$$

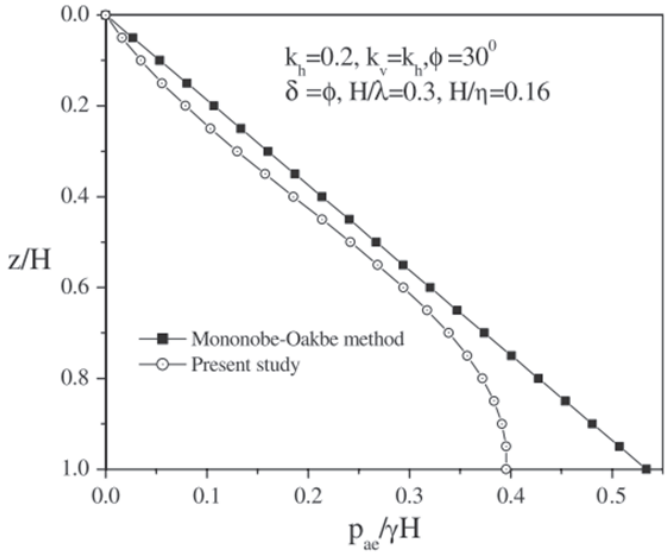

Figure 4.10. A typical comparison of Mononobe-Okabe and Steedman-Zeng method for k_v=k_h=0.2, ϕ=30^o, δ=ϕ, H/λ=0.3, H/η=0.16 (Choudhury and Nimbalkar, 2006).

For very low frequency motions (small H/λ, so the backfill moves essentially in phase), the point of application of the dynamic thrust is at h_d=H/3. For higher frequency motions, the point, where dynamic thrust acts on the wall, moves through the top of the wall, as illustrated in Figure 4.11.

To conclude, in pseudo-dynamic method by considering the time effect and phase change in shear and primary waves propagating in the backfill behind the rigid retaining wall, the seismic active earth pressure distribution as well as the total active thrust behind the retaining wall can be estimated. When compared to Mononobe-Okabe nethod, pseudo dynamic method gives more realistic non-linear active earth pressure distribution behind the retaining wall. Steedman and Zeng (1989) found that the soil thrusts for backfills of different stiffnesses were close to those obtained when the mean shear wave velocities of the backfill were used in the pseudo-dynamic analyses. Choudhury and Nimbalkar (2006) showed that the seismic active thrust is highly sensitive to the friction angle of the soil, ϕ and comparatively less sensitive to the wall friction angle, δ. Backfill amplification effects can also be considered by expressing a_h as a function of depth [rather than as a constant in Equation 4.34] and repeating the integration of Equation 4.36. It should be noted that the loads acting on the wall and the height of the resultant soil thrust increases with backfill amplification (Kramer, 1996). Assuming that a_h(z, t) varied linearly from the input acceleration at the base of the wall to a value twice as large at the top, Steedman and Zeng (1990) showed good agreement with the results of centrifuge tests.

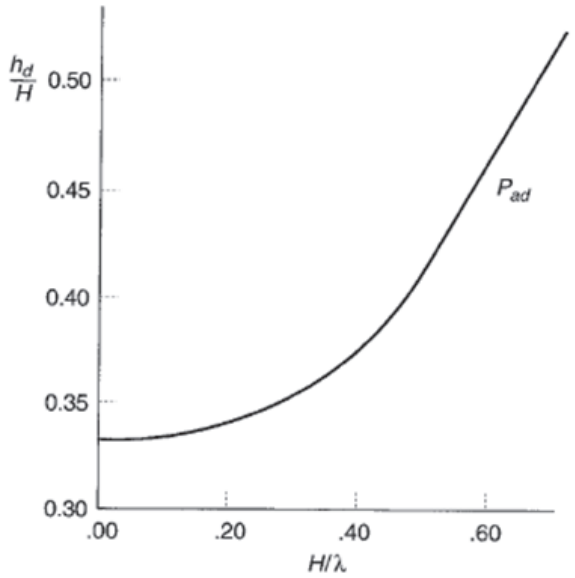

Figure 4.11. Location of dynamic thrust at instant of maximum overturning moment for k_h=0.2 (after Steedman and Zeng, 1990).

Passive state of horizontal earth pressure on the rigid retaining wall for seismic conditions is shown in Figure 4.12. Where, Q_{hp} is the horizontal seismic inertia force in passive case, W_p is the weight of the failure wedge in passive case, F is the soil reaction acting at an angle of ϕ (angle of internal friction of the soil) to the normal to the inclined failure wedge, a_p is the angle of failure plane to the horizontal in passive case, is the P_{PE} Total passive thrust of the soil, δ is the wall friction angle.

Pseudo-dynamic analysis for passive seismic earth pressure conditions is similar to active case. The mass of the thin element of thickness dz, assumed at depth z as shown in Figure 4.12 can be determined using the equation:

$$m_p(z) = \frac{\gamma}{g}\frac{H-z}{tan\alpha_p}dz \tag{4.41}$$

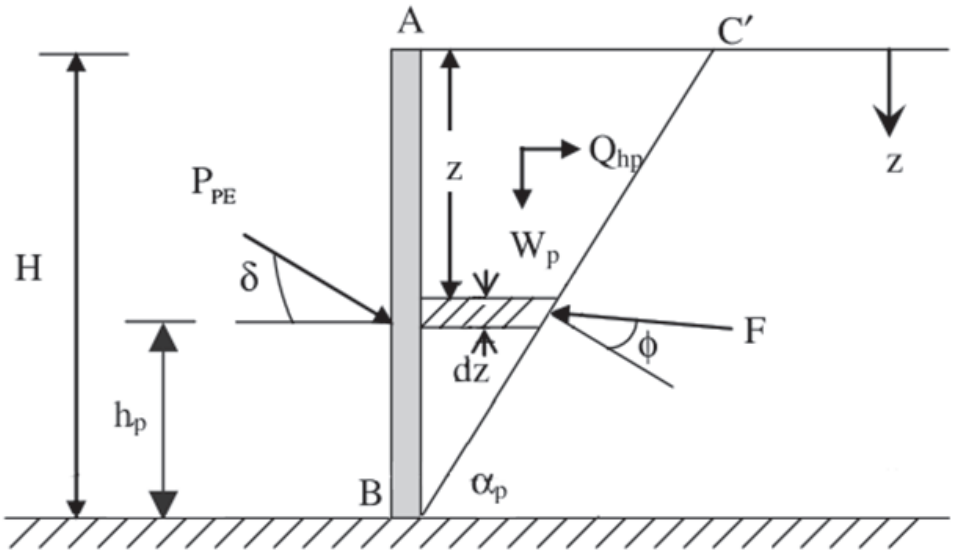

Figure 4.12. Model retaining wall considered for computation of pseudo dynamic active earth pressure (after Choudhury *et al.*, 2006).

The weight of the failure wedge is,

$$W_P = \frac{1}{2}\frac{\gamma H^2}{tan\alpha_p} \tag{4.42}$$

The total horizontal inertia force acting on the wall is given by,

$$Q_h(t) = \int_0^H m_p(z)\alpha_h(z,t)dz = \frac{\lambda\gamma\alpha_h}{4\pi^2 g tan\alpha_p}[2\pi H cos\omega\xi + \lambda(sin\omega\xi - sin\omega t)] \tag{4.43}$$

While determining the minimum seismic passive earth pressure, only the critical directions of Q_h (from left to right or from right to left) is taken into account. The total (seismic+dynamic) passive resistance P_{PE} can be calculated by resolving the forces on the wedge and considering the equilibrium of the forces. Therefore, P_{PE} is given as:

$$P_{PE}(t) = \frac{W_p sin(\alpha_p + \phi) - Q_{hp}(t)cos(\alpha_p\phi)}{cos(\delta + \phi + \alpha_p)} \tag{4.44}$$

P_{PE} is minimized with respect to trial inclination angle of failure surface, σ_p and then the seismic passive earth pressure distribution, p_{PE} can be obtained by differentiating

P_{PE} with respect to depth, z and can be expressed as follows:

$$P_{PE}(t) = \frac{\partial P_{PE}(t)}{\partial Z} = \frac{\gamma z}{tan\alpha_p} \frac{sin(\alpha_p + \phi)}{cos(\delta + \phi + \alpha_p)} - \frac{k_h \gamma z}{tan\alpha_p} \frac{cos(\alpha_p + \phi)}{cos(\delta + \phi + \alpha_p)} sin\left[\omega\left(t - \frac{z}{V_s}\right)\right] \tag{4.45}$$

Chouldhury *et al.*, (2006) stated that the seismic passive earth pressure is more sensitive to wall friction angle as compared to the seismic active earth pressure. By applying the pseudo- dynamic method, the seismic active earth pressures are more and seismic passive earth pressures are less as compared to those calculated by using conventional pseudo-static method of analysis. Thus the pseudo-dynamic method gives the desirable design values of seismic active and passive earth pressure coefficients compared to the existing values by pseudo-static method as it leads to safe approach of design of retaining wall against devastating effect of earthquake (Choudhury *et al.*, 2006).

4.1.3. Seismic Displacements of Retaining Walls

All of the seismic design approaches which are explained in previous sections give beneficial information about the seismic loads acting on retaining walls. Although, they can be used to calculate the factor of safety against failure; they don't provide information about permanent deformations during earthquakes and post earthquake serviceability of the wall. In some cases, even small deformations should be prevented for the serviceability of the wall. Hence, determining the displacements becomes crucial for retaining walls. Several methods have been proposed for predicting permanent deformations of yielding walls.

4.1.3.1. Newmark's Sliding Block Analysis. Newmark (1965) developed a theory to calculate the permanent displacement of a retaining wall for a given input acceleration time history. The purpose of the Newmark (1965) method is to estimate slope deformation for those cases where the pseudo-static factor of safety is less than 1.0. The Newmark (1965) method assumes that the slope will deform only during those portions of the earthquake when the out-of-slope earthquake forces cause the pseudo-static fac-

tor of safety to drop below 1.0. When this occurs, the slope will no longer be stable, and it will be accelerated downslope. The slope deformation increases when the the slope is subjected to a pseudo-static factor of safety below 1.0. On the other hand, if the pseudo-static factor of safety drops below 1.0 for a mere fraction of a second, then the slope deformation will be limited (Day, 2002).

The soil mass is assumed to be a rigid block that fails in a rigid-plastic manner when the ground acceleration exceeds the critical or yield acceleration of the slope (Figure 4.13). Once sliding commences, it is assumed that the rigid mass continues to slide under the actions of the inertia force from the ground acceleration pulse and a constant resisting force. When the acceleration pulse diminishes in magnitude or reverses in direction, the relative velocity between the sliding block and the supporting ground or base eventually reduces to zero and the movement relative to the base ceases. Successive displacements take place each time the ground acceleration exceeds the critical value. Each displacement step is calculated by a double integration of the parts of the input acceleration time-history that are above the critical acceleration value and those parts that are below until the relative velocity (calculated by the first integration) between the sliding mass reduces to zero (Wood, 2008).

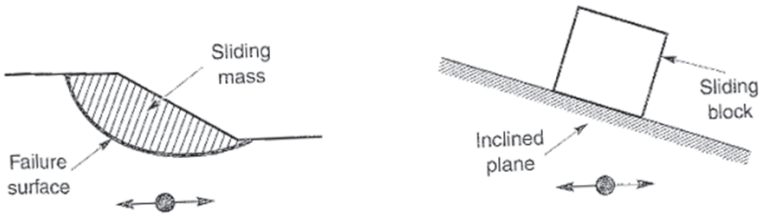

Figure 4.13. Analogy between potential slope failure and block resting on inclined plane.

Under static conditions; the ratio of the available static resisting force, R_s and the static driving force, D_s must be equal or greater than 1.0 in order to achieve equilibrium of the block in the direction parallel to the plane. When the sliding is assumed purely frictional (c=0) and ϕ is the angle of friction between the block and the plane, factor

of safety (FS) is given by:

$$FS = \frac{available resisiting force}{static driving force} = \frac{R_s}{D_s} = \frac{W cos\beta tan\phi}{W sin\beta} = \frac{tan\phi}{tan\beta} \tag{4.46}$$

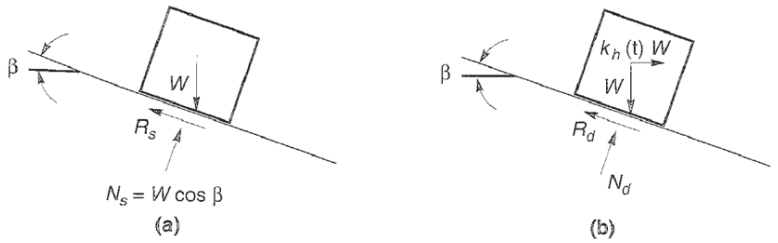

Figure 4.14. Forces acting on a block resting on an inclined plane: (a) static conditions, (b) dynamic conditions.

The effects of vertical accelerations will be neglected for simplicity (Figure 4.14). Therefore, the effect of inertial forces transmitted to the block by horizontal vibration of the inclined plane with acceleration, $a_h(t)=k_h(t)g$ shall be considered for seismic case. Horizontal inertial force k_hW is generated because of the horizontal acceleration of the block. When the inertial force acts in the downslope direction, resolving forces perpendicular to the inclined plane gives:

$$FS_d(t) = \frac{available resisting force}{pseudo - static driving force} = \frac{R_d}{D_d} = \frac{[cos\beta - k_h(t) sin\beta] tan\phi}{sin\beta + k_h(t) cos\beta} \tag{4.47}$$

It can be seen in Equation 4.46 that the FS_d decreases with the increase of k_h. In addition, some positive value of k_h (for a statically stable block) that will produce a factor of safety of 1.0. This k_h coefficient is called *yield coefficient*, k_y, and yield acceleration can be expressed as $a_y=k_hg$. Yield acceleration is the limit value of stability. In other words, it is minimum pseudo-static acceleration required to produce instability of the block and for sliding in the downslope direction it can be expressed as:

$$k_y = tan(\phi - \beta) \tag{4.48}$$

When β and ϕ are small, sliding in the uphill direction can occur. In this case, k_y can

be calculated as:

$$k_y = \frac{tan\phi - tan\beta}{1 + tan\phi tan\beta} \tag{4.49}$$

When $a_y/a_{max} \geq 0.17$, Newmark found that a reasonable upper bound to the permanent displacements, d_{max}, was given by:

$$d_{max} = \frac{v_{max}^2}{2a_y}\frac{a_{max}}{a_y} \tag{4.50}$$

4.1.3.2. Richards-Elms Method. There are very few methods available to estimate seismic displacements of rigid retaining walls. Richard and Elms (1979) proposed a simplified but more rational design criteria consisting in the limitation of the permanent outward displacement of the wall caused by the earthquake to an allowable value. The Richards-Elms development consisted in applying this method to retaining walls assuming that the earth thrust at failure can be computed with the Mononobe-Okabe formula This method was based on Newmarks rigid sliding block analysis (1965) and Franklin and Changs (1977) solution for upper bound permanent displacements for several natural and synthetic ground motions.

The assumptions for the Richards-Elms analysis are:

- The retaining wall is rigid.
- The inertia forces due to the mass of the wall are included.
- Only the sliding of the wall and dry backfill is considered.
- After the horizontal ground acceleration exceeds the yield acceleration, the wall moves away from the backfill until the velocity of the wall motion changes.
- The backfill failure wedge moves as a rigid body with the retaining wall.

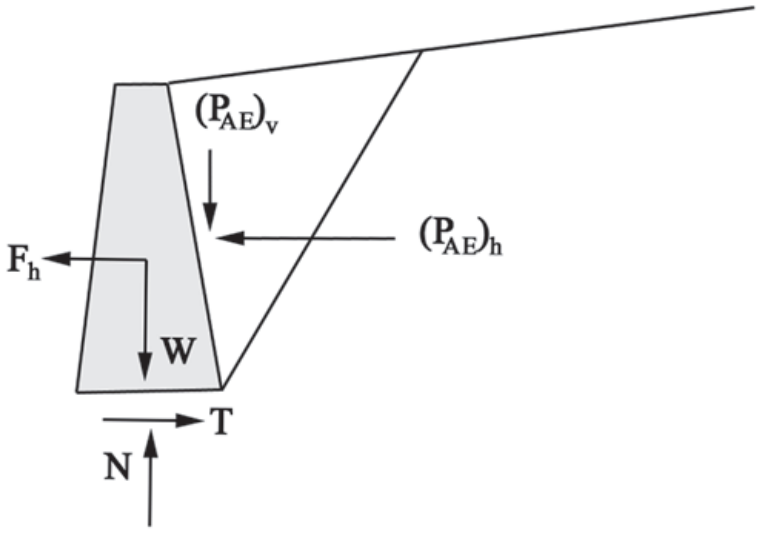

Figure 4.15. Gravity wall acted upon by gravity and pseudo-static acceerations.

Yield acceleration for the wall-backfill system needs to be determined for the application of the Richards-Elms method. When the active wedge is subjected to acceleration acting toward the backfill, the resulting inertial forces will act away from the backfill. The level of acceleration that is just large enough to cause the wall to slide on its base is the yield acceleration. When the acceleration value reaches the value of yield acceleration, from the equilibrium of horizontal and vertical forces:

$$T = F_h + (P_{AE})_h \; and \; N = W + (P_{AE})_v \tag{4.51}$$

Where:

$$T = N tan\phi_b \tag{4.52}$$

$$F_h = a_y \frac{W}{g} \tag{4.53}$$

$$(P_{AE})_h = P_{AE} cos(\delta + \theta) \tag{4.54}$$

$$(P_{AE})_v = P_{AE}sin(\delta + \theta) \tag{4.55}$$

The yield acceleration, a_y can be computed by using substitutions given above:

$$a_y = \left[tan\phi_b - \frac{P_{AE}cos(\delta + \theta) - P_{AE}sin(\delta + \theta)}{W}\right]g \tag{4.56}$$

The value of P_{AE} in Equation 4.56 is calculated by using Mononobe-Okabe method. The yield acceleration a_y must be known to calculate P_{AE} while using Mononobe-Okabe method. Therefore, the solution of the Equation 4.56 must be obtained iteratively. Richards and Elms (1979) prepared the following expression for permanent displacement:

$$d_{perm} = 0.087\frac{v_{max}^2 a_{max}^3}{a_y^4} \tag{4.57}$$

where v_{max} is the peak ground velocity, a_{max} is the peak ground acceleration for the wall-backfill system.

4.1.3.3. Whitman-Liao Method. Richards and Elms (1979) proposed a simplified method which offers a realistic approach to the estimation of gravity wall displacements. Although the assumptions enable the calculation simpler, they neglect some aspects of the dynamic earth pressure problem. Whitman and Liao (1985) determined the various errors which result from the assumptions of the Richards-Elms method. The most important errors are caused by the neglect of:

- dynamic response of the backfill
- kinematic factors
- tilting mechanisms
- vertical accelerations.

After finite element analyses, effects of the dynamic response of the backfill on wall displacements were explained. Analyses show that the compliance of input motions

with the natural period of the backfill causes amplification which produce greater permanent displacement than the rigid block model used by Richards and Elms.

Analyses in which the backfill wedge and wall were treated as separate blocks instead of single block model of Richards and Elms are conducted to determine the effect of kinematic factors. Zarabi-Kashani (1979) used separate blocks approach in their analyses and showed that the kinematic requirements of horizontal and vertical displacement of the backfill wedge cause smaller displacements than the single block approach.

Richards and Elms considered only sliding in their analysis. However, studies in which tilting and sliding was considered together determined that tilting of the wall generally increases the wall displacements.

Finally, consideration of vertical accelerations causes slightly larger displacements than when they are neglected. Whitman and Liao found that the permanent displacements were lognormally distributed with mean value:

$$d_{perm} = \frac{37 v_{max}^2}{a_{max}} exp\left(\frac{-9.4 a_y}{a_{max}}\right) \tag{4.58}$$

4.1.4. Finite Element Analysis

Using numerical techniques for the design and analysis of geosynthetic reinforced soil walls offers several advantages, such as analyzing complex models more realistic and easier. There are various software products that are using numerical methods are available and they give more realistic results when compared with the traditional simplified methods.

Finite element method (FEM) is the most commonly used numerical method. It can be used to analyze various geotechnical structures such as embankments, shallow and deep foundations. Because of their complex mechanism, analyzing the geosynthetic

reinforced retaining walls using finite element method is developed recently. However, finite element analysis provides additional information compared to traditional limit-equilibrium analysis, such as deformation and tensile load in the reinforcement layers that are necessary for understanding the performance of reinforced soil structures. The results obtained from finite element analysis can be used to guide the development of more accurate limit- equilibrium design procedures (Enünlü, 2007).

On the other hand, finite element analysis is very compatible with the computer programming. Software products those using finite element method enables operator to simulate the construction sequences such as such as backfilling and the installation of reinforcement layers and wall facings. Since the computing costs have significantly reduced, modern finite element methods use a discrete approach. The soil, reinforcement, facing and their interactions are modeled separately in discrete approach.

4.2. Stability Analysis For Geosynthetic Reinforced Soil Retaining Walls

In this section, stability analyses for geosynthetic reinforced segmental retaining wall systems under static and seismic loading conditions were investigated. Such analysis consist of separate calculations to determine factors of safety against external, internal and facing modes of failure.

External stability calculations consider the reinforced soil zone and the facing column as a monolithic gravity structure. The calculation of factors of safety for external stability is similar to that used for conventional reinforced concrete gravity structures. Factors of safety against:

- base sliding,
- overturning about the toe,
- foundation bearing capacity

are evaluated for the external stability (Figure 4.16).

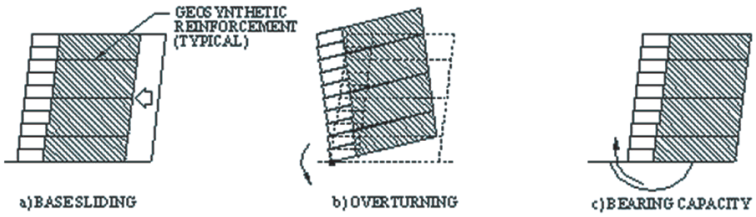

Figure 4.16. Potential external failure mechanisms of MSE wall.

Internal stability analyses for geosynthetic reinforced soil walls are carried out to ensure that the structural integrity of the reinforced zone is preserved with respect to:

- reinforcement over-stressing within the reinforced zone,
- pullout of geosynthetic reinforcement layers from the anchorage zone and
- internal sliding along a reinforcement layer (Figure 4.17).

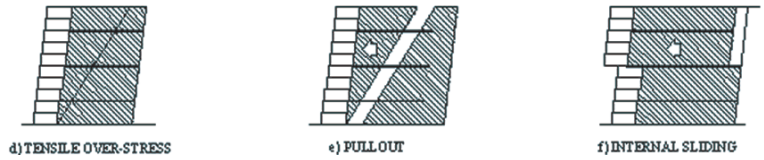

Figure 4.17. Potential internal failure mechanisms of MSE wall.

Facing stability analyses are carried out to ensure that the facing column is stable at all elevations above the toe of the wall and connections between the facing units and reinforcement layers are not over-stressed. Potential facing failure types of MSE walls are:

- shear failure,
- connection failure,
- local overturning,
- crest toppling (Figure 4.18)

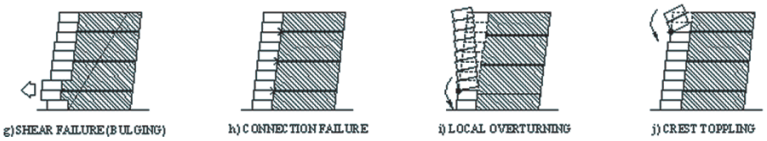

Figure 4.18. Potential facing failure mechanisms of MSE wall.

Minimum recommended factors of safety for static and seismic design of geosynthetic reinforced SRW structures are given in Table 4.1. In general, minimum recommended factors of safety for seismic design are taken as 75% of the values recommended for statically loaded structures following AASHTO/ FHWA practice (Kadayıfçı, 2005).

Table 4.1. Potential external failure mechanisms of MSE wall.

Failure Mode	**Abbr.**	**Static**	**Dynamic**
a) Base Sliding	FS_{sl}	1.5	1.1
b) Overturning	FS_{ot}	1.5	1.1
c) Bearing Capacity	FS_{bc}	2.0	1.5
Global Stability	FS_{gl}	1.3-1.5	1.1
d) Tensile Over-Stress	FS_{os}	1.0	1.0
e) Pull Out	FS_{po}	1.5	1.1
f) Internal Sliding	FS_{sli}	1.5	1.1
g) Shear (Buging)	FS_{sc}	1.5	1.1
h) Connection	FS_{cs}	1.5	1.1
i) Local Overturning	FS_{otl}	1.5	1.1
j) Crest Toppling	FS_{otc}	1.5	1.1

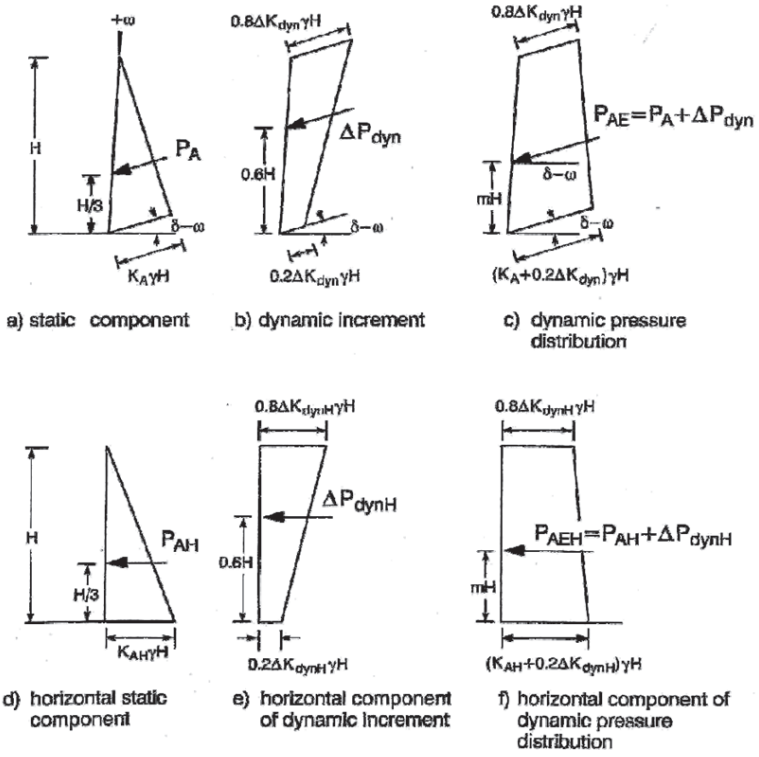

Figure 4.19. Earth pressure distributions due to soil self-weight.

4.2.1. External Stability

External stability calculations are similar to those carried out for conventional (gravity) soil retaining wall structures with the gravity mass now taken as the composite mass formed by the reinforced soil zone and the facing column. The facing column may comprise a significant part of the gravity mass, particularly for low height structures (and hence generate additional inertial forces during a seismic event). For brevity, this gravity mass is called the reinforced mass or reinforced zone in this document.

The dynamic earth pressure distribution shown in Figure 4.19 is used to calculate the destabilizing forces in otherwise conventional expressions for the factor of safety against sliding along the foundation surface, overturning about the toe of the structure and bearing capacity failure of the foundation soils. $k_h = a_c/2g$ is used to calculate the magnitude of the uniformly applied horizontal seismic coefficient value k_h, in all external stability calculations (i.e. k_h=k_h(ext)).

The peak friction angle is taken as $\phi = \phi_b$ in earth pressure and force calculations. The calculation of force components P_{AH} and ΔP_{dynH} assumes full mobilization of inter face friction between the reinforced soil zone and the retained soil (i.e. $\delta = \phi$ with ϕ equal to lesser of ϕ_r and ϕ_b values).

The simplified geometry and body forces illustrated in Figure 4.20 are used in the external stability calculations to follow.

Where, is the W_i Total weight of the reinforced zone extending from the back of the facing column to length L_{min} beyond the face of the wall and having constant height H, is the W_β Contribution of the wedge of soil in the slope above the crest of the wall at height H and is the W_w Total weight of the facing column.

$$W_w = N_w L_w H_w \gamma_w = L_w H \gamma_w \tag{4.59}$$

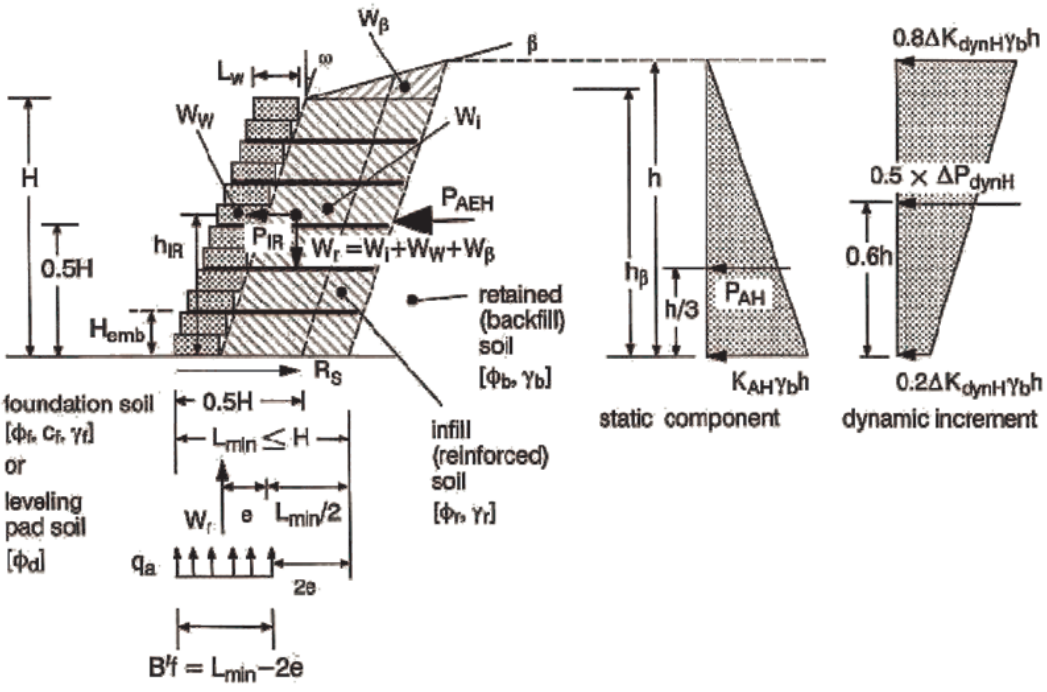

Figure 4.20. Earth pressure distributions due to soil self-weight.

The results of parametric analyses reported by Bathurst and Cai (1995) have illustrated that as the backslope angle β for the infinite slope case increases, the factors

of safety against external stability modes of failure diminish rapidly and reasonable solutions even for modest values of ground acceleration are not possible. This result is due in part to the formulation of earth forces calculated using the Mononobe-Okabe method and the conservative estimates of soil strength parameters that are routinely used for the design and analysis of geosynthetic reinforced wall systems. In order to prevent this problem from developing the following empirical rule is proposed in this design guideline: Regardless of the wall geometry and reinforcement lengths the maximum value of the reinforced zone width Lmin (Figure 4.20) is restricted to the height of the wall H. Hence $L_{min} \leq H$. This approach has been adopted by the Reinforced Earth Company (RECO 1990) for the design of steel strip reinforced soil wails for the same reasons given above.

The total weight of the reinforced soil zone is:

$$W_r = W_w + W_i + W_\beta \tag{4.60}$$

The total weight W_r is used to calculate resisting terms in factor of safety expressions for base sliding and overturning and the applied load in bearing capacity calculations. Quantities W_i and W_β can be calculated using the following expressions:

$$W_i = (L_{min} - L_w)H\gamma_r \tag{4.61}$$

$$W_\beta = \frac{1}{2}\gamma_r(L_{min} - L_w)^2\left(\frac{tan\beta}{1 - tan\beta tan\omega}\right) \tag{4.62}$$

The quantity P_{IR} in Figure 4.20 denotes the horizontal inertial force due to the reinforced mass used in external stability factor of safety calculations. Different strategies have been proposed in North America to compute $P_{IR} < k_h W_r$ to ensure reasonable designs (Bathurst and Alfaro, 1996). The justification is based on the expectation that horizontal inertial forces induced in the reinforced mass and the retained (backfill) soil zone will not reach peak values at the same time during a seismic event.

The method adopted here uses the AASHTO/FHWA approach and assumes that the horizontal inertial force PIR is due to an equivalent mass comprising the facing column and a portion of the reinforced soil zone extending to a distance 0.5H beyond the face of the wall. The general approach is illustrated in Figure 4.20 and applies to any infinite backfill slope condition (i.e. $\beta > 0$). The inertial force PIR is calculated using:

$$P_{IR} = k_h(ext)(W_w + W_i^{'} + W_\beta^{'}) \tag{4.63}$$

Where the reduced inertial zone weights $W_i^{'}$ and $W_\beta^{'}$ are calculated by substituting L_{min}=0.5H in Equation 4.61 and Equation 4.62 Hence:

$$W_i^{'} = (0.5H - L_w)H\gamma_r \tag{4.64}$$

$$W_\beta' = \frac{1}{2}\gamma_r(0.5H - L_w)^2\Big(\frac{tan\beta}{1 - tan\beta tan\omega}\Big) \tag{4.65}$$

The dynamic earth force P_{AE} is applied at the back of the reinforced mass described by the minimum reinforcement length L_{min} and height h. The quantity h can be calculated as:

$$h = H + (L_{min} - L_w)\Big(\frac{tan\beta}{1 - tan\beta tan\omega}\Big) \tag{4.66}$$

For structures with a horizontal backslope ($\beta = 0$) the problem geometry is simplified since h = H.

The horizontal component of dynamic earth force P_{AEH} acting over depth at the back of the reinforced zone is calculated using the following expression:

$$P_{AEH} = P_{AH} + 0.5\Delta P_{dynH} = \frac{k_{AH}\gamma_b h^2}{2} + 0.5\frac{\Delta K_{dynH}\gamma_b h^2}{2} \tag{4.67}$$

Note that only 50% of the dynamic earth force increment, ΔP_{dynH}, acting over height

h is considered in external stability calculations.

The application of the dynamic increment of backfill soil force Δ P_{dynH} differs from the method used by AASHTO/FHWA. AASHTO/FHWA apply Δ P_{dynH} to the back of the inertial zone identified by the dashed line at distance 0.5H behind the wall face in Figure 4.20. For sloped backfills the method used in this document is slightly more conservative but greatly simplifies calculations. For horizontal backfills there is no difference between methods with respect to location of the dynamic force increment. However, AASHTO/FHWA guidelines assume that the interface friction angle at the boundary between the reinforced zone and backfill soil is equal in magnitude to the angle of the constant slope behind the wall crest (i.e. δ=ϕ). However, there is no justification for linking interface friction angle to slope angle. The magnitude of earth pressures for external stability calculations in this document will almost always be less than AASHTO/FHWA values since $\delta = \phi \geq \beta$. In addition, AASHTO/FHWA assumes that ω =0 for walls with $\omega < 10^o$ and this leads to higher earth pressures and hence more conservative static and seismic designs for reinforced SRW structures using their method. The interpretation of Coulomb and Mononobe-Okabe earth pressure theory used in NCMA document provides a seamless transition between the analysis and design of statically loaded structures described in the DMSRW and the methodology for seismic loaded soil retaining wall structures.

4.2.1.1. Base Sliding. The factor of safety against base sliding (FS_{sl}) is expressed by the ratio of resistance horizontal forces to driving horizontal forces. FS_{sl} at the bottom of the reinforced mass (i.e. bottom of the lowermost facing unit and reinforced soil zone) can be expressed as:

$$FS_{sl} = \frac{R_s}{P_{IR} + P_{AH} + 0.5\Delta P_{dynH}} \tag{4.68}$$

The base sliding resistance force, R_s, (Figure 4.20) is calculated as follows: If the reinforced soil (infill) or drainage fill controls:

$$R_s = C_{ds} W_r tan\phi \tag{4.69}$$

with $\phi = \phi_d$ or ϕ_r whichever value has the least magnitude. If the foundation soil controls:

$$R_s = C_{ds}[c_f L_{min} + W_r tan\phi_f] \tag{4.70}$$

Here the quantity C_{ds} is the coefficient of direct sliding and cannot exceed unity. For soil to soil interfaces the value for this parameter can be assumed to be equal to one. For the case of a geosynthetic layer placed at the base of the reinforced soil zone, $C_{ds}<1$ maybe appropriate. The calculated value of FS_{sl} should not be less than 1.1 (Table 4.1).

4.2.1.2. Base Overturning. The factor of safety FS_{ot} against overturning about the toe of the facing column can be expressed as the ratio of the resisting moment M_r and driving moment M_o:

$$FS_{ot} = \frac{M_r}{M_o} \tag{4.71}$$

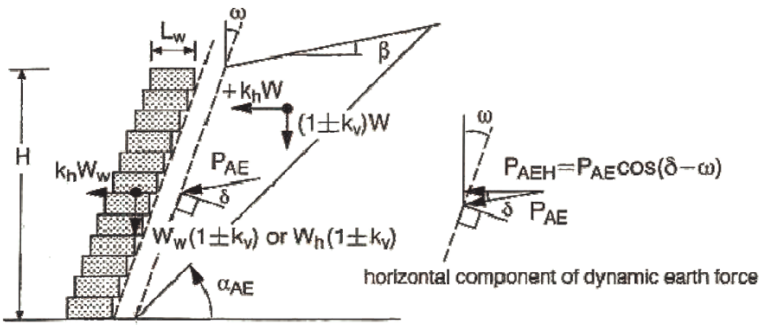

Figure 4.21. Resisting moments for base overturning in external stability calculations for reinforced SRW structures..

The resisting moment, M_r, is given as:

$$M_r = W_w X_w + W_i X_i + W_\beta X_\beta \tag{4.72}$$

where X_w is the horizontal distance from the toe of the wall to the center of gravity of the entire facing column and can be calculated using:

$$X_i = \frac{1}{2}[(N_w - 1)H_w tan\omega] + L_g \tag{4.73}$$

Moment arm quantities X_i and X_β are calculated as follows:

$$X_i = \frac{L_{min} + L_w + Htan\omega}{2} \tag{4.74}$$

$$X_\beta = Htan\omega\frac{1}{3}(L_w + 2L_{min}) \tag{4.75}$$

Then, the driving moment M_o is calculated as:

$$M_o = P_{IR}h_{IR} + P_{AH}\frac{h}{3} + 0.5\Delta P_{dynH}0.6h \tag{4.76}$$

Here:

$$h_{IR}\frac{k_h(ext)W_w\frac{H}{2} + k_h(ext)W_i'\frac{H}{2} + k_h(ext)W_\beta' h_\beta}{P_{IR}} \tag{4.77}$$

$$h_\beta = H + \frac{1}{3}(L_{min} - L_w)tan\beta \tag{4.78}$$

The calculated value of FS_{ot} should not be less than 1.1 (Table 4.1).

4.2.1.3. Bearing Capacity. Conventional bearing capacity analyses are carried out with respect to the base width L of the reinforced (infill) soil mass is assumed to act as a

continuous strip footing and must have sufficient width L to prevent overstressing of the foundation soils that may lead to shear failure of the foundation soils or excessive settlement.

Meyerhof stress distribution approach is utilized to ensure a conservative estimate of applied bearing stress. The effect of eccentricity of the resultant bearing force (net foundation load) (Figure 4.20) is to restrict compressive bearing pressures to an equivalent bearing area B'$_f$ calculated as:

$$B'_f = L_{min} - 2e \tag{4.79}$$

The Meyerhof bearing capacity approach for statically loaded geosynthetic reinforced SRW structures is modified here to include the additional base loading eccentricity developed by the external dynamic force increment ΔP_{dynH} and the inertial force P_{IR}. The factor of safety against bearing capacity failure is expressed as:

$$FS_{bc} = \frac{q_{ult}}{q_a} \tag{4.80}$$

where q_{ult} is the ultimate bearing capacity of the foundation soil and q_a the applied bearing stress at the base of the reinforced soil mass and facing column (composite mass). The magnitude of q_{ult} is calculated as follows:

$$q_{ult} = c_f N_c + \frac{1}{2}\gamma_f B'_f N_f + \gamma_f H_{emb} N_q \tag{4.81}$$

Values of bearing capacity coefficients N_c, N_g and N_q are shown in Table 4.2.

Consistent with the method used in the DMSRW the eccentricity term e can be calculated with respect to the center of the base of the reinforced zone (i.e. at distance $L_{min}/2$ from the toe of the wall) as follows:

$$e = \frac{P_{IR}h_{IR} + P_{AH}\frac{h}{3} + 0.5\Delta P_{dynH}0.6h}{W_r} \tag{4.82}$$

$$\frac{W_w\left(x_w-\frac{L_{min}}{2}\right)-W_i\left(x_i-\frac{L_{min}}{2}\right)-W_x-\left(x_\beta-\frac{L_{min}}{2}\right)}{W_r}$$

The applied bearing capacity stress at the base of the reinforced zone is calculated as:

$$q_a = \frac{W_r}{B'_f} \tag{4.83}$$

The calculated value of FS_{bc} should not be less than 1.5 (Table 4.1).

4.2.2. Internal Stability

4.2.2.1. Reinforcement Loads. The contributory area approach used for the static stability analysis of segmental retaining walls is extended to the dynamic loading case.

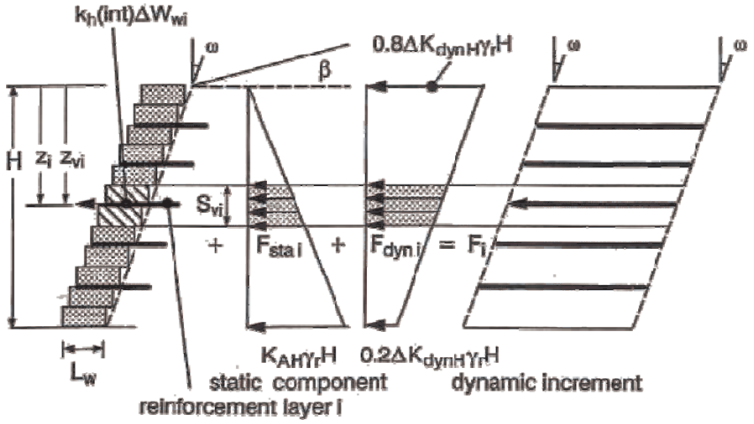

Figure 4.22. Geometry and forces used to calculate reinforcement loads for reinforced SRW structures.

In this method the reinforcement layers are modeled as tie-backs with the tensile force, F_i, in layer i equal to the earth pressure integrated over the contributory area, S_{vi}, at the back of the facing column plus the corresponding wall inertial force increment. Hence:

$$F_i = k_h(int)\Delta W_{wi} + F_{stai} + F_{dyni} \tag{4.84}$$

where, $k_h(int)\Delta W_{wi}$ is the wall inertial force increment, F_{stai} is the static component

Table 4.2. Bearing capacity factors.

ϕ^* ***(degree)***	$\boldsymbol{N_c}$	$\boldsymbol{N_q}$	$\boldsymbol{N_g}$	$\boldsymbol{N_q/N_c}$	$\boldsymbol{tan}\ \phi$
0	5.14	1.00	0.00	0.20	0.00
1	5.38	.09	0.07	0.20	0.02
2	5.63	.20	0.15	0.21	0.03
3	5.90	.31	0.24	0.22	0.05
4	6.19	.43	0.34	0.23	0.07
5	6.49	.57	0.45	0.24	0.09
6	6.81	.72	0.57	0.25	0.11
7	7.16	.88	0.71	0.26	0.12
8	7.53	2.06	0.86	0.27	0.14
9	7.92	2.25	1.03	0.28	0.16
10	8.35	2.47	1.22	0.30	0.18
11	8.80	2.71	1.44	0.31	0.19
12	9.28	2.97	1.69	0.32	0.21
13	9.81	3.26	1.97	0.33	0.23
14	10.37	3.59	2.29	0.35	0.25
15	10.98	3.94	2.65	0.36	0.27
16	11.63	4.34	3.06	0.37	0.29
17	12.34	4.77	3.53	0.39	0.31
18	13.10	5.26	4.07	0.40	0.32
19	13.93	5.80	4.68	0.42	0.34
20	14.83	6.40	5.39	0.43	0.36
21	15.82	7.07	6.20	0.45	0.38
22	16.88	7.82	7.13	0.46	0.40
23	18.05	8.66	8.20	0.48	0.42
24	19.32	9.60	9.44	0.50	0.45
25	20.72	10.66	10.88	0.51	0.47

Table 4.2. Bearing capacity factors.

ϕ^* ***(degree)***	N_c	N_q	N_g	N_q/N_c	$tan\ \phi$
26	22.25	11.85	12.54	0.53	0.49
27	23.94	13.20	14.47	0.55	0.51
28	25.80	14.72	16.72	0.57	0.53
29	27.86	16.44	19.34	0.59	0.55
30	30.14	18.40	22.40	0.61	0.58
31	32.67	20.63	25.99	0.63	0.60
32	35.49	23.18	30.22	0.65	0.62
33	38.64	26.09	35.19	0.68	0.65
34	42.16	29.44	41.06	0.70	0.67
35	46.12	33.30	48.03	0.72	0.70
36	50.59	37.75	56.31	0.75	0.73
37	55.63	42.92	66.19	0.77	0.75
38	61.35	48.93	78.03	0.80	0.78
39	67.87	55.96	92.25	0.32	0.81
40	75.31	64.20	109.41	0.85	0.84
41	83.86	73.90	130.22	0.88	0.87
42	93.71	85.38	155.55	0.91	0.90
43	105.11	99.02	186.54	0.94	0.93
44	118.37	115.31	224.64	0.97	0.97
45	133.88	134.88	271.76	1.01	1.00
46	152.10	158.51	330.35	1.04	1.04
47	173.64	187.21	403.67	1.08	1.07
48	199.26	222.31	496.01	1.12	1.11
49	229.93	265.51	613.16	1.15	1.15
50	266.89	319.07	762.89	1.20	1.19
* Use ϕ_f the phi angle for foundation soils					

of reinforcement load, F_{dyni} is the dynamic component of reinforcement load.

The quantity ΔW_{wi} is the weight of the facing falling with the contributory area S_{vi} of the corresponding reinforcement layer and hence can be calculated as follows:

$$\Delta W_{wi} = S_{vi} L_w \gamma_w \tag{4.85}$$

referring to Figure 4.22:

$$F_{stai} = K_{AH} \gamma_r Z_{vi} S_{vi} \tag{4.86}$$

$$F_{stai} = \left[0.8 - 0.6\frac{Z_{vi}}{H}\right] \Delta K_{dynH} \gamma_r H S_{vi} \tag{4.87}$$

The quantity z_{vi} is the distance from the crest of the wall to the mid-elevation of the contributory area S_{vi}. For constant reinforcement spacings $z_{vi} = z_i$. For non-uniform spacings $z_{vi} \neq z_i$. The contributory area for the topmost reinforcement layer is taken from the wall crest to mid-elevation between the first and second reinforcement layers from the crest. The contributory area for the bottommost layer is taken from the mid-elevation between the bottom layer and the layer immediately above, and the base elevation of the reinforced soil mass. The value of horizontal seismic coefficient (k_h=k_h(int)) used to calculate the wall inertial force increment (k_h(int) Δ W_{wi} in Equation 4.84) and dynamic component of reinforcement load (i.e. Δ K_{dynH} term in Equation 4.87) is determined from Equation 4.88.

$$k_h = \frac{a_h}{g}\left(1.45 - \frac{a_h}{g}\right) \tag{4.88}$$

4.2.2.2. Overstressing of Reinforcement. The dynamic factor of safety, FS_{os}, against over-stressing of reinforcement layer i is given by:

$$FS_{os} = \frac{T_{a(dyn)}}{F_i} \tag{4.89}$$

Here, $T_{a(dyn)}$ is the allowable tensile load for the reinforcement under seismic loading. AASHTO/FHWA guidelines recommend that the allowable strength for seismic loaded structures can be calculated using the same reduction factor approach used for statically loaded structures but with the creep reduction factor RF_{CR}=1. Equivalently, the allowable strength calculated according to the DMSRW for statically loaded structures can be modified according to:

$$T_{a(dyn)} = T_a RF_{CR} \tag{4.90}$$

The calculated value of FS_{os} should not be less that 1.0 (Table 4.1). In other words, $T_{a(dyn)}>F_i$.

4.2.2.3. Reinforcement Anchorage (Pull-out Failure). The reinforcement tensile load Fi must be carried by the reinforcement anchorage length which is located between the internal active failure plane (oriented at a_{ae} from horizontal) and the reinforcement free end (Figure 4.23). A common approach for anchorage capacity design is to use a simple Coulomb-type interface model in which anchorage capacity is taken to be linearly proportional to anchorage length, overburden pressure and soil shear strength.

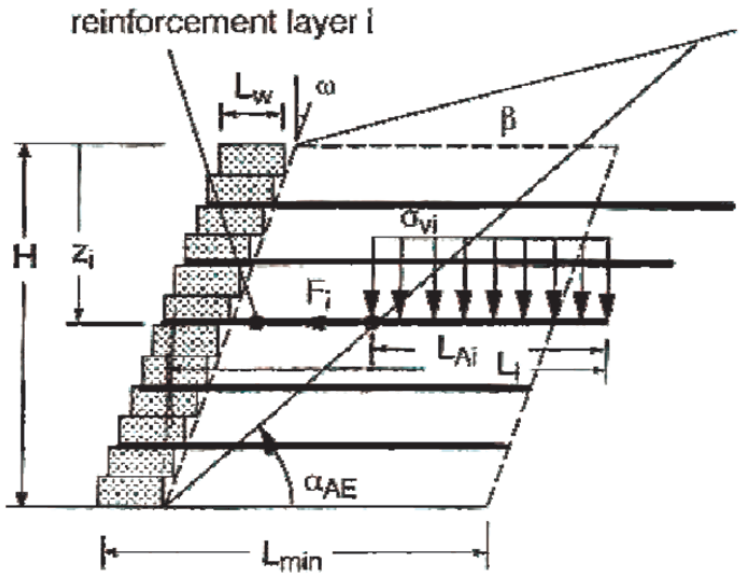

Figure 4.23. Geometry and forces used to calculate anchorage capacity of reinforcement layers in SRW structures.

The anchorage capacity T_{pull} i, corresponding to reinforcement layer i is calculated as follows:

$$T_{pulli} = 2L_{Ai}C_i\sigma_{vi}tan\phi_r \tag{4.91}$$

where; L_{Ai} is the anchorage length for reinforcement layer i, C_i is the coefficient of interaction for pullout, σ_{vi} is the average overburden pressure acting over anchorage length L_{Ai} and ϕ_r is the peak friction angle of reinforced (infill) soil. The anchorage length L_{Ai} can be expressed as:

$$L_{Ai} = L_iL_w + (H - z_i)\left[tan\omega - tan\left(\frac{\pi}{2} - \alpha_{AE}\right)\right] \tag{4.92}$$

Here L_i is the total length of reinforcement layer i taken from the front face of the wall to the soil embedded end of the layer, and α_{AE} is calculated in accordance with Equation 4.22 using ψ=0. The average normal stress acting over the anchorage length

can be calculated using the following expression:

$$\sigma_{vi} = \left[z_i + \left(\frac{H - z_i}{tan\alpha_{AE}} - Htan\omega + \frac{L_{Ai}}{2} \right) tan\beta \right] \tag{4.93}$$

and the factor of safety against pullout failure is expressed as:

$$FS_{po} = \frac{T_{pulli}}{F_i} \tag{4.94}$$

The calculated value of FS_{po} should not be less than 1.1 (Table 4.1).

4.2.2.4. Internal Sliding. The factor of safety against internal sliding FS_{sli} along a reinforcement layer located at depth z below the crest of the wall can be expressed as:

$$FS_{sli} = \frac{R_s(z_i)}{\Delta P_{IR}(z_i) + \Delta P_{AEH}(z_i)} \tag{4.95}$$

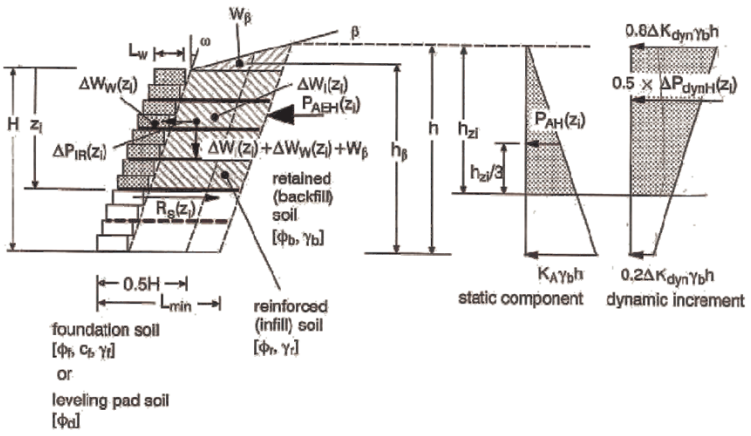

Figure 4.24. Geometry and forces used to calculate internal sliding of reinforcement layers in SRW structures.

The internal force contribution $\Delta P_{IR(zi)}$ is calculated as:

$$\Delta P_{IR}(z_i) = k_h(ext)(\Delta W_w(z_i) + \Delta W_i'(z_i) + \Delta W_\beta') \tag{4.96}$$

The value of k_h(ext) used to calculate the inertial force contribution is determine from k_h=a_c/2g. Quantity Δ W_w (z_i) is the total weight of the facing column above the sliding surface located at depth z_i. Similar to the approach adopted for base sliding, the reduced reinforced zone weight $\Delta W'_i$ (z_i) is calculated using:

$$\Delta W'_i(z_i) = (0.5H - L_w) z_i \gamma_r \tag{4.97}$$

Finally, the reduced reinforced zone weight in the slope above the reinforced mass, W'_β, is calculated using Equation 4.65.

$$\begin{aligned} P_{AEH}(z_i) &= P_{AH}(z_i) + 0.5\Delta P_{dynH}(z_i) \\ &= \frac{K_{AH}\gamma_b h_{zi}^2}{2} + \left[0.8h_{zi} - 0.3\frac{h_{zi}^2}{h}\right]\Delta K_{dynH}\gamma_b h \end{aligned} \tag{4.98}$$

The value of k_h, used to calculate the horizontal component of the dynamic force increment (Δ P_{dynH} (z_i)) is determined from k_h=a_c/2g). The quantity h_{zi} can be calculated as:

$$h_{zi} = z_i + (L_{min} - L_w)\left(\frac{tan\beta}{1 - tan\beta tan\omega}\right) \tag{4.99}$$

For structures with a horizontal backslope (β=0) the problem geometry is simplified since h_{zi}=z_i. The sliding resistance RS(z_i) corresponding to interface i is calculated using:

$$R_s(z_i) = V_u(z_i) + C_{ds}(\Delta W_i(z_i) + \Delta W_\beta) tan\phi_r \tag{4.100}$$

The quantity $V_u(z_i)$ is the peak interface shear capacity between facing column units calculated using:

$$V_u(z_i) = a_u + \Delta W_h(z_i) tan\lambda_r \tag{4.101}$$

The quantity C_{ds} in Equation 4.99 is the coefficient of direct sliding for the soil geosyn-

thetic interface and cannot exceed unity. Quantity Δ W$_i$ (z_i) is calculated as:

$$\Delta W_i(z_i) = (L_{min} - L_w) z_i \gamma_r \tag{4.102}$$

and W$_\beta$ is calculated using Equation 4.62.

Only 50% of the external dynamic earth force increment, Δ P$_{dynH}$ (z_i), acting over the height h$_{zi}$ is considered for internal sliding stability calculations. The calculation of force components P$_{AH}$ (z_i) and Δ W$_i$ (z_i) assumes full mobilization of interface friction between the reinforced soil zone and the retained soil (i.e. δ=ϕ with ϕ equal to the lesser of ϕ_r and ϕ_b). The calculated value of FS$_{sli}$ should not be less than 1.1 (Table 4.1).

4.2.3. Facing Stability

In pseudo-static seismic analysis of the facing stability of reinforced SRW structures, the following potential failure mechanisms must be examined: interface shear failure; overturning; crest toppling; and connection failure (Figure 4.18).

4.2.3.1. Interface Shear. The influence of interface shear transmission on facing column stability can be analyzed by treating the facing column as a beam in which the integrated lateral pressure (i.e. distributed load) must equal the sum of the reactions (forces in reinforcement layers). The calculation of interface shear force under dynamic loading must include the effect of wall facing inertia. The general approach is illustrated in Figure 4.25. The locally maximum interface shear forces will occur at reinforcement elevations.

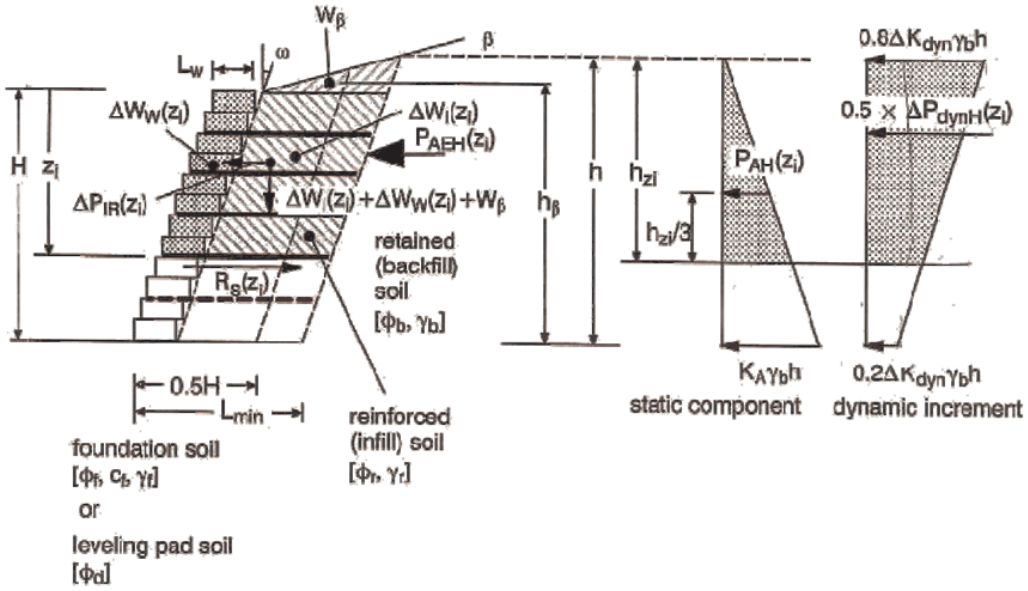

Figure 4.25. Geometry and forces used to calculate interface shear (bulging) and overturning of the facing column for reinforced SRW structures.

The out-of-balance horizontal force S_i transmitted to an interface at depth z_i (corresponding to reinforcement layer i) is the difference in magnitude between the horizontal component of dynamic earth force plus facing column inertia) force and the sum of the horizontal loads carried by the reinforcement layers above the target interface. Hence:

$$S_i(z_i) = k_h(int)\Delta W_w(z_i) + P_{AEH}(z_i) - \sum_{i+1}^{N} F_j \tag{4.103}$$

Here N is the number of reinforcement layers. The horizontal component of dynamic earth force P_{AEH} (z_i) acting over the depth z_i at the back of the facing column is calculated using the following expression;

$$\begin{aligned} P_{AEH}(z_i) &= P_{AH} + \Delta P_{dynH}(z_i) \\ &= \frac{K_{AH}\gamma_r z_i^2}{2} + \left[0.8z_i - 0.3\frac{z_H^2}{H}\right]\Delta K_{dynH}\gamma_r H \end{aligned} \tag{4.104}$$

Coefficients of earth pressure (K_{AH} and Δ K_{dynH}) are calculated using ϕ=ϕ_r and 0 $\leq \delta \leq \phi_r$. Typically is taken as $2\phi_r/3$ for facing stability calculations. Quantity

Δ K_{dynH} in Equation 4.102 is calculated using Equation 4.87. The summation of reinforcement reactions can be calculated using Equation 4.83. The factor of safety against interface shear failure (FS_{sc}) at a reinforcement layer is:

$$FS_{sc} = \frac{V_u(z_i)}{S_i(z_i)} \tag{4.105}$$

where V_u (z_i) is the peak shear capacity of the interface calculated usingEquation 4.99, The selection of interface shear strength parameters should be based on the results of laboratory interface shear data simulating the geosynthetic-modular block interface. The calculated value of FSsc should not be less than 1.1 (Table 4.1).

4.2.3.2. Connection Failure. The dynamic factor of safety, FS_{cs}, against connection failure of the reinforcement layer with the facing column can be expressed as:

$$FS_{cs} = \frac{T_{ci}}{F_i} \tag{4.106}$$

Here, F_i is the tensile load in the reinforcement layer i calculated using Equation 4.83 and T_{ci} is the peak connection capacity for that layer calculated as:

$$T_{ci} = a_{cs} + \Delta W_h(z_i) tan\lambda_s \tag{4.107}$$

The quantity acs is the minimum available peak connection strength in kN/m and λ_{cs} is the apparent peak interface friction angle describing the connection failure envelope (degrees) corresponding to the range of normal weight over which Δ W_h(z_i) applies. The calculated value of FScs should not be less than 1.1 (Table 4.1).

4.2.3.3. Local Overturning. The distribution of internal moments at interface elevations can also be calculated using the beam analog described in Section 4.2.3.1 for interface shear stability calculations. Internal moments that cause net outward moment at the toe of a facing unit, provide a possible failure mechanism for which an adequate factor of safety should be checked. Local peak destabilizing moments will

occur at reinforcement elevations.

The factor of safety FS_{otl} against local overturning about the toe of the facing column at depth z_i below the crest of the wall can be expressed as the ratio of the resisting moments to driving moments:

$$FS_{otl} = \frac{M_r(z_i) + \sum_{i+1}^{N} T_{cj} x y_i}{M_o(z_i)} \tag{4.108}$$

The resisting moment M_r (z_i) due to the facing column is calculated using:

$$M_r(z_i) = \Delta W_h(z) \Delta X_h(z) \tag{4.109}$$

where:

$$\Delta X_h = \frac{1}{2}[(N_z - 1) H_W tan\omega] + L_g \tag{4.110}$$

and the driving moment due to earth forces, $M_o(z_i)$, is calculated using:

$$\begin{aligned} M_o(z_i) &= k_h \Delta W(z_i) \frac{z_i}{2} + \frac{P_{AH}(z_i) z_i}{3} + \Delta P_{dynH}(z_i) y_{dyn}(z_i) \\ &= k_h \Delta W(z_i) + \frac{K_{AH} \gamma_b z^3}{6} \left[\left(0.8 z_i - 0.3 \frac{z_i^2}{H} \right) \Delta K_{dynH} \gamma_b H \right] y_{dyn}(z) \end{aligned} \tag{4.111}$$

where:

$$y_{dyn}(z_i) = \frac{0.4 H Z_i - 0.1 z_i^2}{0.8 H - 0.3 z_i} \tag{4.112}$$

The value of k_h used in this moment calculation is based on the value from the equation k_h=(a_h/g)(1.45-a_h/g)). The summation with T_{cj} X y_j terms in Equation 4.107 denotes the resisting moment due to the peak connection capacities of reinforcement layers and their corresponding moment arms from the target point of rotation. The calculated value of FSotl should not be less than 1.1 (Table 4.1).

4.2.3.4. Crest Toppling. Local (crest) toppling refers to the overturning of the top unreinforced portion of the facing column (Figure 4.18). This analysis is identical to that described in Section 4.2.3.3 for conventional gravity structures but using Equation 4.88. The critical portion of the facing column is taken as the height of wall starting at the elevation of the topmost layer of reinforcement. The calculated value of FS_{otc} should not be less than 1.1 (Table 4.1).

4.3. Simplified Design Rules For Tiered Walls

Tiered walls are often used with an offset distance between adjacent tiers due to its advantage which is the aesthetics (beauty and artistic). Leschinsky and Han (2004) mentioned that the tensile strength in the reinforcement increases rapidly with increasing wall height in the current design of geosynthetic reinforced soil walls. So, the economics also can be one of the advantages of geosynthetic reinforced soil retaining walls for greater height. However, a rational design approach for tiered geosynthetic reinforced soil walls that accurately predicts wall performance is derived without theoretical or experimental bases, while FHWA guidelines limited to a maximum of two tiered walls, denoted as superimposed wall hereafter.

For superimposed geosynthetics reinforced earth structures, FHWA guidelines, "Mechanically stabilized earth walls and reinforced soil slopes design and construction guidelines" (FHWA-NHI-00-43, 2009), is mainly for design of two tier geosynthetics reinforced earth walls. An offset distance D is defined between the faces of the upper tier and lower tier walls. The design of tiered geosynthetic reinforced soil walls is using simplified design rules for locating the internal failure plane, for internal stability as shown in Figure 4.26. In the FHWA design guideline, maximum tensile force lines are defined as internal failure surfaces in relation to the offset distance.

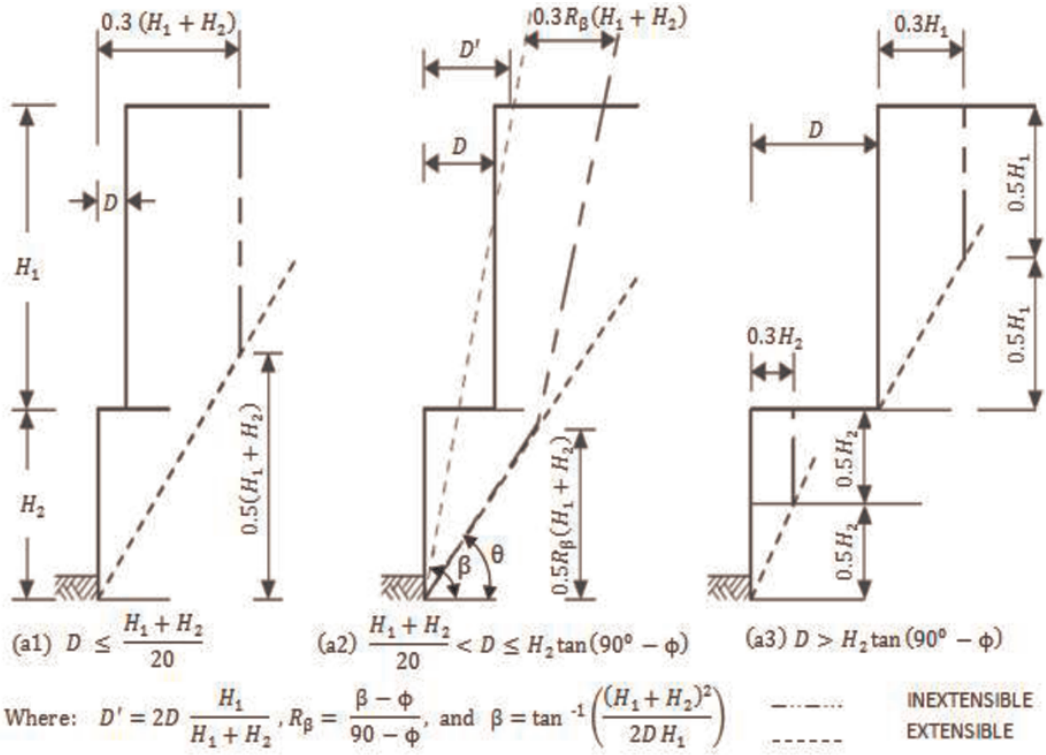

Figure 4.26. Maximum tension lines assumed in FHWA Guidelines (2009).

For superimposed geosynthetics reinforced earth structures, FHWA guidelines, "Mechanically stabilized earth walls and reinforced soil slopes design and construction guidelines" (FHWA-NHI-00-43, 2009), is mainly for design of two tier geosynthetics reinforced earth walls. An offset distance D is defined between the faces of the upper tier and lower tier walls. The design of tiered geosynthetic reinforced soil walls is using simplified design rules for locating the internal failure plane, for internal stability as shown in Figure 4.26. In the FHWA design guideline, maximum tensile force lines are defined as internal failure surfaces in relation to the offset distance.

For preliminary design, if the offset distance is smaller than $(H_1+H_2)/20$ as shown in Figure 4.26, where H_1 and H_2 is the height of the upper and lower tier, respectively, the wall should be designed as a single wall of height $H = H_1 + H_2$. The failure surface does not fundamentally change and it is simply adjusted laterally by the offset distance D.

In FHWA (2009) guidelines, if the offset distance is between $(H_1+H_2)/20$ and $H_2\tan(45\text{-}\phi/2)$, intermediate offset distances, the minimum values for reinforcement length for the top-tier and the lower tier walls should be greater than $0.7H_1$ and $0.6(H_1+H_2)$, respectively. The location of the failure surface is varied according to the offset distance, as shown in Figure 4.26.

If the offset distance is greater than $H_2\tan(45\text{-}\phi/2)$ where ϕ is the friction angle of the reinforced fill, the two tiers are designed independently with the failure surface shown in Figure 4.26. If the offset distance is greater than $H_2\tan(90\text{-}\phi)$, the walls are not considered as a superimposed wall but two independent walls. It is assumed that the upper wall is not taken as an equivalent uniform surcharge affecting the lower wall (no interaction).

It should be stated that although FHWA guidelines deal with superimposed wall, the approach is derived without theoretical or experimental bases. In reality, despite the lack of design guidelines for tiered geosynthetic reinforced earth wall, walls with even more than five tiers are successfully and economically constructed. Hence, there is a clear need for a rational geotechnical engineering approach to deal with the design of realistic tiered wall systems.

4.4. Previous Research Studies Related to Reinforced Soil Retaining Walls

The first commercial proprietary mechanically stabilized earth (MSE) wall system was introduced in the U.S. in the 1960s. It utilized metallic strips to reinforce the soil and precast concrete panels that retain the soil at the face of the wall. Its use worldwide has increased dramatically since the 1970s, mainly due to its economics and aesthetics. Competitive wall systems using welded wire grids were introduced in the mid 1970s. Geosynthetic reinforced walls were introduced in the 1980s. In the 1990s, the use of geosynthetic reinforced walls increased dramatically by the introduction of segmental retaining walls (SRW) (Leshchinsky and Han, 2004).

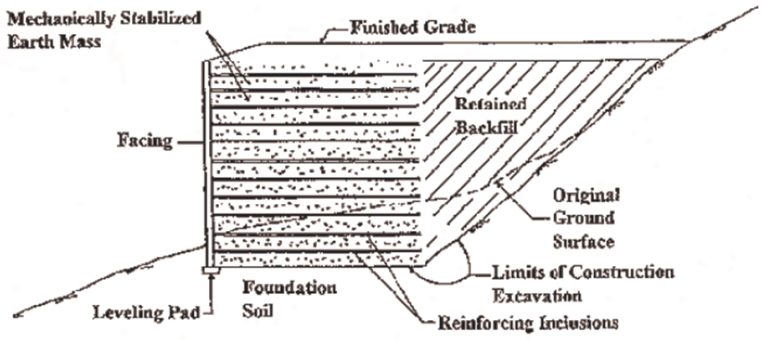

Figure 4.27. A typical MSE wall-cross sectional view.

Scarborough (2004) presented two case histories of mechanically stabilized earth (MSE) retaining walls. Both of the walls were constructed using geosynthetic reinforcement within clayey soil backfill. One of the walls failed and the other experienced large deformation, but remain in service. The author argued that, the catastrophic failure of Wall "A" was most likely due to poor drainage. Water pressure was allowed to build up behind the wall facing due to a lack of adequate drainage resulting wall failure. Other contributing factors were inconsistent compaction of fill soils, increased height of wall, and the use of clayey backfill within the reinforced zone. The serviceability failures of wall "B" was due to inadequate geogrid reinforcements. This can be directly linked to not performing global stability analysis during the design of Wall "B". The contributing factor may be the use of clayey backfill within the reinforced zone. The author provided the following recommendations to prevent this type of failure in future: to pay more attention to important design considerations, such as, drainage, use of local construction materials, global stability analysis and ensure proper control during the construction phase.

Budge *et al.*, (2006) explained the process used to calibrate PLAXIS software model using the vertical deformations measured during the construction of a MSE wall located at Salt Lake City, Utah. The wall was constructed on a soft clay foundation, and instrumentation was placed in this material to monitor foundation response. Several photographs showing the wall during and after construction are shown in Figure 4.28. To understand the response of the wall, extensive instrumentation was also placed within the wall. During the course of construction, measurements were taken to moni-

tor vertical and horizontal deformations within the wall and in the foundation material. Stresses in the wall reinforcement, and increase in vertical stresses within the wall are also measured as construction progressed. Constant rate of strain (CRS) consolidation tests and the triaxial tests were conducted to determine required strength and stiffness parameters for the soils. With the appropriate wall geometry and estimated soil properties, a model was developed using PLAXIS. The position of horizontal inclinometers and extensometer casings are also provided (Figure 4.29).

Figure 4.28. Photographs of the MSE wall constructed at 3600 South and I-15 (Budge *et al.*, 2006).

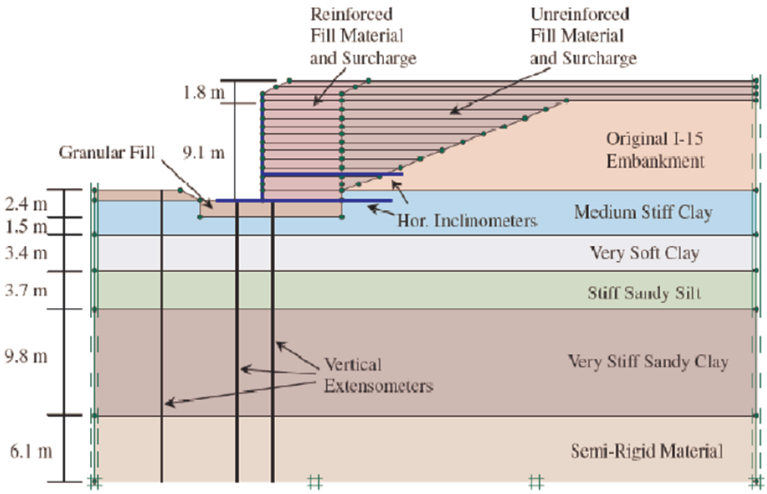

Figure 4.29. Soil profile and selected instrumentation for MSE wall on I-15 (Budge *et al.*, 2006).

Once the MSE wall was modeled using PLAXIS, the deformations measured in the vertical extensometer within the wall footprint were compared to vertical deformations obtained using the numerical modeling. Figure 4.30 shows the comparison of the

PLAXIS model results and the measured vertical extensometer deformation plotted with respect to a reference datum elevation. Figure 4.31 shows the PLAXIS model results compared to the measured horizontal inclinometer readings at the end of primary consolidation. The simulated vertical settlement in the model matches quite well with the measured data for the wall. The effect of the very soft clay layer is evident in the significant deformation between reference elevations 96 m and 92 m, which were the upper and lower bounds of the soft clay. Figure 4.31 also shows a nice calibration for the vertical movement along the lower horizontal inclinometer. The horizontal inclinometer comparison seems to confirm that the model is able to replicate the measured foundation response.

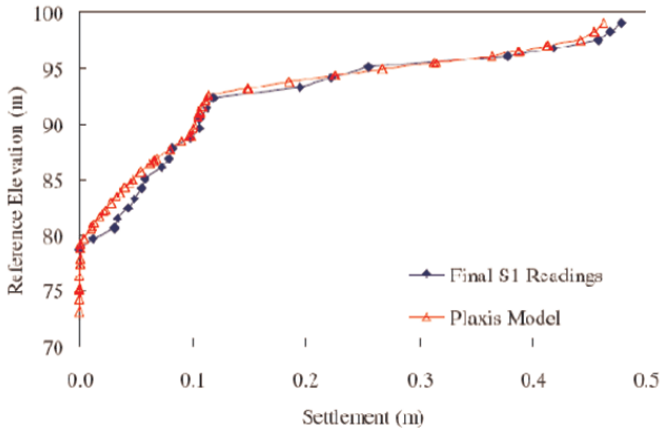

Figure 4.30. Comparison of vertical extensometer data to PLAXIS model data (Budge *et al.*, 2006).

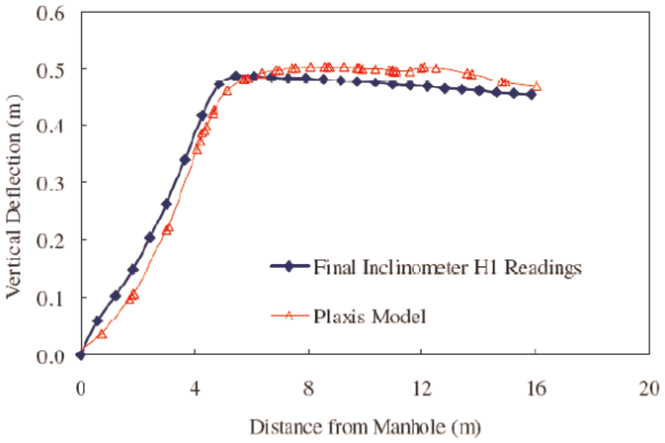

Figure 4.31. Comparison of horizontal inclinometer data to PLAXIS model data (Budge *et al.*, 2006).

Han and Leshchinsky (2004) used limit equilibrium and continuum mechanics-based numerical methods to investigate the stability of MSE walls. For LE analysis the Bishop option in RESSA (2.0) software, developed by ADAMA Engineering (2002) was used. The finite difference program (FLAC 2D Version 4.0) which is based on continuum mechanics, was adopted in their study for numerical analysis. The result showed a difference in the location of the critical slip surface predicted by the LE method and the numerical method. The factor of safety computed by the LE and the numerical method is almost same. Since the factor of safety is the key to designing MSE walls in terms of stability, properly adopted LE approach can be used to fulfill the purpose. However, progressive failure of MSE wall cannot be simulated using LE method.

Armour *et al.*, (2004) presented a case history of the failure and rehabilitation of a 25 year old mechanically stabilized earth (MSE) bridge abutment and approach retaining walls in Soda Springs, Idaho. This MSE bridge abutment was constructed in 1978. But unfortunately, after 24 years of construction, in the summer 2002, approximately six of the precast concrete facing panels "popped out" in a localized area of one of the MSE earth retaining walls supporting the bridge approaches. The cause of failure was corrosion of the galvanized steel soil reinforcing strips at the panel connection to a point where the lateral earth pressures exceeded the connections remaining capacity (Figure 4.32). Some of the remedial measures were installing horizontal drilled and grouted crosstie ground anchors in the approach walls, anchored soldier piles at the abutments and a reinforced shotcrete facing structurally attached to the existing MSE facing panels. A class one corrosion protection system was utilized for all of the rock anchors and crossties. Each strand was coated with a corrosion inhibitor and then encapsulating each stands in a plastic shell. To complete the structure rehabilitation a thick reinforced shotcrete wall was designed to span between the crossties and rock anchors. The corrosive nature of the fill material should be closely monitored to prevent failure to all future projects of this type.

Figure 4.32. Corroded metallic soil reinforcements (Armour, 2004).

San *et al.*, (1994) presented the comparisons of potential failure surface and the maximum tensile force developed in the geosynthetic reinforcement layers between finite element (FE) method and limit equilibrium (LE) method. First, reinforced slopes with dense and loose backfill, for three slope inclinations (75, 60 and 45 degree) were analyzed by the LE analysis. The analysis was conducted using STRATASLOPE, a LE slope stability analysis computer code. The backfill material properties correspond to data from triaxial tests, but the co-efficient of earth pressure (K_0) was chosen so that the LE result of one arbitrary slope inclination would fit the FE result. Then using the same parameters, FE analysis for other slopes was performed. The FE analysis was performed utilizing Duncan and Chang model. The critical lengths of the reinforced obtained from LE analysis for a safety factor of one, were used as an input in the FE analysis. Finally, the maximum reinforcement tensile force and the failure pattern of the reinforced slopes obtained from both LE and FE analysis were compared. The results were almost identical in term of both location of critical slip surfaces and required strength of reinforcement. So, using a consistent value of K0, the results of FE analysis agreed reasonably well with LE results.

Narejo and Ramsey (2001) emphasized hydrologic design issues, to be the major

cause of MSE wall failure. According to the authors, a comprehensive drainage and filtration plan should address the drainage at the top of a wall, and drainage and filtration at the front. The cost and benefit analysis was also conducted. The total cost of a drainage and filtration system for a wall included design, material and installation cost. The design of the filtration and drainage system was assumed to add a cost of $1.00/m^2$ of the wall face. The choice of drainage and filtration system, and materials to be used, will be site-specific. "Flowing" out of blocks of MSE walls can be prevented by using a filter geotextile, i.e. nonwoven needle-punched geotextile at the back of the blocks. The high benefit/cost ratio suggested that a geosynthetic filtration and drainage system should be considered for all MSE walls.

Narejo and Ramsey (2001) showed some of the common drainage schemes utilized at the top of a typical MSE wall (Figure 4.33). Runoff water at the top may be drained towards the face of a wall as shown in Figure 4.33 (a. lined ditch directly behind the blocks) and Figure 4.33 (b.low-permeability layer to catch infiltrating water). Alternatively, runoff water may be collected and discharged by a drainage pipe installed at suitable intervals along the wall as shown in Figure 4.33 (c. drainage pipe at suitable intervals along the wall). Figure 4.33 (d. drainage away from wall face) shows another scheme in which runoff water is drained away from the wall face. In Figure 4.33 (b. low-permeability layer to catch infiltrating water), a second line of defense against any infiltrating water is provided by a geomembrane or geosynthetic clay liner (GCL) used along with a geotextile-wrapped pipe. The drainage ditch shown in Figure 4.33 (a. lined ditch directly behind the blocks), Figure 4.33 (b. low-permeability layer to catch infiltrating water) and Figure 4.33 (d. drainage away from wall face) should be lined with a geomembrane, GCL, clay or a combination thereof in order to prevent infiltration. In certain cases, especially in built-up areas, a layer of asphalt may be used as a surfacing. Suitable discharge points should be located along the drainage ditch to minimize travel paths and excessive accumulation of surface water. The water may be discharged in a storm water drain if one is located close to the wall. It is the authors opinion that the alternatives shown in Figure 4.33 (a. lined ditch directly behind the blocks) and Figure 4.33 (c. drainage pipe at suitable intervals along the wall) should be used only if no other option is available. If water is to be drained towards the face

of the wall, then the schematic shown in Figure 4.33 (b. low-permeability layer to catch infiltrating water) should be used. If a drainage pipe is to be used then it should, preferably, be located outside the reinforced zone. If allowed by the site topography, the schematic shown in Figure 4.33 (d. drainage away from wall face) has the least risk associated with it and is the most economical to implement.

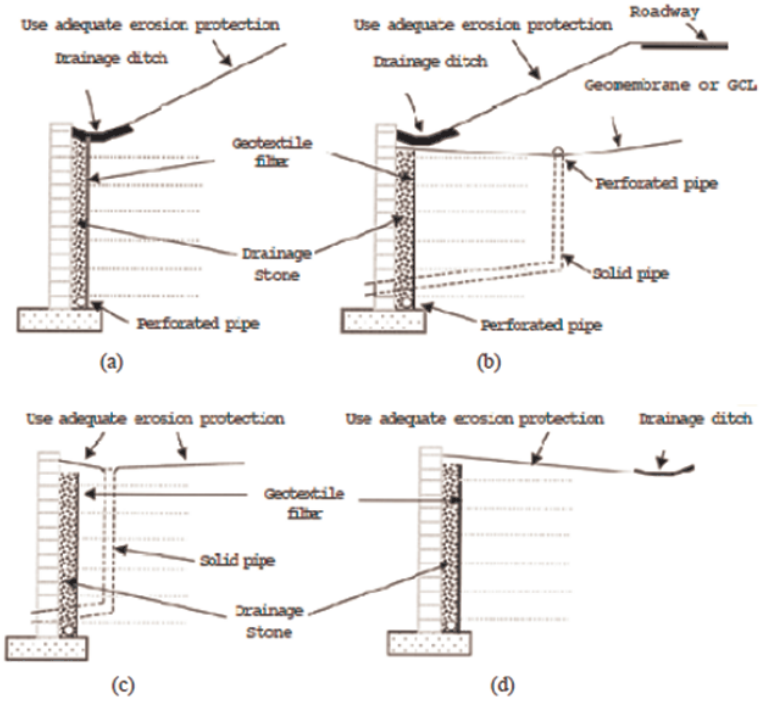

Figure 4.33. Drainage of run-off water at the top of a MSE wall using: (a) lined ditch directly behind the blocks; (b) low-permeability layer to catch infiltrating water; (c) drainage pipe at suitable intervals along the wall; (d) drainage away from wall face (Narejo and Ramsey, 2001).

Figure 4.34 (a. chimney and bottom drains) and Figure 4.34 (b. horizontal drains) show two alternative drainage schemes at the back of a wall currently being used by the industry. In Figure 4.34, (a. chimney and bottom drains) a combination of chimney drain and bottom drain is utilized, whereas Figure 4.34 (b. horizontal drains) shows horizontal drainage layers placed within the reinforced zone. The alternative shown in Figure 4.34 (b. horizontal drains) is used where seepage water is expected in the reinforced zone or where horizontal drains are provided in addition to the chimney drain shown in Figure 4.34 (a. chimney and bottom drains). There is currently

much controversy regarding the effectiveness of the schematic shown in Figure 4.34 (b. horizontal drains). Further testing and research is needed in this area to better understand the mechanism. In both cases, the intercepted water should be discharged at the face of the wall by one or more solid pipes located at suitable intervals along the wall (Narejo and Ramsey, 2001).

In simple situations, all that may be required is a nonwoven needle-punched geotextile. Figure 4.35 shows a wall; where the reinforced soil is "flowing" out of the blocks as a result of water infiltrating from the top of the wall. Using a filter geotextile at the back of the blocks could have prevented this problem (Narejo and Ramsey, 2001).

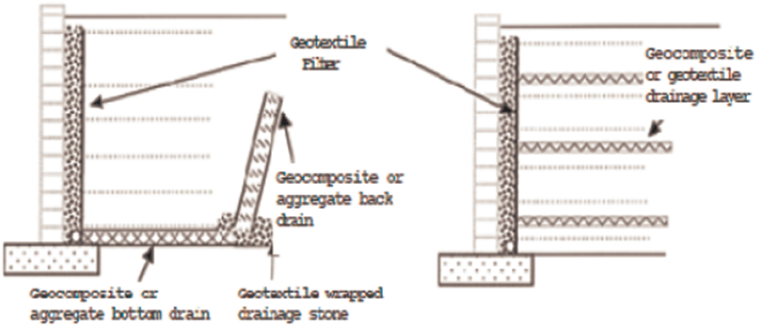

Figure 4.34. Drainage alternatives for seepage and infiltrating water: (a) chimney and bottom drains; (b) horizontal drains (Narejo and Ramsey, 2001).

Figure 4.35. An example of reinforced soil flowing from block due to water infiltrating at the top of a wall (Narejo and Ramsey, 2001).

Retaining walls narrower than the walls in design guidelines are referred as "Narrow" retaining walls. Yang and Liu (2007) presented finite element analysis of earth pressure in narrow retaining walls for both at-rest and active conditions. The predicted data showed a favorable agreement with measured data from centrifuge tests. The result showed that the earth pressure decreases in the case of narrow walls for both at-rest and active conditions. This happens due to arching effects and boundary constraint of narrow walls. According to the authors, earth pressure theories and design guidelines based on conventional MSE wall is somewhat overly conservative and uneconomical when applying to the design of narrow walls. A reconsideration and revision of design guidelines specifically for narrow MSE walls was conducted in their study. The calculated earth pressure profiles were compared to the FHWA design guidelines and then a new design method modified from FHWA design guidelines was described by a practical example. The new design method recommended the use of shorter and weaker reinforcement in narrow walls, when the wall was not slender, that is when the internal stability is the main mode of failure. But in case of slender wall ($L/H<0.3$), the failure mode transforms from internal failure to external failure. Lawson and Yee (2005) suggested attaching the reinforcement to anchors and nails inserted into an existing stable wall or stable rock to ensure the external stability and to dissipate the residual tension at the rear of reinforcement. However, this method may rack the stability of existing stable walls and create potential weak interfaces at stable wall faces. The authors recommended an alternative option. Their suggestion was to extend the upper reinforcements over the top of an existing stable wall. If the fill is too narrow, cast in place concrete is a good alternative.

Chalermyanont and Benson (2005) used a two-phase approach to develop a reliability sbased design (RBD) method for external stability of mechanically stabilized earth (MSE) walls. In the first phase, a parametric study was done by using Monte Carlo simulation to identify parameters that affect the probability of external failure of MSE walls. Three modes of failure were considered here. They are: sliding, overturning, and bearing capacity. External stability was assessed by treating the reinforced soil as a rigid mass using the same procedures employed for conventional gravity-type wall systems. Results from the parametric study indicated that the mean and coeffi-

cient of variation of the backfill friction angle are significant for sliding, the mean and coefficient of variation of the friction angle of the backfill and coefficient of variation of the unit weight of the backfill are significant for overturning, and the mean and coefficient of variation of the friction angle of the foundation soil and the mean of the backfill friction angle are significant for bearing capacity. In the second phase, a series of additional simulations were conducted where the significant parameters identified in the parametric study were varied over a broad range. Results of these simulations were used to develop a set of RBD charts for external stability of MSE walls. Comparison of the required reinforcement lengths indicated that similar reinforcement lengths were obtained using RBD and conventional methods and that the inherent probability of external failure in conventional deterministic design was ≤ 0.001. This probability of external failure was similar to inherent probability of failure reported by other investigators for similar geotechnical structures. Parameters used in calculating external stability of an MSE wall were the wall height (H), length of reinforced soil mass (L, equals the reinforcement length), backfill friction angle (ϕ), backfill unit weight (γ), friction angle of the foundation soil (ϕ_f), and unit weight of the foundation soil (γ_f). Normal distributions, defined by their mean (μ) and coefficient of variation (COV), were used to describe the friction angle and unit weight of the backfill and the foundation soil. The wall height was varied between 3 to 9 m, and the distance from the wall facing to the back of the retained soil was set at 10 m to be consistent with the MSE wall used in Chalermyanont and Benson (2004). The backfill and the retained soil were assumed to be the same, to be cohesionless, and to have a mean friction angle ($\mu\phi$) ranging from 25^o to 40^o and a mean unit weight ($\mu\gamma$) ranging from 16 to 21 kN/m^3. The foundation soil was assumed to be cohesionless and to have a mean friction angle ($\mu\phi_f$) ranging from 25^o to 45^o and a mean unit weight ($\mu\gamma_f$) ranging from 16 to 21 kN/m^3. Factors of safety corresponding to sliding, overturning, and bearing capacity modes were computed using classical analyses for gravity-type wall systems (i.e., the MSE wall was treated as a rigid mass subjected to body forces and active thrust).

Chalermyanont and Benson (2005) developed a technique to calculate the system probability of failure or system reliability of MSE walls. The system probability of failure is the sum of the probabilities of failure corresponding to the four common modes

of failure: slope stability, sliding, overturning and bearing capacity. The reliability is the complement of the system probability of failure. Probability of internal failure is obtained from analysis of MSE walls using design charts. Probabilities for each external failure mode are calculated using a mean factor of safety computed with conventional design equations and mean values for the soil properties as input, and a standard deviation of the factor of safety computed using an empirical equation. The analysis showed that the probability of failure typically is smaller than 0.0003, which is approximately one order of magnitude lower than the failure rate (0.01 to 0.001) for similar type of structures.

Chen *et al.*, (2007) described a successful failure analysis to determine the causes of loss of backfill sand from a mechanically stabilized earth (MSE) wall, and cracks on the concrete approach slabs on top of it. The cracks on the approach slabs may be related to the excessive loss of backfill from behind the MSE walls, and that the embankment structure may be unsafe due to potential voids under the concrete slab. Several cubic meters of sugar sand had washed out of the wall and deposited adjacent to the paneled walls. A series of destructive and nondestructive tests were conducted to determine the causes of the problems. It was found that the cracking of the approach slab and the loss of backfill were unrelated. The loss of sand is usually associated with significant amounts of water that can enter the embankment through joints, ruptured drainage pipes, approach slabs, or in the vicinity of bridge abutments. As water enters the top of the wall in any appreciable quantity, it will seek a path out through any breach in the filter fabric covering the wall panels. Once this process begins, piping will occur, carrying out the fine sand backfill with the water. To achieve these goals, some important tests were performed. They are: i) Coring- to determine the concrete material characteristics; ii) Ground penetration radar (GPR)- to determine the locations and extent of voids under the slab; i) Impulse response (IR)- to determine the locations and extent of voids behind the wall; iv) Dynamic cone penetrometer (DCP)- to verify the voids and their extent; and v) Video survey- to determine the condition of the drainage system in the embankment structure.

It was suspected that the source of the water that was causing the seepage of

embankment sand was a ruptured pipe within the embankment. The main cause of the loss of sand was attributed to the ruptured drainage pipe (As shown in Figure 4.36). The water was eroding and transporting the fine sand through the wall panels where the geotextile filter ruptured. Grouts were used to repair areas where the geotextile filter was breached. This repair was not effective, as the grout could not resist the water pressure.

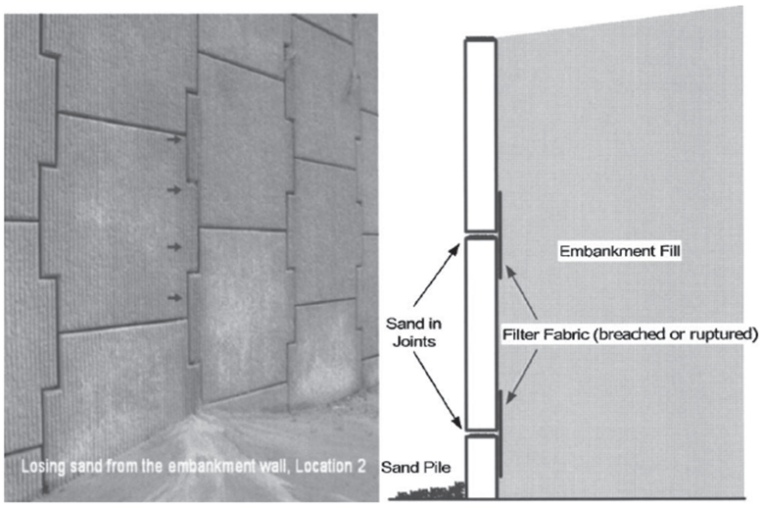

Figure 4.36. Water carried sand through breached or ruptured filter fabric (Chen *et al.*, 2007).

Although there may be other reasons (e.g., high pouring temperature) that caused the cracks, aggregate is one of the main contributing factors to cracking. The southbound and northbound approach slabs were constructed with similar designs, but at different times. Apparently siliceous gravel was substituted on the southbound approach slabs only. The increased thermal expansion/contraction was therefore not adequately accommodated, leading the writers to believe it is a primary cause of the cracking. It is believed that the cracks occurred shortly after placement (e.g., the first month after construction) due to temperature variation. The spilling probably occurred gradually as pavement aged. The probability of the cracks being caused by the loss of backfill is low. It is just a coincidence that the cracks on the bridge approach slabs occurred where there is sand loss. A close inspection of the MSE wall revealed a 50 mm open gap between the riprap and the sidewall, as shown in Figure 4.37. District personnel indicated that the settlement of the riprap shortly after construction caused

the riprap joint to open. It was also observed that the water drained from the bridge deck directly fell on the riprap joint, as shown in Figure 4.38. Because of the wide opening of this particular joint, water could easily enter the embankment. The water then carried the sand out wherever the geotextile filters were breached. Water was also observed flowing out of this joint when the drain pipe was flushed. IR tests were carried out on the face of the wall to quantify the extent of the damage to the wall (Chen *et al.*, 2007).

Kim and Bilgin (2007) had studied the effect of concrete key size for varying reinforcement lengths and foundation soil friction angles. Numerical analyses were performed using PLAXIS. The results indicated that longer key lengths result in decreased wall deformations. The effect of the longer key lengths in reducing wall deformations was more significant for the walls with shorter reinforcement lengths and for the walls placed over weaker soils. A 10 m-high MSE wall was studied and parametric study was performed to investigate the effect of concrete key size on the behavior of MSE walls. Overall geometry of the model analyzed and the details of the MSE wall are shown in Figure 4.39.

Figure 4.37. Wide opening between riprap joint and sidewall permits water to enter riprap. Water carries sand through breached or rupture filter fabric (Chen *et al.*, 2007).

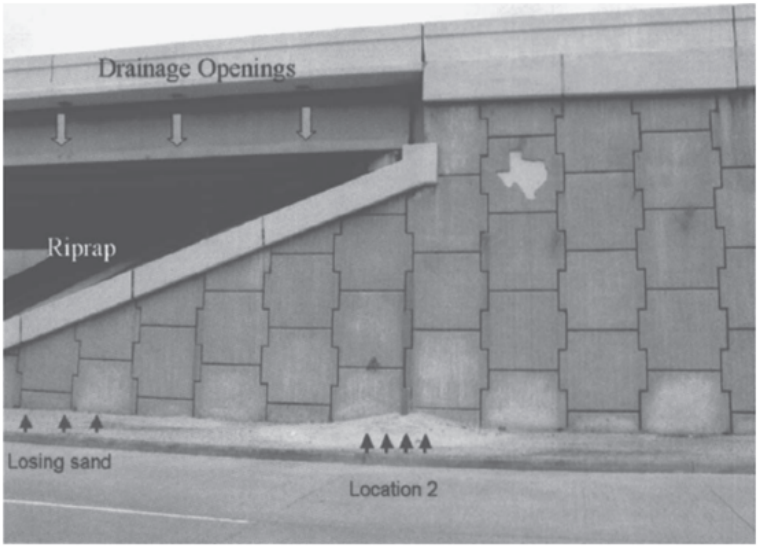

Figure 4.38. Drainage opening on bridge deck that permits water to fall straight through riprap joint (Chen *et al.*, 2007).

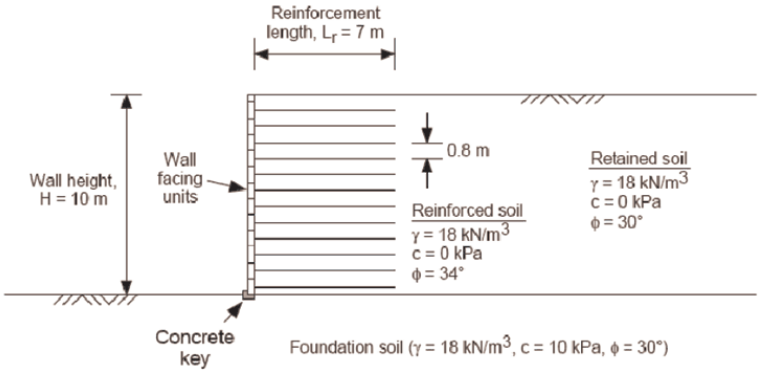

Figure 4.39. Baseline model of MSE wall for numerical analysis (Kim and Bilgin, 2007).

PLAXIS was chosen to perform the numerical analysis. The finite element modeling comprised of two-dimensional plane strain analysis. Finite elements used were triangular elements with 15-nodes. The finite element model mesh consisted of approximately 620 elements and 5,500 nodes. Due to the stress concentration in and around the wall, a finer mesh used in these areas and mesh became coarser in the zones away from the wall. The loading was simulated by adding soil in layers. The thickness of the soil lifts was 0.8 m, equal to the vertical spacing of reinforcement and the facing panel height. A total unit weight, $\gamma = 18$ kN/m^3 and secant elastic modulus at 50%

mobilized strength level, E50 = 50,000 kPa were used for all soil materials modeled; reinforced, retained, and foundation soils. The soil friction angle, $\phi = 34^o$ and 30^o used for the reinforced and retained soils, respectively. The foundation soil had internal friction angle, $\phi_{sub} = 30^o$ and cohesion, c = 10 kPa for the baseline model and ϕ_{sub} of 35^o and 40^o were also studied for parametric study. Subsurface soil conditions were assumed to be composed of one uniform soil layer. The effect of concrete key length on the horizontal wall deformations for varying reinforcement lengths and foundation soil friction angle is shown in Figure 4.40. Each curve in the figure represents the final deformed shape of wall face at the end of construction for varying key length, L_k, reinforcement length, L_r, and ϕ_{sub} values. All the cases presented in Figure 4.40 indicate that as the key length increases the wall deformations decrease regardless of the reinforcement length and the foundation soil strength. The effect of the concrete key on maximum wall deformations as a function of varying reinforcement lengths and foundation soil strengths is shown in Figure 4.41. The figure shows that the concrete key can reduce maximum wall deformations significantly, especially for the walls with shorter reinforcement.

Dov Leshchinsky and Jie Han (2004) investigated the stability of multi tiered reinforced SRWs by two independent types of analysis: i) Limiting Equilibrium (LE) and ii) Continuum mechanics. These two methods show nearly the same factor of safety against collapse of the MSE wall. This research work also study the effect of some important parameters on MSE Wall failure. They study the effect of offset distance, reinforced length and stiffness, fill quality, foundation soil, water, surcharge and number of tiers. The effect of each parameter was investigated by changing its value from the baseline case while keeping all other parameters unchanged. Then the FS was computed for each individual case by using FLAC and RESSA. The outcomes are almost identical. From this study, they identify some cause of MSE wall failure, such as: small offset distance, higher height of MSE Wall, low quality fill soil and insufficient reinforcement length. A sudden draw down of water may also greatly decrease the overall stability of wall. Bearing or deep seated failure could control the failure if, the foundation soil is weak. The study also provides some remedial measures to prevent failure from these causes. They came up with some graphical

charts which are useful for making a balanced relation between height of MSE wall, offset distance and reinforcement length. Again by using high quality fill soil and by improving foundation soil; the FS against failure can be increased.

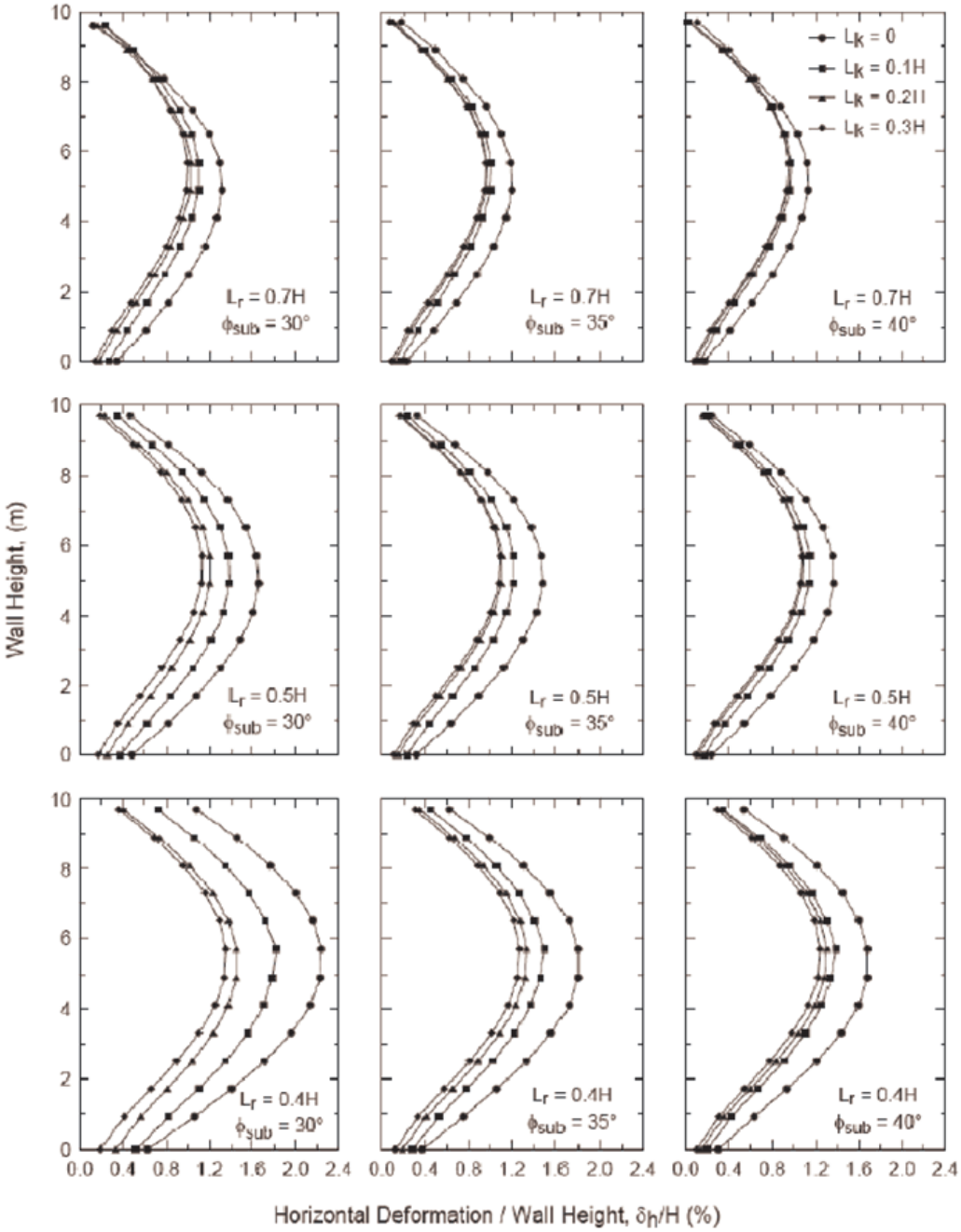

Figure 4.40. Effect of concrete key length on wall deformations (Kim and Bilgin, 2007).

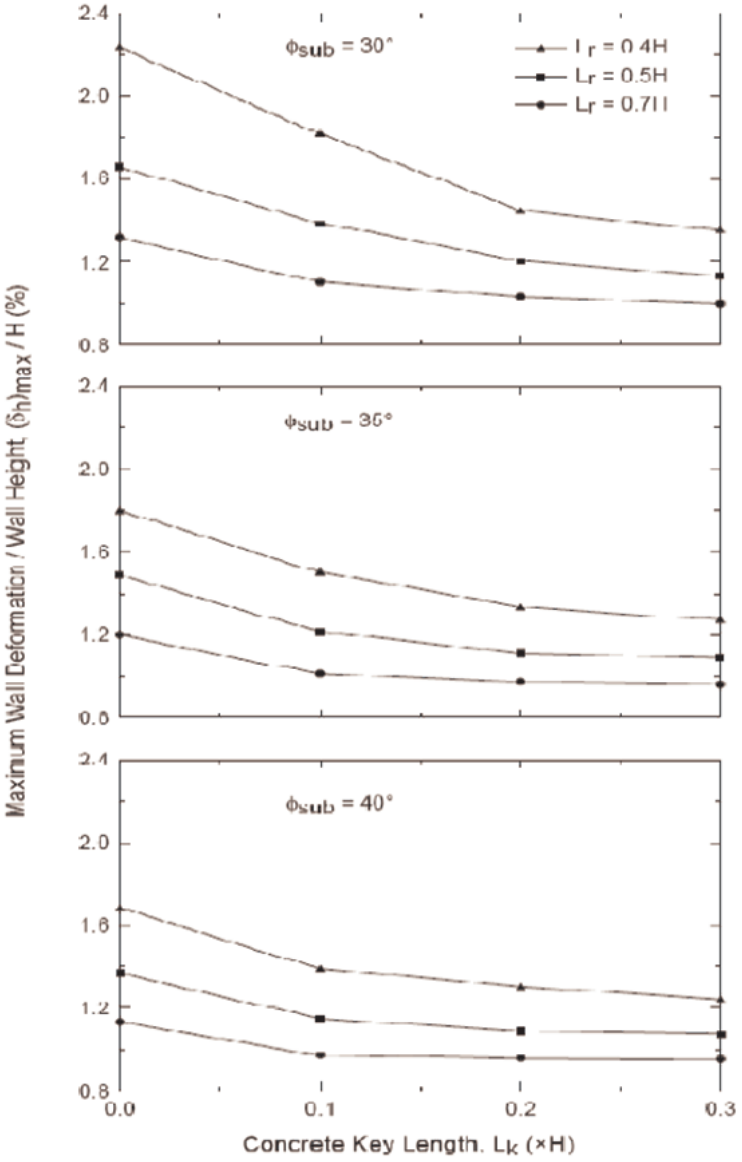

Figure 4.41. Effect of concrete key length on maximum wall deformations (Kim and Bilgin, 2007).

The geometry and material properties of the baseline model used in this study are shown in Figure 4.42, where γ, c, and ϕ are the unit weight, cohesion, and friction angle of soils or blocks, respectively and Ta is the tensile strength of reinforcement. The effect of offset distance on the required reinforcement strength is presented in Figure 4.43. Each tier in this Figure is 3 m high; offsets between adjacent tiers are equal. It can be seen that an increase of offset distance reduces the required reinforcement strength. The effects of reinforced and retained fill quality were investigated by using a lower

friction angle of the fill compared with the baseline case. Figure 4.44 shows the effects of offset distance on the required reinforcement strength; the trends are similar to the baseline case. However, the maximum offset distance for the tiered walls to function independently is larger when the low-quality fill is used. The low-quality fill requires higher reinforcement strength. The behavior exhibited by low-quality fill is obvious since it provides less shear resistance thus requiring stronger and longer reinforcement. An increase in the number of tiers results in a significant increase of required strength of reinforcement.

Two different reinforcement lengths were used to investigate the length effects. The longer reinforcement length of 6.3 m (baseline case) was selected based on 70% height of three tier walls while the shorter reinforcement length of 4.2 m was selected based on 70% height of two-tier walls. The results of required strength of reinforcement with these two reinforcement lengths are presented in Figure 4.45. It can be seen that no difference in strength exists for two tiered walls for the lengths used; simply, even the shorter reinforcement was long enough to resist pullout and develop its strength. However, the difference in required tensile strength of reinforcement is obvious for the three-tiered walls when the offset distance is less than 1.8 m (equivalent to 60% height of individual walls).

Figure 4.46 shows the shear zone predicted by FLAC and Figure 4.47, which was also produced by FLAC, shows that bearing failure under the facing instigates the global failure.

Yoo *et al.*, (2011) conducted a series of reduced scale model tests with different offset to identify internal failure patterns for GRS walls. A series of Finite Element (FE) analyses in conjunction with the shear strength reduction method was also conducted to further investigate the critical offset distance and minimum reinforcement lengths for two tier GRS walls with different offset distances. The analyses results show the critical offset distance beyond which two tiers act independently set by the Federal Highway Administration (FHWA) design guideline is considerably larger than that obtained from the current study. Also indicate that the lower tier reinforcement length has a

greater effect on the overall wall stability than the upper tier reinforcement length, as the minimum reinforcement length changes more drastically with the offset distance S for the lower tier than for the upper tier.

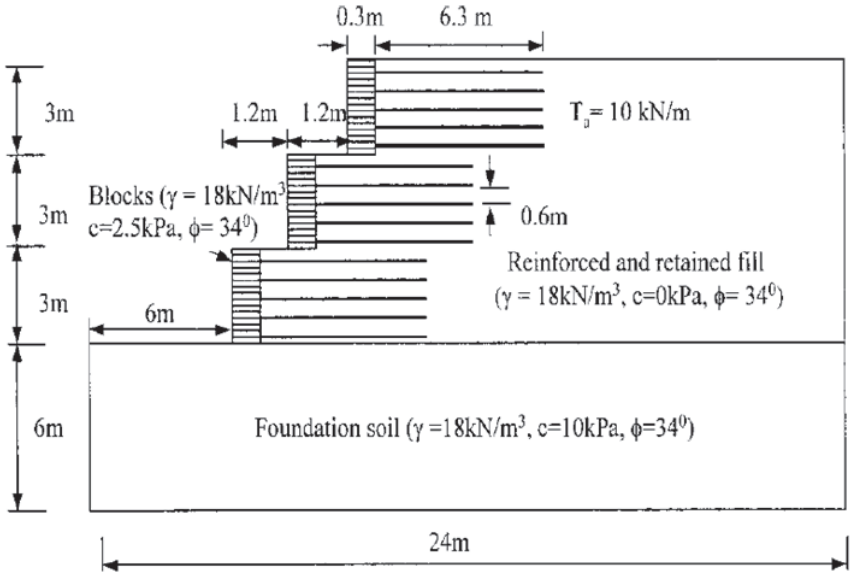

Figure 4.42. Baseline model for limit equilibrium and numerical analyses (Leshchinsky *et al.*, 2004).

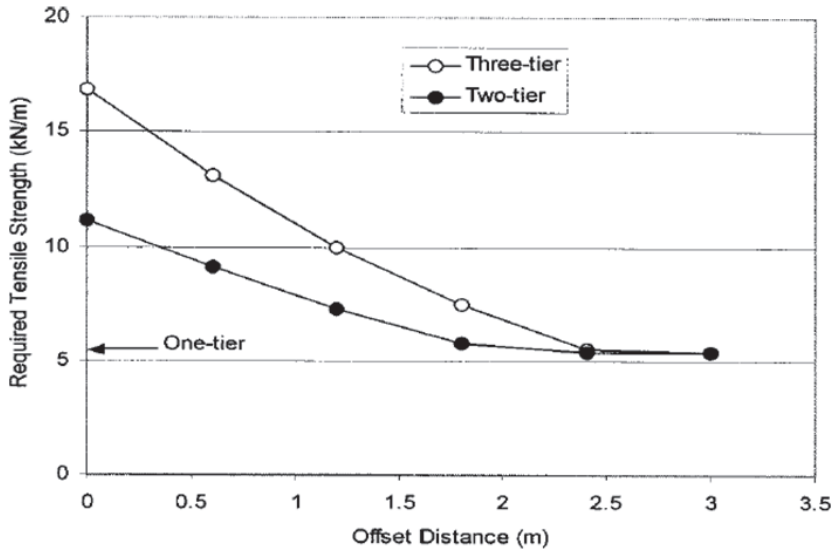

Figure 4.43. Effect of offset distance on required reinforcement strength (Leshchinsky *et al.*, 2004).

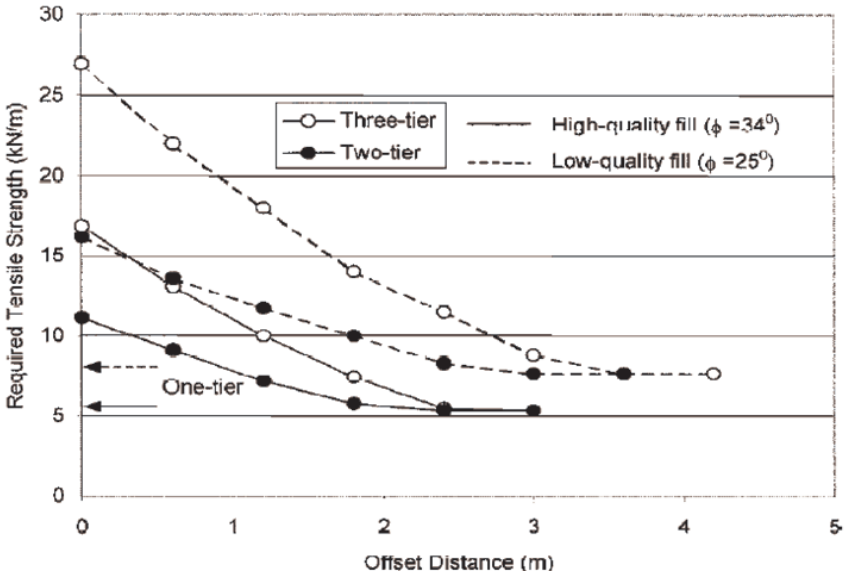

Figure 4.44. Effect of fill quality on required reinforcement strength (Leshchinsky *et al.*, 2004).

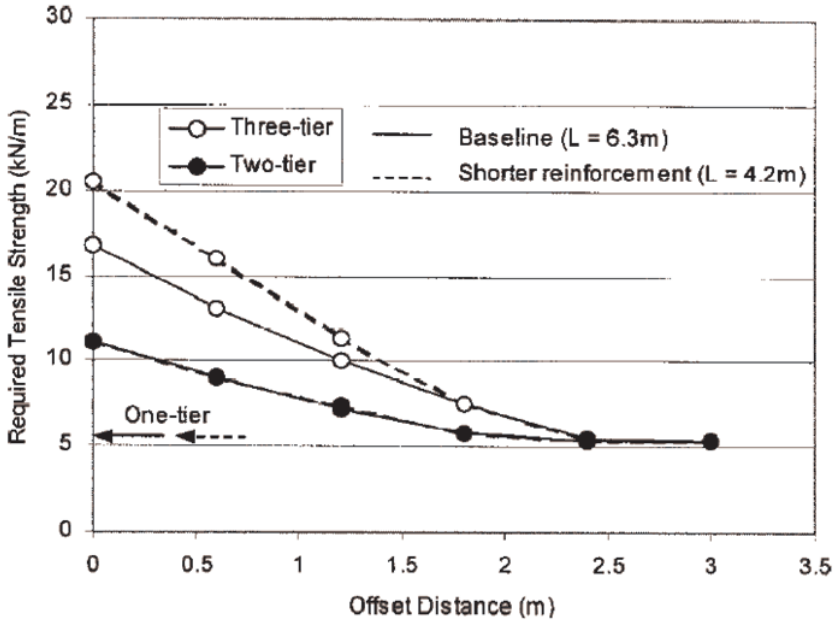

Figure 4.45. Effect of reinforcement length on required reinforcement Strength (Leshchinsky *et al.*, 2004).

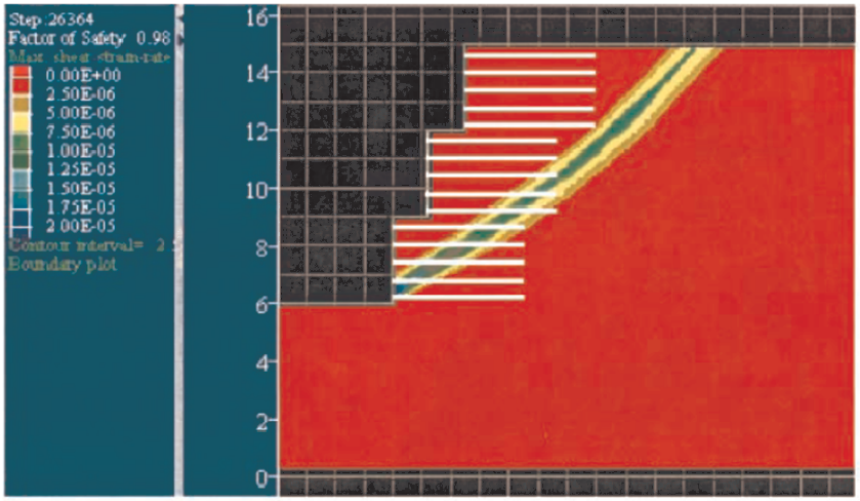

Figure 4.46. Critical surfaces for short reinforcement in FLAC, Predicted shear zone superimposed over reinforcement layout (Leshchinsky *et al.*, 2004).

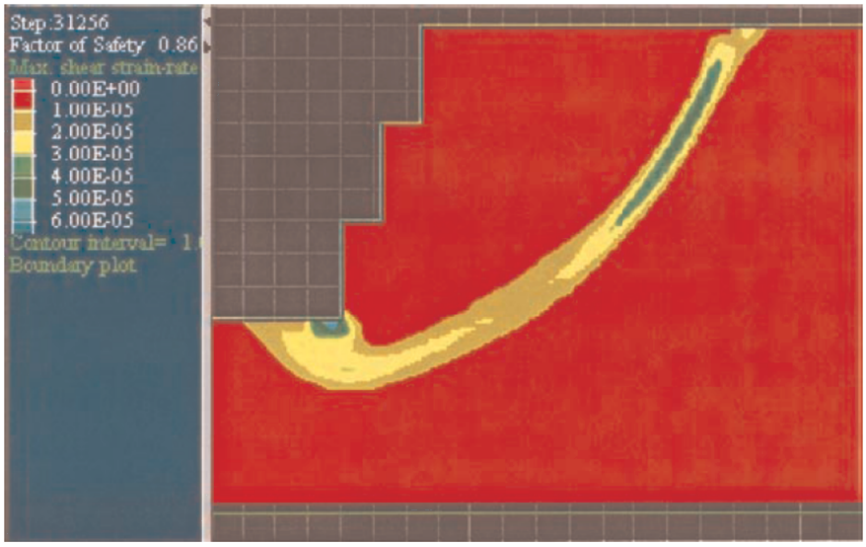

Figure 4.47. Bearing failure of multi-tiered mechanically stabilized earth wall in FLAC (Leshchinsky *et al.*, 2004).

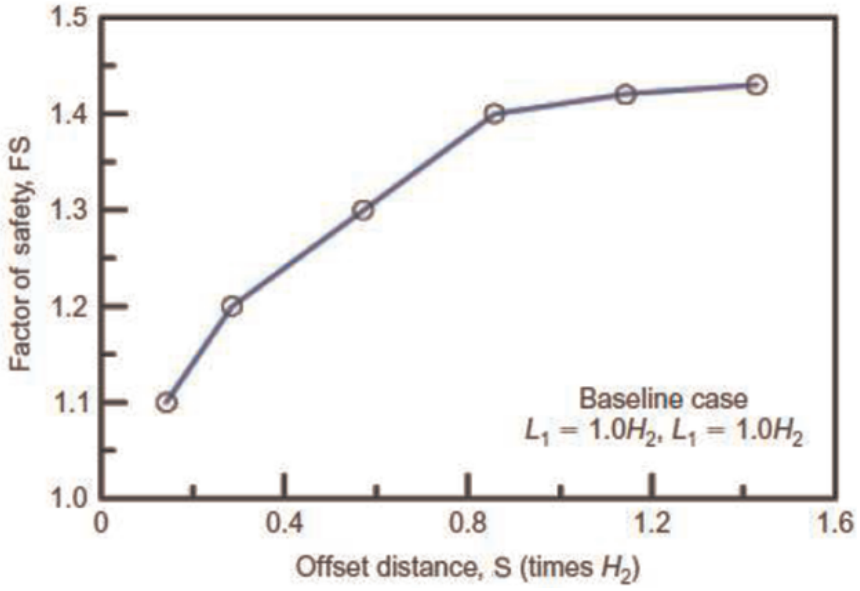

Figure 4.48. Variation of FS with offset distance S (Yoo *et al.*, 2011).

Yoo and Kim (2008) analyzed a two-tier, 5 m high, geosynthetic reinforced segmental retaining wall (GR-SRW) subjected to a surcharge load by a full-scale load test and a 3D finite element analysis. Figure 4.49 shows the geometry of the test two-tier wall had an exposed height (H) of 5 m with the lower and upper tier height of 3.4 and 2.2 m, respectively. The results of the load test at working stress condition revealed that the GR-SRWs response to the test load was well within the serviceability limits, and that the currently available design guideline tends to over-estimate the surcharge load-induced reinforcement forces. The predicted results for the surcharge load well in excess of the test load indicated that the surcharge load-induced reinforcement strains exponentially decrease with depth, showing a good agreement in qualitative terms with that assumed in the FHWA design guideline. The predicted wall deformation at the allowable bearing pressure of 200 kPa was within the serviceability level demonstrating an excellent load carrying capacity of the GR-SRW.

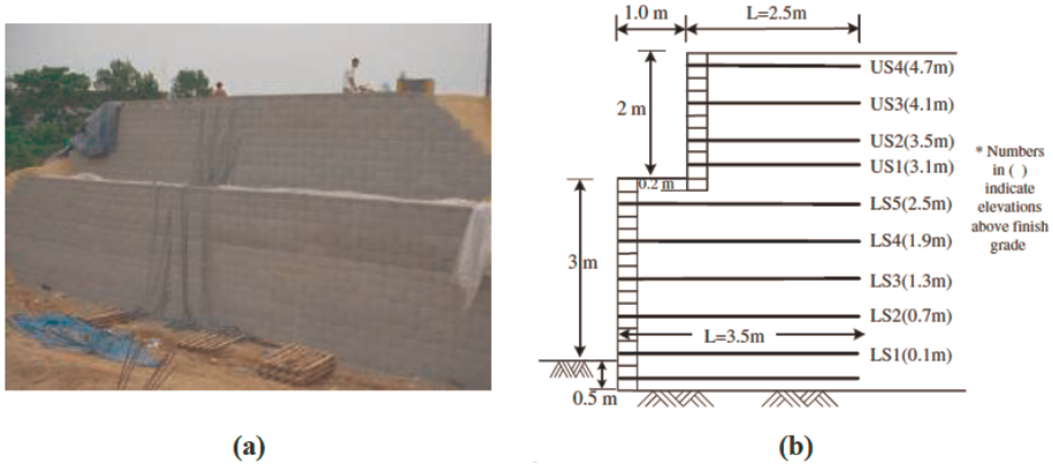

Figure 4.49. Test wall configuration: (a) photo of completed wall; (b) sectional view (Yoo and Kim, 2008).

5. METHODOLOGY

5.1. Model Used In Analyses

In this chapter; the model used in numerical analyses, methodology of the analyses and the program used to compute analyses will be presented. At first, 42 analyses (Figure 5.1) were conducted in this study to investigate the effects of reinforcement length (L), offset distance (S) and reinforced soil type on multi-tiered reinforced retaining walls. Then, additional 16 models were analyzed to determine the critical offset distances. Additonal models were made to determine the offset distance at which each wall behaves like a separate wall. In the end, 58 models were analyzed by using Plaxis v8.2 program which is based on finite element methods. An example of the tiered reinforced soil retaining wall is shown in Figure 5.1.

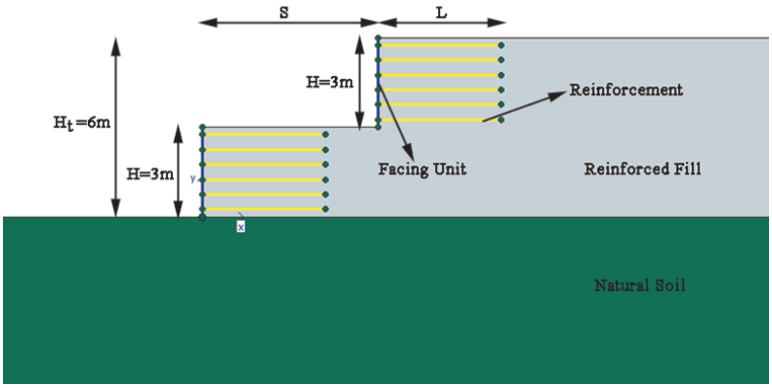

Figure 5.1. Tiered reinforced soil retaining wall.

The Plaxis program was created by the research studies conducted on the use of finite element methods for geotechnical design. It is a finite element code for 2D plane strain and axi-symmetric or 3D modeling of soil and rock behavior for use on personal computers . In addition to soil models, various structural elements exist to model plates, anchors and geogrids. Interface elements can be used to simulate a proper soil-structure, soil-soil or soil-reinforcement interaction. The code uses automatic calculation procedures, and interactive menus combined with direct graphical output. Either 15-noded or 6-noded elements can be used to generate meshes used

in the model. The actual construction process can be realistically simulated by using staged construction feature of the program.

Plaxis code and its material models were developed with intensive care. However, the simulation of reality remains an approximation which implicitly involves some inevitable numerical and modeling errors. It should be noted that the accuracy depends highly on the experience and knowledge of the user regarding the modeling of the problem.

5.2. Modeling of Reinforced Soil Retaining Walls With Plaxis

While simulating the model of the GRS-RW, geometry of the model should be defined first. Points and lines are used to define the boundaries of the GRS-RW in Plaxis. Moreover, lines enclose the areas to form clusters. Clusters are automatically recognized by the Plaxis program after an enclosed area is formed by using lines. The clusters are filled with the soils whose material properties are already composed by the user. Soil is always considered homogenous in each cluster. After defining the geometry and soils; plates, distributed loads, single loads and geogrids can be used to simulate the reinforced soil retaining wall. An example of the model used in Plaxis and interface of the input module of the program can be seen in Figure 5.2.

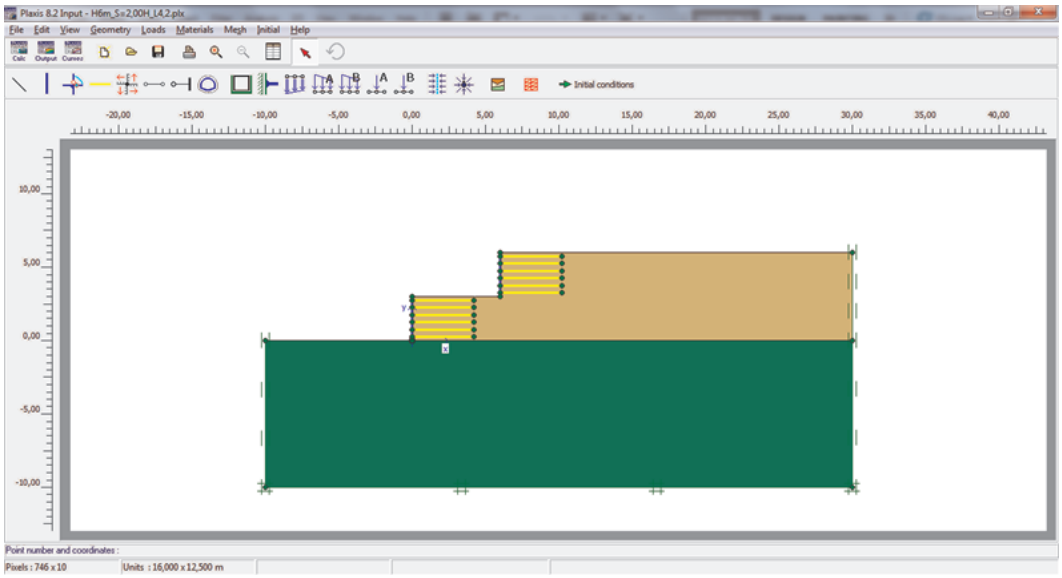

Figure 5.2. A model used in analyses.

5.2.1. Material Modeling

5.2.1.1. Modeling of Soils. Stress-strain behaviour of soil and rock can be modeled at several levels of sophistication because of their non-linear behaviour under load. The number of model parameters depends on the level of sophistication of the model. Therefore, the number of parameters which are required to build model, increases with the level of sophistication.

Plaxis provides some soil models such as linear elastic soil model, Mohr-Coulomb soil model, soft soil model, hardening soil model, soft soil creep model and jointed rock model. Also, Plaxis supports a user defined model option. All soils were modeled in Mohr-Coulomb soil model in this study. The well-known Mohr-Coulomb model can be considered as a first order approximation of real soil behavior. This elastic perfectly-plastic model requires five basic input parameters, namely a Youngs modulus, E, a Poissons ratio, ν, a cohesion, c, a friction angle, ϕ, and a dilatancy angle, ψ. Moreover, Plaxis provides drained and undrained options for the soil model. The shear modulus of the soil is calculated by program using the formula of;

$$G = \frac{E}{2(1+\nu)} \tag{5.1}$$

In this study, two types of reinforced fill and a natural soil is modeled for the analyses. Reinforced fill, as the name suggests, is used in the reinforced zone of the wall. In this study, granular and cohesive soils are modeled for the reinforced fill. According to FHWA, reinforced fill should be non cohesive and angle of internal friction should be at least 34^o. The underlying foundation soil, which is called natural soil in this study, was assumed to have a friction angle of 30 degrees, a value that current FHWA guidelines suggest as a typical lower limit. The soil properties which are used in this study are summarized in Table 5.1.

Table 5.1. Material properties of soil layers.

Material Properties	**Symbol**	**Unit**	Reinforced Fill (Cohesive)	Reinforced Fill (Non-Cohesive)	**Natural Soil**
Model	-	-	Mohr-Coulomb	Mohr-Coulomb	Mohr-Coulomb
Unit Weight	γ_{dry}	kN/m^3	19	19	18
Modulus of Elasticity	E	kN/m^2	20000	50000	10000
Poisson Ratio	ν	-	0,3	0,3	0,35
Cohesion	c	kN/m^2	25	1	3
Angle of Internal Friction	ϕ	^{o}	5	38	30
Dilatency Angle	ψ	^{o}	1	8	1
Shear Modulus	G	kN/m^2	7692	19230	3704

5.2.1.2. Modeling of Reinforcement. Soil reinforcements can be modeled by using geogrid feature of the program. Either elastic or elastoplastic behaviour can be simulated while modeling the reinforcement. Reinforcements are thin elements and they have only axial stiffness, not bending stiffness. Furthermore, they can only resist tensile forces so there is no compression in them. Reinforcements are used to model geotextile, geogrid or metal strip. The parameters used to simulate reinforcement in the program are axial stiffness, EA and tensile strength, N_p. If the material is selected as elastic, there wont be a requirement for the tensile strength. Axial stiffness entered in units of force per unit width and calculated by multiplying the modulus of elasticity of the reinforcement by its thickness.

In this study, reinforcements were considered elastic and EA value was selected 10000 kN/m. The reinforcement layers were placed 0.5m in vertical spacing in all analyses. In order to investigate the influence of reinforcement length, L, on wall behaviour, various lengths are used. Lengths used in this study are L/H_t=0.5, L/H_t=0.7 and L/H_t=1.0 where H_t is the total height of the wall. In other words, H_t is the sum of the height of all tiers. In this study, the wall has two tiers and height of each wall (H) is 3m, so H_t is equal to 6m.

5.2.1.3. Modeling of Facing Unit. The facing elements were of concrete modular block type and they were modeled with line elements. The linear elastic model was opted for the facing elements. Properties of the plate element used in analyses are shown in Table 5.2.

Table 5.2. Material properties of facing unit.

Plate Facing					
Model	**Axial Stifness (EA)**	**Flexural Rigidity (EI)**	**Thickness (d)**	**Weight (w)**	**Poisson Ratio (ν)**
-	kN/m	kNm^2/m	m	kN/m/m	-
Elastic	4500000	8438	0.15	0.8	0.1

5.2.1.4. Modeling of Interfaces. Modeling the interaction between different materials is as important as the material properties. In Plaxis, interfaces are used to model the interaction between two different materials.A suitable value for the strength reduction factor (R_{inter}) is selected to model the roughness of the interaction. Interface strength is related to the soil strength by using strength reduction factor. Therefore, the interface properties are calculated by using soil properties and the strength reduction. The formulas used in calculations are shown below;

$$c_{inter} = R_{inter} x c_{soil} \tag{5.2}$$

$$tan\phi_{inter} = R_{inter} x tan\phi_{soil} \tag{5.3}$$

In this study, interface elements were not placed between materials. Analyses made to investigate the effect of interface elements around reinforcements on horizontal displacement of the top point of the wall. The analyses yielded insignificant changes between the models with and without interface around reinforcement elements. Interface elements are shown schematicaly in Figure 5.3.

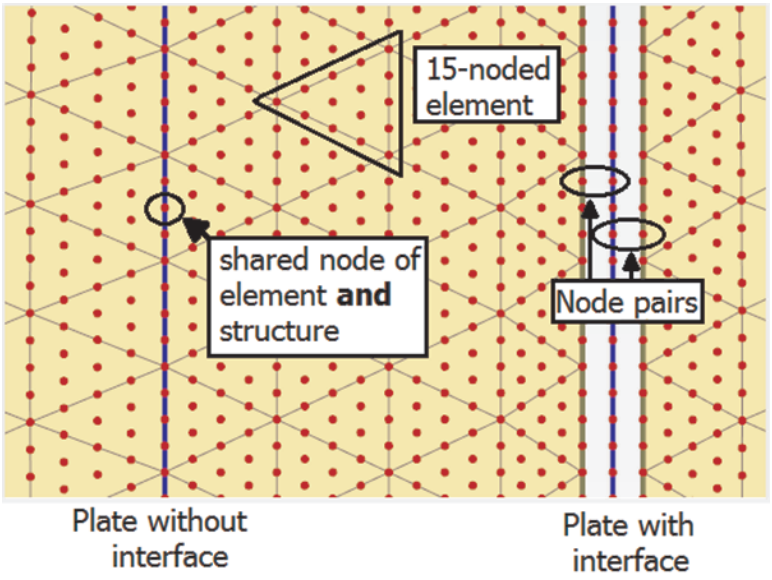

Figure 5.3. Interface elements used in models.

5.2.2. Boundary Modeling

In Plaxis, horizontal and vertical fixities are used to identify boundaries. Horizontal fixity disables the horizontal displacement and vertical fixity disables the vertical displacement as well. Horizontal and vertical fixities can be used separately and together. In the geometry of our model, the right and the left boundary had horizontal fixity and the bottom boundary had total fixity which means a combination of both horizontal and vertical fixities.

5.2.3. Mesh Generation

In finite element analysis, geometry of the model is divided into smaller elements to perform the calculations. A composition of finite element is called a finite element mesh and mesh generation is done automatically in Plaxis. The mesh generation takes full account of the position of points and lines in geometry model, so that the exact position of layers, loads and structures is accounted for in the finite element mesh. The generation process is based on a robust triangulation principle thet search for optimized triangles and which results in an unstructured mesh. Unstructured meshes are not formed from regular patterns of elements. The numerical performance of these meshes

is usually better than structured meshes with regular arrays of elements (Brinkgreve and Yogendrakumar, 1992).

Plaxis also enables to make refinement of mesh where we want the calculations must be more accurate than the other part of the model. Refinement wasnt used in this study. The approximate number of elements was 646 and the number of nodes were 5341 in our models. The finite element is shown in Figure 5.4.

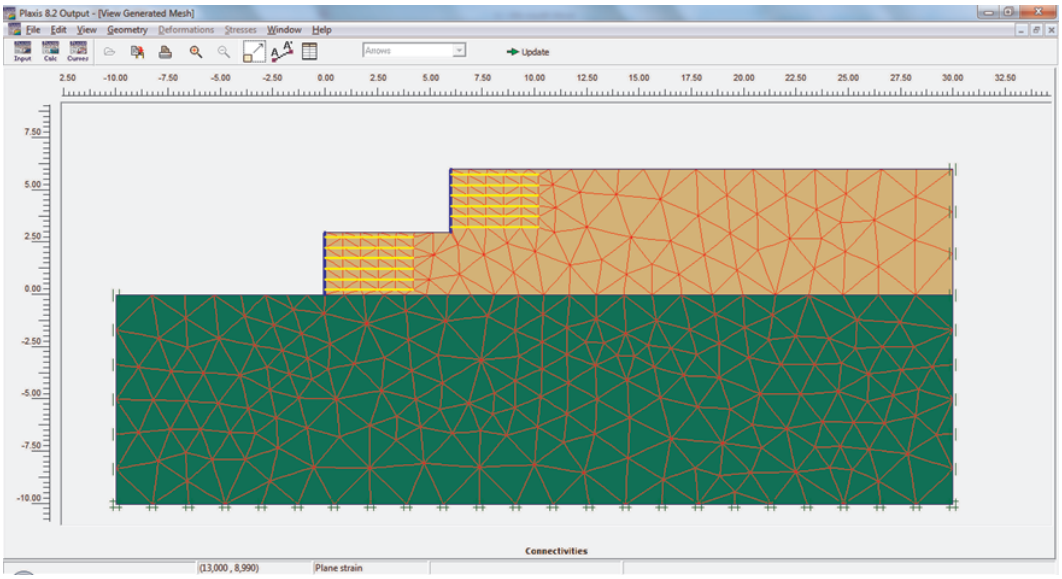

Figure 5.4. Finite element mesh of a model.

5.2.4. Determining the Initial Conditions

After creating the model geometry, defining the material properties and the mesh generation; the initial stress state also initial situations must be determined. Also groundwater level and water pressures are determined in this step. The initial stresses in a soil body were characterized by an initial vertical stress $\sigma_\nu 0$ which is related by the coefficient lateral earth pressure at rest K_0 where;

$$\sigma_{h0} = K_0 x \sigma_{\nu 0} \tag{5.4}$$

Initial stress state of a model is show in Figure 5.5.

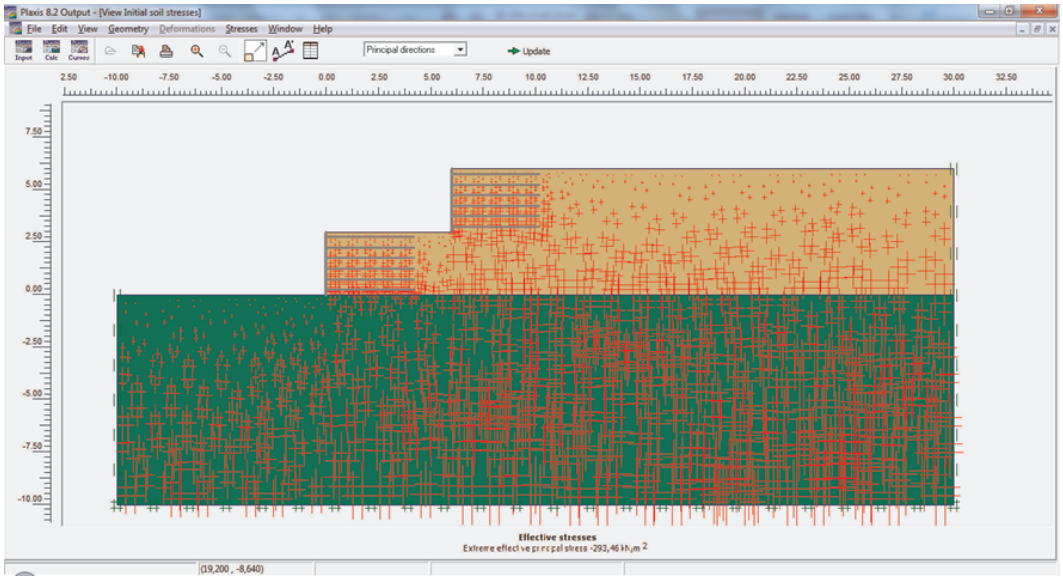

Figure 5.5. Initial conditions of a model.

5.3. Calculations

5.3.1. Staged Construction (Plastic Analysis)

In the analysis of the numerical models conducted in this study, this type of calculation and loading was adopted till to the phi/c reduction phase. The staged construction is the most important type of loading input where it is possible to change the geometry and load configuration by deactivating or reactivating loads, volume clusters or structural objects as created in the geometry input. In this case, the total level to be reached at the end of the construction phase is defined by specifying a new geometry and load configuration, and/or pore pressure distribution. Staged construction is performed using the load advancement ultimate level procedure, which terminates the calculation when the specified state or load level is reached or when soil failure is detected. The ultimate load level is controlled by a total multiplier parameter (ΣMstage). This multiplier generally starts at zero and it is expected to reach the ultimate level of 1.0 at the end of the calculation phase (Enünlü, 2007).

5.3.2. Phi/c Reduction Analysis

The phi/c reduction calculation is an important step in which safety of the structure is analyzed. When doing a safety analysis using the phi/c reduction method, tan(phi) and c are reduced according to the rule:

$$\Sigma Msf = \frac{tan\phi'_{input}}{tan\phi'_{reduced}} = \frac{C'_{input}}{C'_{reduced}} \tag{5.5}$$

This relationship is different for models that do not have the Mohr-Coulomb failure criterion, like the Hoek-Brown model.

Due to this (artificial) strength reduction, user will introduce out-of-balance forces in the model. This out-of-balance will be solved by the calculation kernel, which will result in deformations.

These additional displacements that are generated do not have a physical meaning, but the incremental displacements and/or incremental shear strains in the final step (once a stable solution for ΣMsf is reached), give an indication of the likely failure mechanism. The displacements just before the maximum ΣMsf is reached may be used to get an order of magnitude of the displacements at the moment of failure.

The idea of phi/c reduction is that the soil strength is gradually reduced and when failure occurs the corresponding strength reduction factor can be considered a factor of safety on soil strength. We can recognize whether failure occurs based on the idea that when a small reduction of strength is applied this leads to a large change of strains and displacements.

It should be noted that when more additional steps are used to calculate the safety factor by a phi/c reduction, and a stable value of ΣMsf is reached, you will generate more additional displacements.

In order to determine the safety factor as calculated by a phi/c reduction, user

should check if model has a stable value for ΣMsf: prior to the calculation one can select a control point that is likely to be in the failure zone. Afterwards, it should be checked if the control point is indeed in the failure zone and then the displacements of this point against ΣMsf can be plotted. Moreover, it should be checked to see if a stable value for ΣMsf is reached. If this is not the case, the phase must be calculated with more additional steps (Plaxis, 2012).

6. RESULTS AND DISCUSSIONS

This study was carried out to investigate the behaviour of tiered reinforced soil retaining walls in static conditions, by using finite element analysis. Plaxis 8.2, a commercial computer program was used to conduct the analyses. The main geometry and terminology used in analyses are shown in Figure 6.1. Also, models used in this study is shown in Table 6.1 and Table 6.2. It should be noted that the upper tier is called Tier 2 and the other one is called Tier 1 in this section.

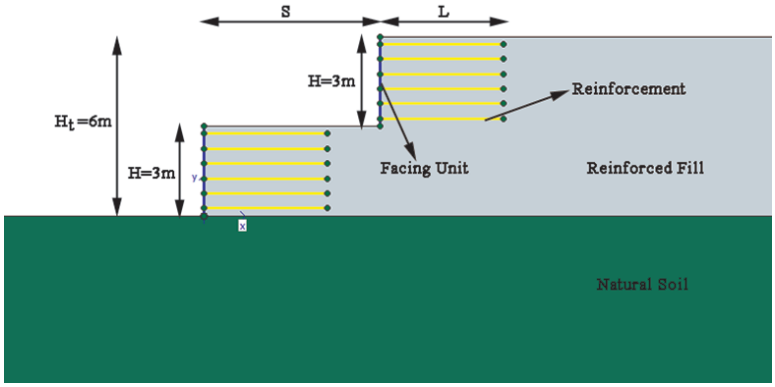

Figure 6.1. Multi tiered reinforced soil retaining wall.

This study is divided into two parts. In all models, height of each tier was selected as 3m and vertical spacing of the reinforcemend was seected as 0.5m. In first part of the study; effects of reinforcement length, type of reinforced fill and offset distance were investigated. Reinforcement length (L) was selected as $0.5H_t$, $0.7H_t$ and $1H_t$. Cohesive and non cohesive soils were used in the reinforced part and offset distance (S) is selected as 0H, 0.5H, 1H, 1.5H, 2H, 2.5H and 3H. Factor of safety and permanent displacements of the models are calculated by using Plaxis. Models used in the first part of the study are summarized in Table 6.1.

Table 6.1. Models used in the first part of the study.

Models Used In Analyses (1-42)													
Model No	**H_t (m)**	**Tiers**	**H (m)**	**L/H_t**	**Fill Type**	**S/H**	Model No	**H_t (m)**	**Tiers**	**H (m)**	**L/H_t**	**Fill Type**	**S/H**
Model 1	6	2	3	0.5	Non Cohesive	0.00	Model 22	6	2	3	0.5	Cohesive	0,00
Model 2	6	2	3	0.5	Non Cohesive	0.50	Model 23	6	2	3	0.5	Cohesive	0,50
Model 3	6	2	3	0.5	Non Cohesive	1.00	Model 24	6	2	3	0.5	Cohesive	1,00
Model 4	6	2	3	0.5	Non Cohesive	1.50	Model 25	6	2	3	0.5	Cohesive	1,50
Model 5	6	2	3	0.5	Non Cohesive	2.00	Model 26	6	2	3	0.5	Cohesive	2,00
Model 6	6	2	3	0.5	Non Cohesive	2.50	Model 27	6	2	3	0.5	Cohesive	2,50
Model 7	6	2	3	0.5	Non Cohesive	3.00	Model 28	6	2	3	0.5	Cohesive	3,00
Model 8	6	2	3	0.7	Non Cohesive	0.00	Model 29	6	2	3	0.7	Cohesive	0,00
Model 9	6	2	3	0.7	Non Cohesive	0.50	Model 30	6	2	3	0.7	Cohesive	0,50
Model 10	6	2	3	0.7	Non Cohesive	1.00	Model 31	6	2	3	0.7	Cohesive	1,00
Model 11	6	2	3	0.7	Non Cohesive	1.50	Model 32	6	2	3	0.7	Cohesive	1,50
Model 12	6	2	3	0.7	Non Cohesive	2.00	Model 33	6	2	3	0.7	Cohesive	2,00
Model 13	6	2	3	0.7	Non Cohesive	2.50	Model 34	6	2	3	0.7	Cohesive	2,50
Model 14	6	2	3	0.7	Non Cohesive	3.00	Model 35	6	2	3	0.7	Cohesive	3,00
Model 15	6	2	3	1.0	Non Cohesive	0.00	Model 36	6	2	3	1.0	Cohesive	0,00
Model 16	6	2	3	1.0	Non Cohesive	0.50	Model 37	6	2	3	1.0	Cohesive	0,50
Model 17	6	2	3	1.0	Non Cohesive	1.00	Model 38	6	2	3	1.0	Cohesive	1,00
Model 18	6	2	3	1.0	Non Cohesive	1.50	Model 39	6	2	3	1.0	Cohesive	1,50
Model 19	6	2	3	1.0	Non Cohesive	2.00	Model 40	6	2	3	1.0	Cohesive	2,00
Model 20	6	2	3	1.0	Non Cohesive	2.50	Model 41	6	2	3	1.0	Cohesive	2,50
Model 21	6	2	3	1.0	Non Cohesive	3.00	Model 42	6	2	3	1.0	Cohesive	3,00

Table 6.2. Models used in the second part of the study.

Models Used In Analyses (43-58)							
Model No	**H_t (m)**	**Tiers**	**H (m)**	**F.S.**	**Fill Type**	**S/H**	**L/H_t**
Model 43	6	2	3	1.50	Non Cohesive	0	Variable
Model 44	6	2	3	1.50	Non Cohesive	0.5	Variable
Model 45	6	2	3	1.50	Non Cohesive	1	Variable
Model 46	6	2	3	1.50	Non Cohesive	1.5	Variable
Model 47	6	2	3	1.50	Non Cohesive	2	Variable
Model 48	6	2	3	1.50	Non Cohesive	2.25	Variable
Model 49	6	2	3	1.50	Non Cohesive	2.5	Variable
Model 50	6	2	3	1.50	Non Cohesive	3	Variable
Model 51	6	2	3	1.50	Cohesive	0	Variable
Model 52	6	2	3	1.50	Cohesive	0.5	Variable
Model 53	6	2	3	1.50	Cohesive	1	Variable
Model 54	6	2	3	1.50	Cohesive	1.5	Variable
Model 55	6	2	3	1.50	Cohesive	2	Variable
Model 56	6	2	3	1.50	Cohesive	2.25	Variable
Model 57	6	2	3	1.50	Cohesive	2.5	Variable
Model 58	6	2	3	1.50	Cohesive	3	Variable

Second part of the study was conducted to determine required reinforcement length that gives the factor of safety as 1.5. Therefore, various reinforcement lengths were used and the one that gives the factor of safety as 1.5 was determined for each offset distance. By doing this, the critical offset distance at which walls start to behave like two separate walls with respect to reinforcement length was investigated. Models used in the second part of the study are summarized in Table 6.2.

6.1. Results for L=0.5H_t

Effects of offset distance were investigated by using L=0.5H_t reinforcement length in non cohesive and cohesive reinforced soils. Factor of safety and permanenet horizontal displacements were provided by Plaxis 8.2. Safety factors and maximum horizontal displacements of the walls are summarized in Table 6.3.

Table 6.3. Results for L=0.5H_t.

Results for L=0.5H_t									
Model No	**H_t (m)**	**H (m)**	**S/H**	**L (m)**	**L/H_t**	**L/H**	**Reinforced Fill**	**F.S.**	Max. Hor. Displacement, max Δx (mm)
Model 1	6	3	0	3	0.5	1	Non Cohesive	1.2	39.302986
Model 2	6	3	0.5	3	0.5	1	Non Cohesive	1.39	38.63667
Model 3	6	3	1	3	0.5	1	Non Cohesive	1.35	36.6629265
Model 4	6	3	1.5	3	0.5	1	Non Cohesive	1.52	33.574109
Model 5	6	3	2	3	0.5	1	Non Cohesive	1.69	30.027545
Model 6	6	3	2.5	3	0.5	1	Non Cohesive	1.87	28.012673
Model 7	6	3	3	3	0.5	1	Non Cohesive	1.89	26.901643
Model 22	6	3	0	3	0.5	1	Cohesive	1.27	45.503793
Model 23	6	3	0.5	3	0.5	1	Cohesive	1.29	45.152313
Model 24	6	3	1	3	0.5	1	Cohesive	1.24	43.142371
Model 25	6	3	1.5	3	0.5	1	Cohesive	1.4	40.583421
Model 26	6	3	2	3	0.5	1	Cohesive	1.54	38.983253
Model 27	6	3	2.5	3	0.5	1	Cohesive	1.69	37.098951
Model 28	6	3	3	3	0.5	1	Cohesive	1.81	35.464755

Detailed wall displacements for non cohesive reinforced fill are shown in Table 6.4. Also, relationship between offset distance (S) and permanent horizontal displacements for cohesive soils are shown in Figure 6.2.

Table 6.4. Horizontal displacements for non cohesive fill and L=0.5H_t.

Height (m)		**Horizontal Displacements (Non Cohesive Soil)**						
		S=0	**S=0.5H**	**S=1H**	**S=1,5H**	**S=2H**	**S=2,5H**	**S=3H**
		Δx	**Δx**	**Δx**	**Δx**	**Δx**	**Δx**	**Δx**
		(mm)	**(mm)**	**(mm)**	**(mm)**	**(mm)**	**(mm)**	**(mm)**
Tier 1	0	36,86	37,82	36,42	33,57	29,73	27,72	26,40
	1	38.24	38.42	36.66	33.46	29.99	27.96	26.73
	2	39.09	38.64	36.55	33.03	30.03	28.01	26.87
	3	39.30	38.62	36.25	32.43	29.94	27.95	26.90
Tier 2	3	39.30	38.13	33.50	30.66	27.31	25.74	24.43
	4	38.99	36.04	31.82	29.51	26.84	24.34	23.51
	5	38.33	33.87	30.08	28.32	26.26	22.88	22.43
	6	37.53	31.65	28.58	27.07	25.60	21.36	21.27

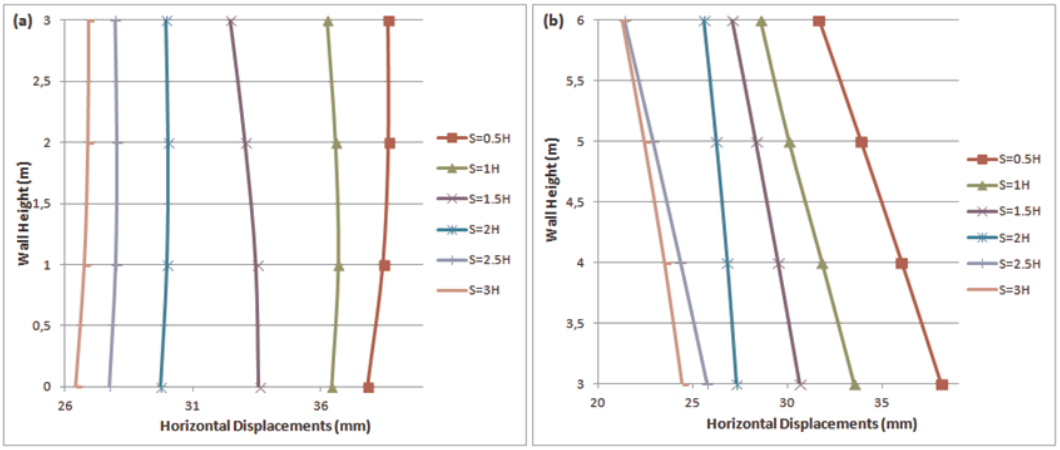

Figure 6.2. Permanent displacements with respect to offset distance for non cohesive soils and L=0.5H_t (a) Tier 1 (b) Tier 2.

Detailed wall displacements for cohesive reinforced fill are shown in Table 6.5. Also, relationship between offset distance (S) and permanent horizontal displacements for non cohesive soils are shown in Figure 6.3.

Table 6.5. Horizontal displacements for cohesive fill and L=0.5H_t.

Height (m)		Horizontal Displacements (Cohesive Soil)						
		S=0	S=0.5H	S=1H	S=1.5H	S=2H	S=2.5H	S=3H
		Δx (mm)	Δx (mm)	Δx (mm)	Δx (mm)	Δx (mm)	Δx (mm)	Δx (mm)
Tier 1	0	45,50	43,84	41,85	39,25	37,13	35,16	33,47
	1	45.41	44.78	42.79	40.17	38.21	36.26	34.57
	2	44.52	45.15	43.14	40.54	38.75	36.83	35.16
	3	42.81	44.99	43.13	40.58	38.98	37.10	35.46
Tier 2	3	42.81	41.83	39.84	37.25	34.94	33.00	31.21
	4	40.79	40.32	38.33	35.52	33.21	31.25	29.52
	5	38.76	38.86	36.87	33.85	31.48	29.52	27.82
	6	36.76	37.41	35.42	32.17	29.73	27.75	26.08

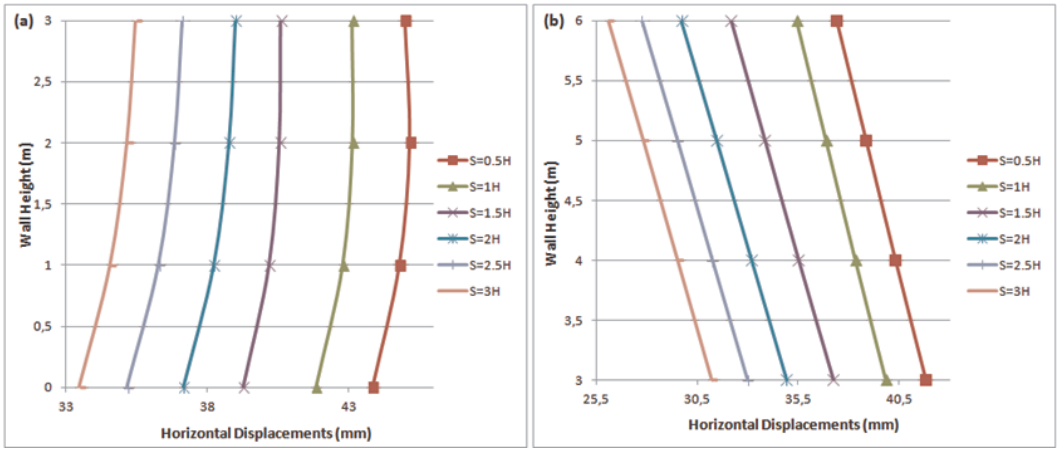

Figure 6.3. Permanent displacements with respect to offset distance for cohesive soils and L=0.5H_t (a) Tier 1 (b) Tier 2.

Maximum horizontal wall displacements for both cohesive and non cohesive fills are shown in Figure 6.4.

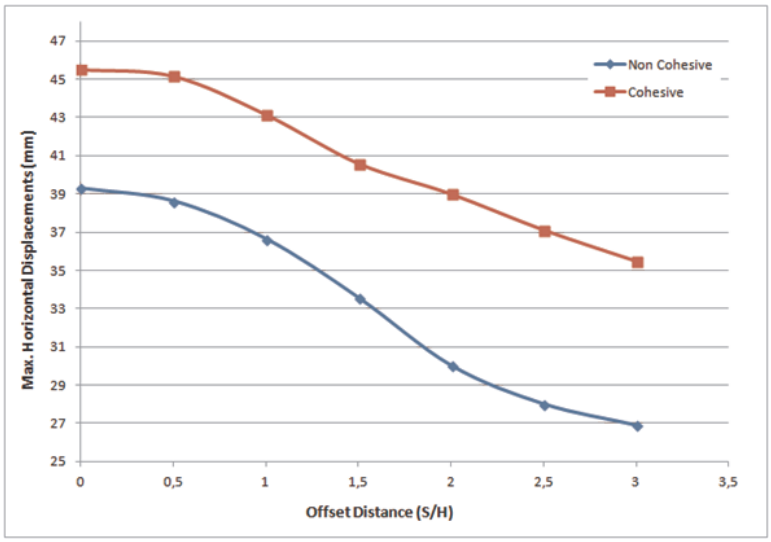

Figure 6.4. Maximum horizontal wall displacements with respect to offset distance for L=0.5H_t.

Factor of safety for both cohesive and non cohesive fills are shown in Figure 6.5.

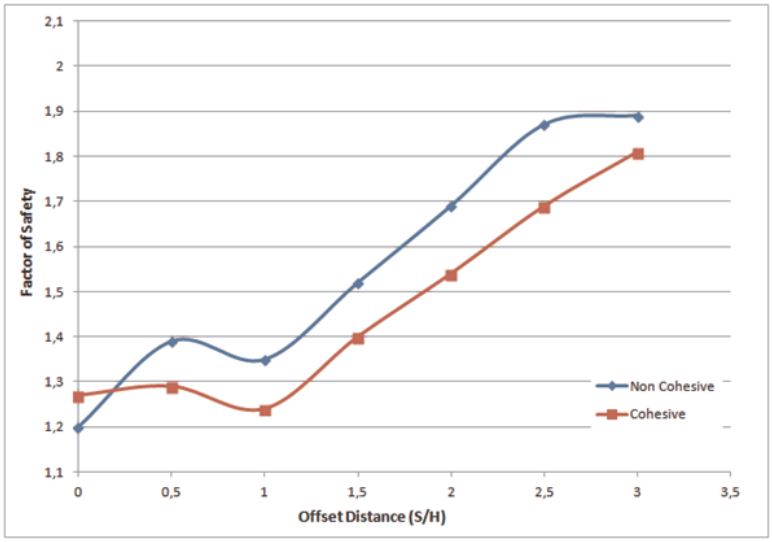

Figure 6.5. Factor of safety with respect to offset distance for L=0.5H_t.

For L=0.5H_t case in cohesive and non cohesive reinforced fill, analyses showed that the factor of safety increases with the increase of offset distance. Also, it can be seen that displacements decrease with the increasing offset distance. When compared to cohesive reinforced fill, non cohesive fill gives higher safety factors and less displacements. Failure surfaces for non cohesive fill is shown in Figure 6.6 and they are shown in Figure 6.7 for cohesive fill.

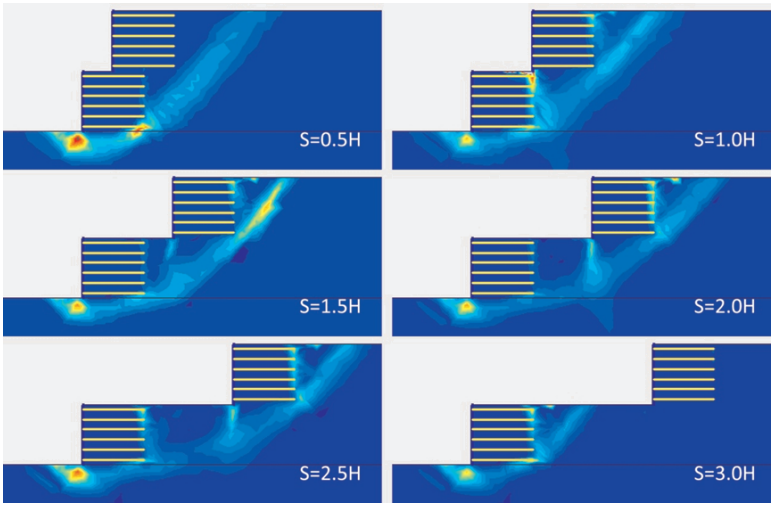

Figure 6.6. Failure surfaces for non cohesive fill.

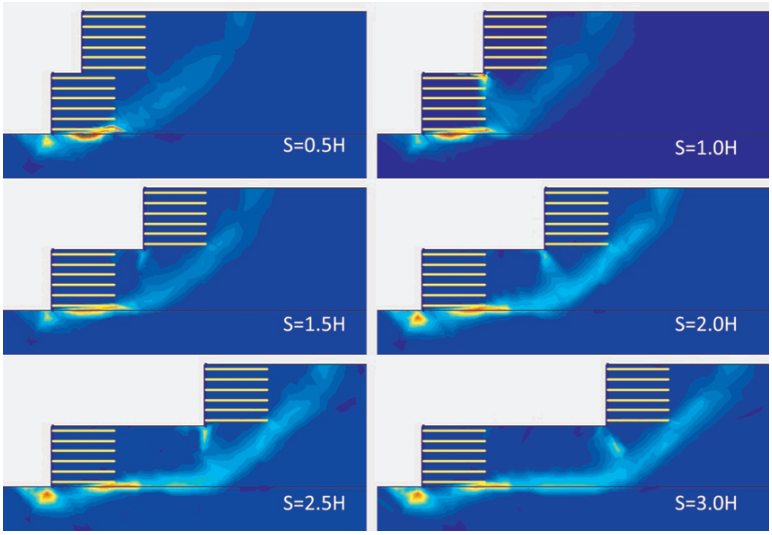

Figure 6.7. Failure surfaces for cohesive fill.

6.2. Results for L=0.7H_t

Effects of offset distance were investigated by using L=0.7H_t reinforcement length in non cohesive and cohesive reinforced soils. Factor of safety and permanent horizontal displacements were provided by Plaxis 8.2. Safety factors and maximum horizontal displacements of the walls are summarized in Table 6.6.

Table 6.6. Results for L=0.7H_t.

Results for L=0.7H_t									
Model No	**H_t (m)**	**H (m)**	**S/H**	**L (m)**	**L/H_t**	**L/H**	**Reinforced Fill**	**F.S.**	Max. Hor. Displacement, max Δx (mm)
Model 8	6	3	0	4.2	0,7	1.4	Non Cohesive	1.47	43.10
Model 9	6	3	0.5	4.2	0,7	1.4	Non Cohesive	1.57	34.65
Model 10	6	3	1	4.2	0,7	1.4	Non Cohesive	1.59	32.63
Model 11	6	3	1.5	4.2	0,7	1.4	Non Cohesive	1.61	31.19
Model 12	6	3	2	4.2	0,7	1.4	Non Cohesive	1.83	29.15
Model 13	6	3	2.5	4.2	0,7	1.4	Non Cohesive	1.97	27.80
Model 14	6	3	3	4.2	0,7	1.4	Non Cohesive	2.15	26.53
Model 29	6	3	0	4.2	0,7	1.4	Cohesive	1.39	43.39
Model 30	6	3	0.5	4.2	0,7	1.4	Cohesive	1.43	42.60
Model 31	6	3	1	4.2	0,7	1.4	Cohesive	1.43	41.34
Model 32	6	3	1.5	4.2	0,7	1.4	Cohesive	1.41	40.08
Model 33	6	3	2	4.2	0,7	1.4	Cohesive	1.57	38.27
Model 34	6	3	2.5	4.2	0,7	1.4	Cohesive	1.71	36.54
Model 35	6	3	3	4.2	0,7	1.4	Cohesive	1.83	34.86

Detailed wall displacements for non cohesive reinforced fill are shown in Table 6.7. Also, relationship between offset distance (S) and permanent horizontal displacements for non cohesive soils are shown in Figure 6.8.

Table 6.7. Horizontal displacements for non cohesive fill and L=0.7H$_t$.

Height (m)		Horizontal Displacements (Non Cohesive Soil)						
		S=0	S=0,5H	S=1H	S=1,5H	S=2H	S=2,5H	S=3H
		Δx (mm)	Δx (mm)	Δx (mm)	Δx (mm)	Δx (mm)	Δx (mm)	Δx (mm)
Tier 1	0	36.46	34.65	32.63	31.19	29.08	27.58	26.14
	1	38.33	34.39	32.45	31.13	29.15	27.79	26.43
	2	39.85	33.81	32.01	30.84	29.01	27.80	26.53
	3	40.97	33.02	31.42	30.41	28.75	27.69	26.51
Tier 2	3	40.97	32.86	30.82	29.25	27.01	25.11	23.67
	4	41.80	31.49	29.17	27.89	26.15	24.71	23.41
	5	42.48	30.02	27.57	26.50	25.28	24.19	23.00
	6	43.10	28.49	26.13	25.09	24.38	23.61	22.50

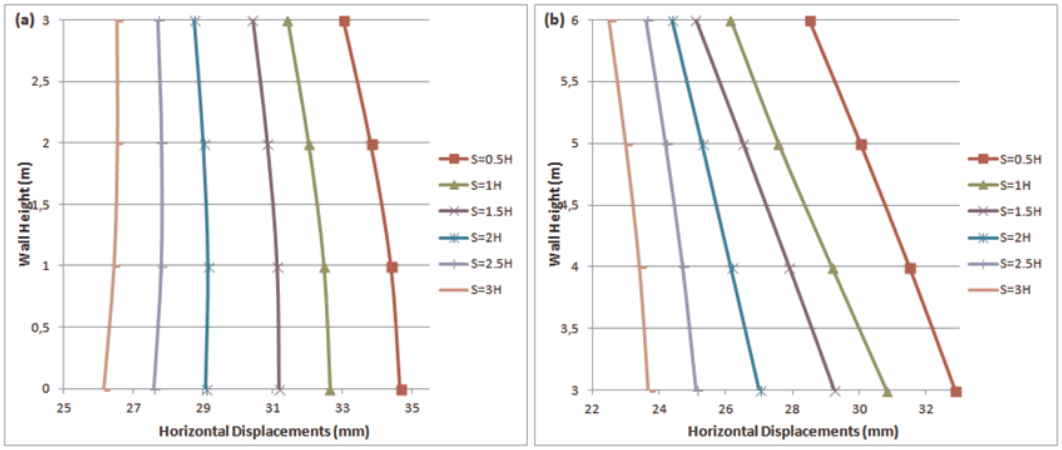

Figure 6.8. Permanent displacements with respect to offset distance for non cohesive soils and L=0.7H$_t$ (a) Tier 1 (b) Tier 2.

Detailed wall displacements for cohesive reinforced fill are shown in Table 6.8. Also, relationship between offset distance (S) and permanent horizontal displacements for non cohesive soils are shown in Figure 6.9.

Table 6.8. Horizontal displacements for cohesive fill and L=0.7H_t.

Height (m)		Horizontal Displacements (Cohesive Soil)						
		S=0	S=0,5H	S=1H	S=1,5H	S=2H	S=2,5H	S=3H
		Δx	Δx	Δx	Δx	Δx	Δx	Δx
		(mm)	(mm)	(mm)	(mm)	(mm)	(mm)	(mm)
Tier 1	0	43.39	42.00	40.79	39.14	36.97	35.07	33.29
	1	42.84	42.60	41.34	39.89	37.87	36.01	34.25
	2	41.70	42.56	41.31	40.08	38.22	36.43	34.70
	3	40.08	42.13	40.93	39.94	38.27	36.54	34.86
Tier 2	3	40.08	41.51	39.33	36.82	34.75	32.71	30.93
	4	38.39	40.01	37.45	35.01	32.78	30.85	29.11
	5	36.79	38.50	35.61	33.27	30.91	29.02	27.33
	6	35.24	36.96	33.78	31.53	29.05	27.19	25.53

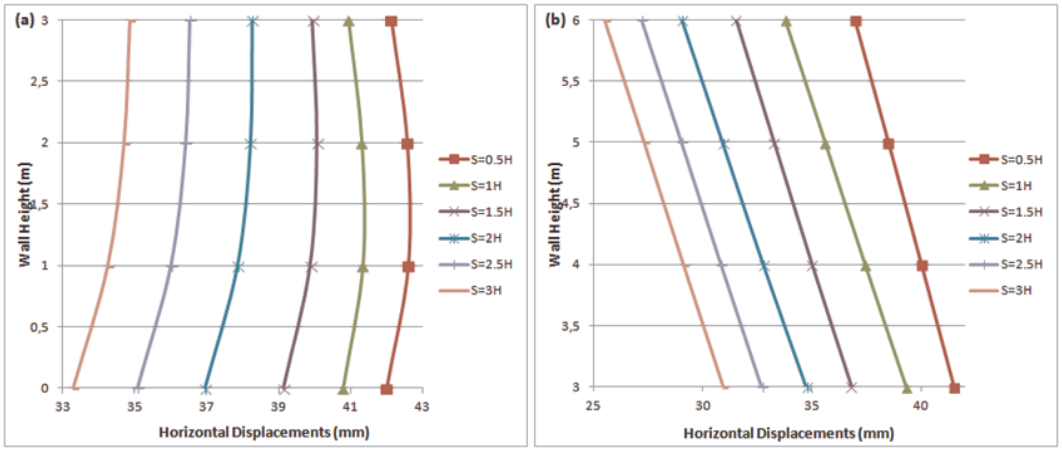

Figure 6.9. Permanent displacements with respect to offset distance for cohesive soils and L=0.7H_t (a) Tier 1 (b) Tier 2.

Maximum horizontal wall displacements for both cohesive and non cohesive fills are shown in Figure 6.10.

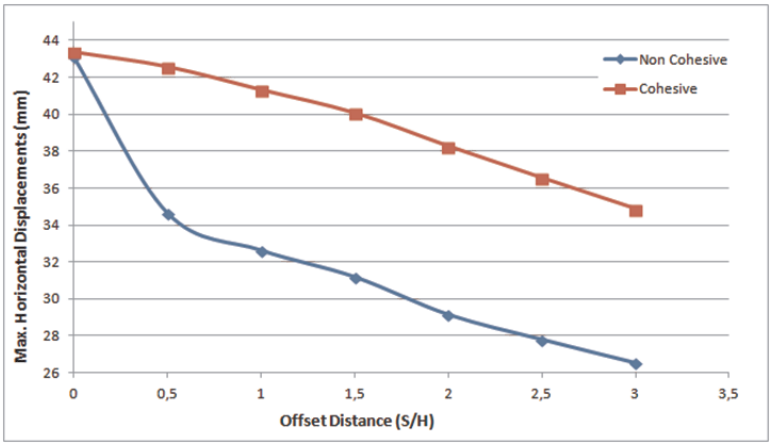

Figure 6.10. Factor of safety with respect to offset distance for L=0.7H_t.

Factor of safety for both cohesive and non cohesive fills are shown in Figure 6.11.

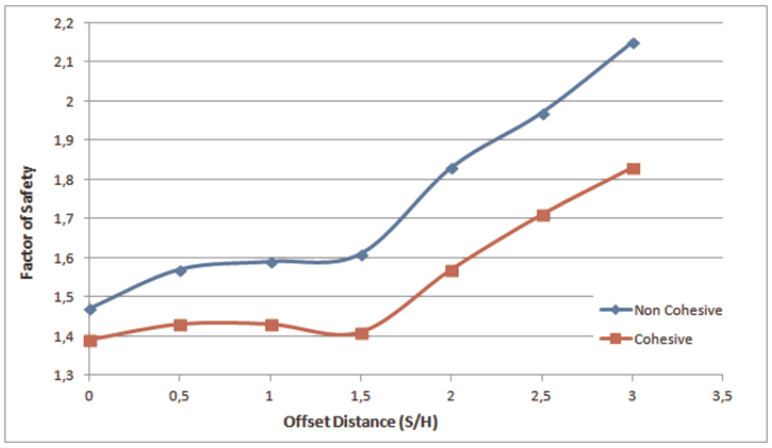

Figure 6.11. Factor of safety with respect to offset distance for L=0.7H_t.

For L=0.7H_t case in cohesive and non cohesive reinforced fill, analyses showed that the factor of safety increases with the increase of offset distance. Also, it can be seen that displacements decrease with the increasing offset distance. When compared to cohesive reinforced fill, non cohesive fill gives higher safety factors and less displacements. Failure surfaces for non cohesive fill is shown in Figure 6.12 and they are shown in Figure 6.13 for cohesive fill.

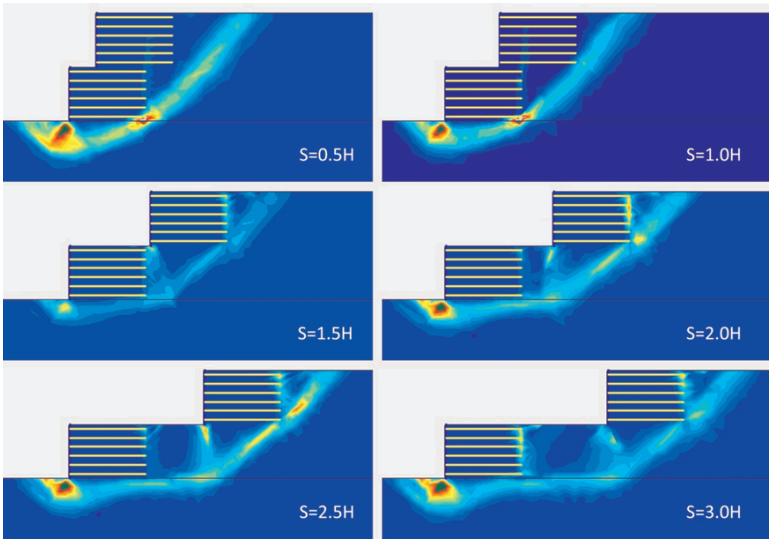

Figure 6.12. Failure surfaces for non cohesive fill.

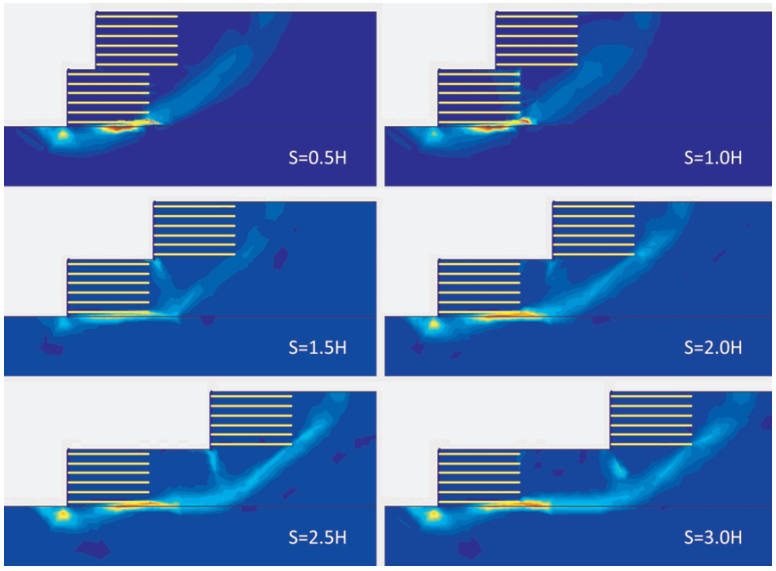

Figure 6.13. Failure surfaces for cohesive fill.

6.3. Results for L=1.0H_t

Effects of offset distance were investigated by using L=1.0H_t reinforcement length in non cohesive and cohesive reinforced soils. Factor of safety and permanent horizontal displacements were provided by Plaxis 8.2. Safety factors and maximum horizontal displacements of the walls are summarized in Table 6.9. Detailed wall displacements for non cohesive reinforced fill are shown in Table 6.10. Also, relationship between

Table 6.9. Results for L=1.0H_t.

Results for L=1H_t									
Model No	**H_t (m)**	**H (m)**	**S/H**	**L (m)**	**L/H_t**	**L/H**	**Reinforced Fill**	**F.S.**	Max. Hor. Displacement, max Δx (mm)
Model 15	6	3	0	6	1	2	Non Cohesive	1.71	32.55
Model 16	6	3	0,5	6	1	2	Non Cohesive	1.82	32.45
Model 17	6	3	1	6	1	2	Non Cohesive	1.83	31.08
Model 18	6	3	1.5	6	1	2	Non Cohesive	1.93	31.35
Model 19	6	3	2	6	1	2	Non Cohesive	1.96	29.08
Model 20	6	3	2.5	6	1	2	Non Cohesive	2.12	27.33
Model 21	6	3	3	6	1	2	Non Cohesive	2.27	26.04
Model 36	6	3	0	6	1	2	Cohesive	1.56	41.60
Model 37	6	3	0.5	6	1	2	Cohesive	1.65	41.40
Model 38	6	3	1	6	1	2	Cohesive	1.62	40.14
Model 39	6	3	1.5	6	1	2	Cohesive	1.64	38.82
Model 40	6	3	2	6	1	2	Cohesive	1.66	37.78
Model 41	6	3	2.5	6	1	2	Cohesive	1.78	36.05
Model 42	6	3	3	6	1	2	Cohesive	1.91	34.38

offset distance (S) and permanent horizontal displacements for non cohesive soils are shown in Figure 6.14.

Table 6.10. Horizontal displacements for non cohesive fill and L=1.0H_t.

Height (m)		**Horizontal Displacements (Non Cohesive Soil)**						
		S=0	**S=0,5H**	**S=1H**	**S=1,5H**	**S=2H**	**S=2,5H**	**S=3H**
		Δx (mm)	**Δx (mm)**	**Δx (mm)**	**Δx (mm)**	**Δx (mm)**	**Δx (mm)**	**Δx (mm)**
Tier 1	0	32.31	32.45	31.08	31.35	28.92	27.20	25.77
	1	32.55	32.03	30.55	30.82	29.08	27.33	26.00
	2	32.49	31.31	29.79	30.01	29.04	27.27	26.04
	3	32.10	30.40	28.90	29.05	28.88	27.10	25.98
Tier 2	3	30.36	30.36	28.67	28.09	25.48	24.26	22.77
	4	31.48	29.52	27.53	27.05	25.23	23.85	22.37
	5	30.75	28.60	26.27	25.95	24.88	23.37	21.87
	6	29.98	27.62	24.94	24.81	24.38	22.83	21.31

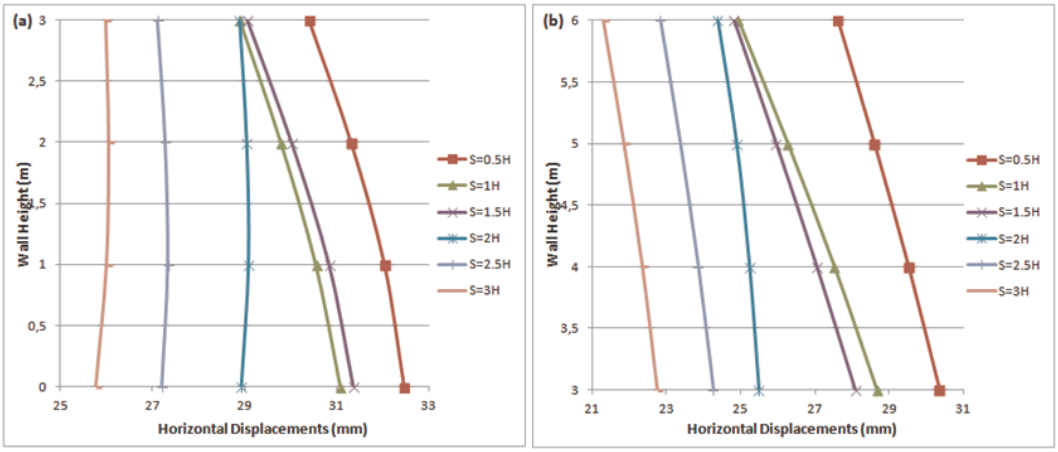

Figure 6.14. Permanent displacements with respect to offset distance for non cohesive soils and L=1.0H_t (a) Tier 1 (b) Tier 2.

Detailed wall displacements for cohesive reinforced fill are shown in Table 6.11. Also, relationship between offset distance (S) and permanent horizontal displacements for non cohesive soils are shown in Figure 6.15.

Table 6.11. Horizontal displacements for cohesive fill and L=1.0H_t.

Height (m)		**Horizontal Displacements (Cohesive Soil)**						
		S=0	**S=0,5H**	**S=1H**	**S=1,5H**	**S=2H**	**S=2,5H**	**S=3H**
		Δx	**Δx**	**Δx**	**Δx**	**Δx**	**Δx**	**Δx**
		(mm)	**(mm)**	**(mm)**	**(mm)**	**(mm)**	**(mm)**	**(mm)**
Tier 1	0	41.60	41.02	39.77	38.31	36.81	34.93	33.12
	1	40.75	41.40	40.14	38.82	37.56	35.74	33.97
	2	39.43	41.19	39.95	38.78	37.78	36.04	34.31
	3	37.82	40.60	39.43	38.44	37.71	36.05	34,38
Tier 2	3	37.82	40.04	38.18	36.35	34.32	32.40	30.55
	4	36.29	38.48	36.37	34.35	32.26	30.33	28.49
	5	34.92	36.90	34.54	32.35	30.28	28.34	26.50
	6	33.61	35.29	32.68	30.35	28.32	26.36	24.50

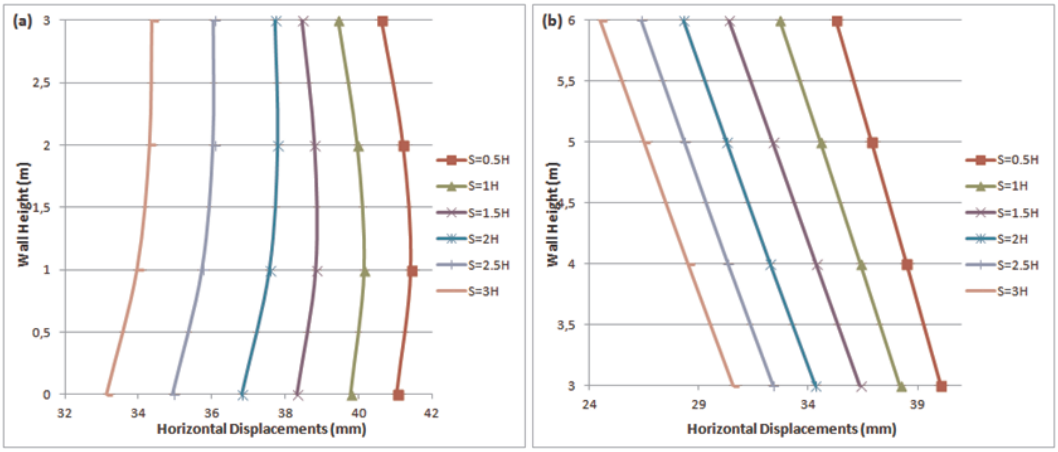

Figure 6.15. Permanent displacements with respect to offset distance for cohesive soils and L=1.0H_t (a) Tier 1 (b) Tier 2.

Maximum horizontal wall displacements for both cohesive and non cohesive fills are shown in Figure 6.16.

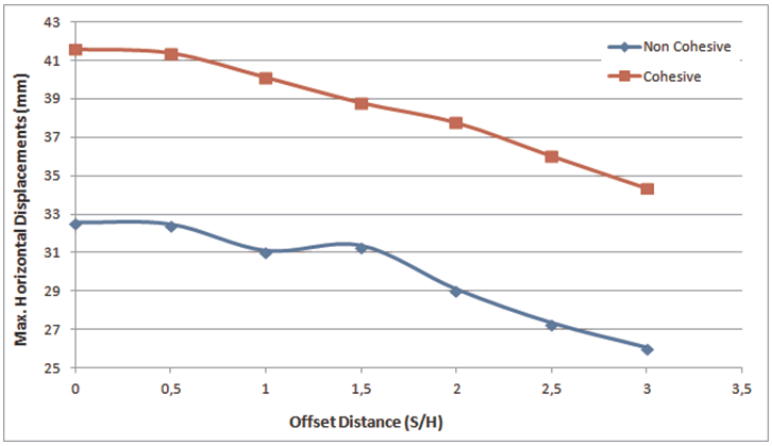

Figure 6.16. Maximum horizontal wall displacements with respect to offset distance for L=1.0H_t.

Factor of safety for both cohesive and non cohesive fills are shown in Figure 6.17.

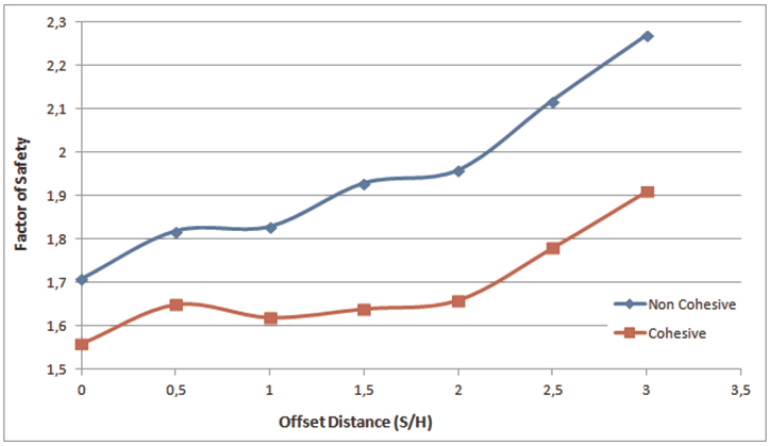

Figure 6.17. Factor of safety with respect to offset distance for L=1.0H_t.

For L=1.0H_t case in cohesive and non cohesive reinforced fill, analyses showed that the factor of safety increases with the increase of offset distance. Also, it can be seen that displacements decrease with the increasing offset distance. When compared to cohesive reinforced fill, non cohesive fill gives higher safety factors and less displacements. Failure surfaces for non cohesive fill is shown in Figure 6.18 and they are shown in Figure 6.19 for cohesive fill.

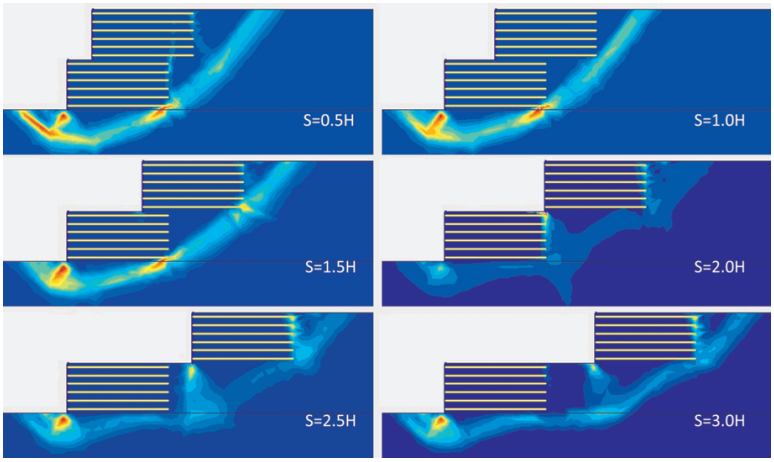

Figure 6.18. Failure surfaces for non cohesive fill.

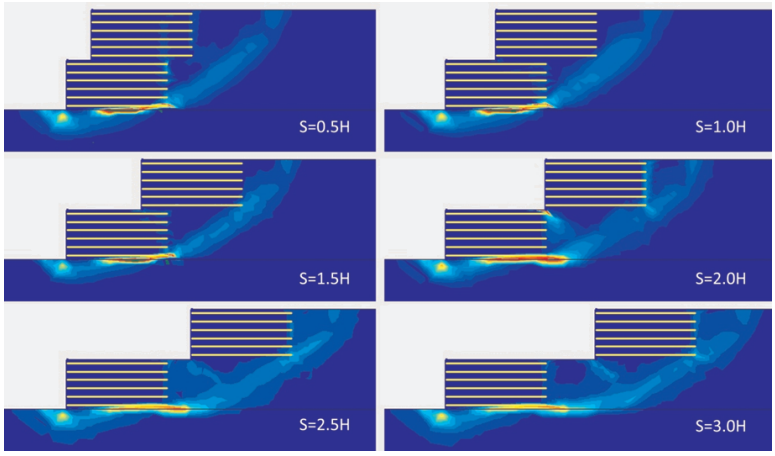

Figure 6.19. Failure surfaces for cohesive fill.

6.4. Effects of Reinforcement Length

Analysis showed that the horizontal wall displacements were reduced with the increase in reinforcement length (Figure 6.20 and Figure 6.21). However, displacement values obtained closer for higher offset distances. Also, it was seen that the factor of safety values can be increased by using longer reinforcements. Effects of reinforcement length on factor of safety can be seen in Figure 6.22 and Figure 6.23.

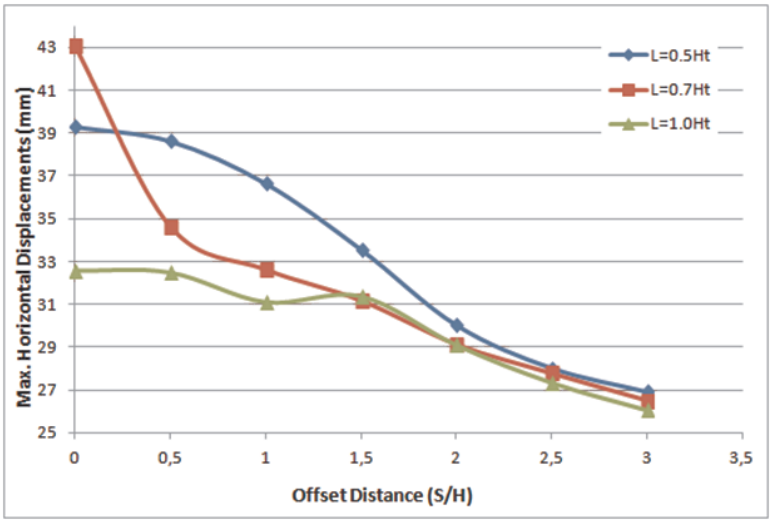

Figure 6.20. Maximum horizontal wall displacements for non cohesive reinforced fill.

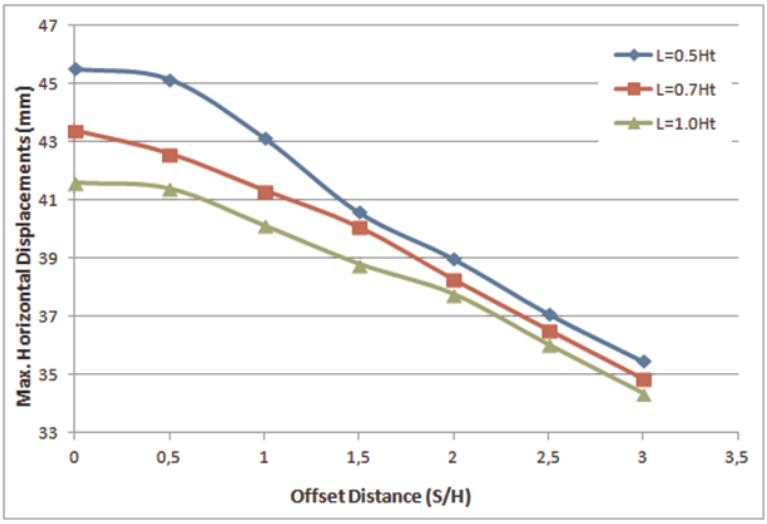

Figure 6.21. Maximum horizontal wall displacements for cohesive reinforced fill.

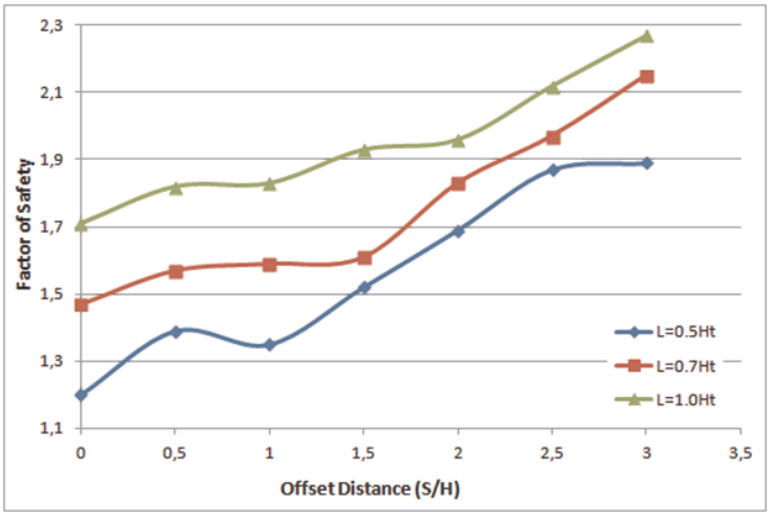

Figure 6.22. Factor of safety values for non cohesive reinforced fill.

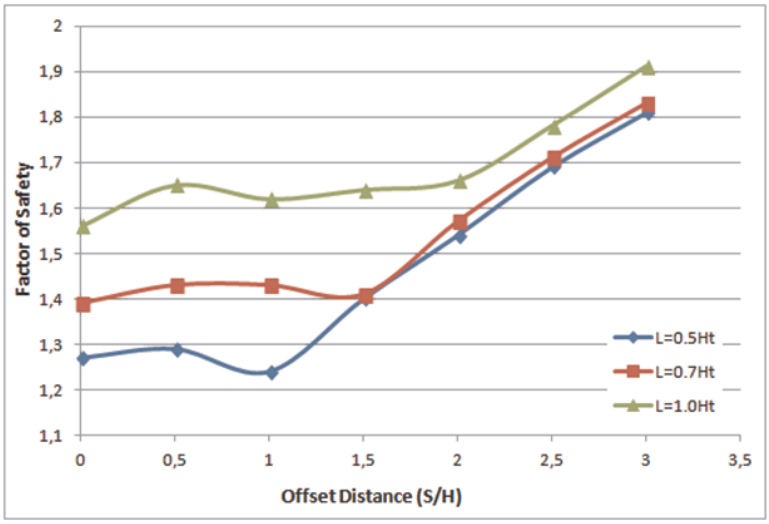

Figure 6.23. Factor of safety values for cohesive reinforced fill.

6.5. Investigation of Critical Offset Distance

Second part of the study will be discussed in this section. In this section, minimum reinforcement length which gives the factor of safety as 1.5 is investigated for various offset distances. Then, the critical offset distance is determined for non cohesive fill and cohesive fill cases.. Required reinforcement lengths for each offset distance to obtain F.S.=1.5 are shown in Table 6.12 and Table 6.13.

Table 6.12. Results for non cohesive soil.

NON COHESIVE REINFORCED FILL					
H_t (m)	H (m)	S/H	L (m)	L/H_t	L/H
6	3	0	4.4	0.733	1.467
6	3	0.5	3.9	0.650	1.300
6	3	1	3.6	0.600	1.200
6	3	1.5	2.8	0.467	0.933
6	3	2	1.6	0.267	0.533
6	3	2.25	1.5	0.250	0.500
6	3	2.5	1.5	0.250	0.500
6	3	3	1.5	0.250	0.500

Table 6.13. Results for cohesive soil.

COHESIVE REINFORCED FILL					
H_t (m)	**H (m)**	**S/H**	**L (m)**	**L/H_t**	**L/H**
6	3	0	5.2	0.867	1.733
6	3	0.5	5.0	0.833	1.667
6	3	1	4.9	0.817	1.633
6	3	1.5	4.9	0.817	1.633
6	3	2	3.0	0.500	1.000
6	3	2.25	0.5	0.083	0.167
6	3	2.5	0.5	0.083	0.167
6	3	3	0.5	0.083	0.167

Figure 6.24 shows that the effect of offset distance on required reinforcement length which gives the factor of safety as 1.5. It can be seen that the increase in offset distance causes decrease of the required reinforcement length to obtain the factor of safety as 1.5.

In the case of non cohesive fill; analyses showed that when the offset distance is greater than 2H, required reinforcement length becomes stable. In other words, increasing offset distance more than 2H causes no change in the required reinforcement length. Therefore, tiered walls in which non cohesive fill used as reinforced fill, starts to behave like two single tiered separate walls with respect to reinforcement length when the offset distance exceeds 2H. It can be concluded that 2H is the critical offset distance when the non cohesive fill is used.

In the case of cohesive fill; analyses showed that when the offset distance is greater than 2.25H, required reinforcement length becomes stable. In other words, increasing offset distance more than 2.25H causes no change in the required reinforcement length. Therefore, tiered walls in which cohesive fill used as reinforced fill, starts to behave like two single tiered separate walls with respect to reinforcement length when the offset distance exceeds 2.25H. It can be concluded that 2.25H is the critical offset distance when the cohesive fill is used.

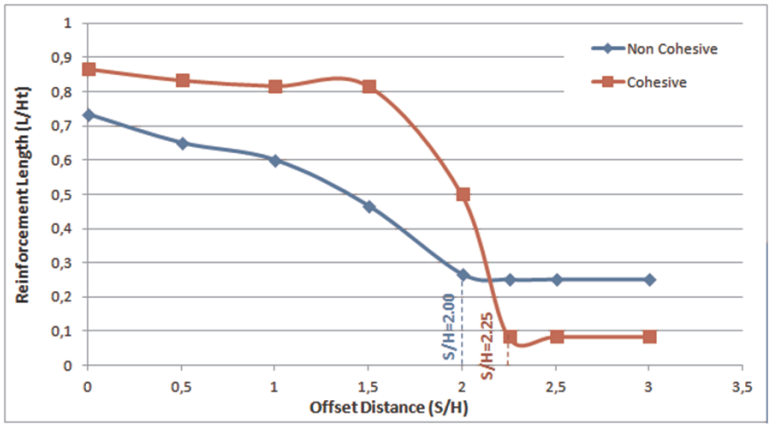

Figure 6.24. Influence of offset distance on the required reinforcement length to obtain a factor of safety equals to 1.5.

7. CONCLUSIONS

This study was carried out to investigate the behaviour of tiered reinforced soil retaining walls in static conditions, by using finite element analysis. Plaxis 8.2, a commercial computer program was used to conduct the analyses.

This study is divided into two parts. In the first part; effects of reinforcement length (L), type of reinforced soil and offset distance between tiers (S) on the behaviour of two tiered reinforced soil retaining wall was investigated using numerical analyses.

In the first part of the study, 42 analyses were conducted by choosing total height (H_t) as 6m and each tier height (H) as 3m. Reinforcement lengths were selected as L=0.5H_t, L=0.7H_t and L=1H_t. Offset distances were selected as S=0H, S=0.5H, S=1H, S=1.5H, S=2H, S=2.5H and S=3H for cohesive and non cohesive reinforced fills.

Increasing the L/H_t ratio causes increase in factor of safety and decrease in displacements for both non cohesive and cohesive reinforced fills. These effects of the reinforcement length were observed at all offset distances. However, effects of reinforcement length decrease significantly when the offset distance exceeds 1.5H. In other words; when offset distance exceeds 1.5H, factor of safety values and displacement magnitudes for various reinforcement lengths becomes similar.

Increasing the offset distance (S) increases the factor of safety for both cohesive and non cohesive reinforced fills. These effects of the offset distance were observed at all reinforcement lengths. Moreover, permanent horizontal displacements were reduced with the increasing offset distance between the walls. Moreover, it was observed from the failure planes and changes in safety factors that increasing the offset distance has similar effects with decreasing the angle of a slope.

For the soil parameters used in this study, the wall with a non cohesive reinforced fill gave higher factor of safety values and lower displacement magnitudes when com-

pared to cohesive soils. These effects of soil type are valid for all reinforcement lengths and all offset distances.

In the second part of the study, 16 analyses were conducted by using various offset distances such as S=0H, S=0.5H, S=1H, S=1.5H, S=2H, S=2.25H, S=2.5H, S=3H. In each offset distance, aimed factor of safety was 1.5. Various reinforcement lengths were used and the one that gives the factor of safety as 1.5 was determined for each offset distance. Therefore, minimum required reinforcement length was obtained for each offset distance. By doing this, the critical offset distance at which walls start to behave like two separate walls with respect to reinforcement length was investigated.

Analyses showed that the minimum required reinforcement length decreases with the increasing offset ratio, as expected.

For the type of reinforced soil, type of reinforcement and wall height used in this study; analyses showed that when the offset distance is greater than 2.00H, required reinforcement length becomes fixed. When offset distance exceeds 2.00H, two tiered wall can be considered two single tiered walls with respect to reinforcement length. Therefore; in case of non cohesive fill, 2H can be considered the crtitical offset distance where walls behave completely separate.

For the type of reinforced soil, type of reinforcement and wall height used in this study; it was observed that when the offset distance exceeds 2.25H, required reinforcement length becomes fixed. When offset distance exceeds 2.25H, two tiered wall can be considered two single tiered walls with respect to reinforcement length. Therefore; in case of cohesive fill, 2.25H can be considered the crtitical offset distance where walls behave completely separate.

This research has thrown up many questions in need of further investigation. This study can be expanded by investigating the behaviour of the wall;

- by using different wall heights (H_t),

- by using 3 or more tiers,
- by using different tier heights (H1, H2,...),
- by using different reinforcement lengths in tiers (L1, L2, ...),
- By using various reinforceent orientations.

As an obtained implementation from this study, we can conclude that some experimental research studies must be conducted in the future to prove the findings of numerical simulations with scaled experimental models. Experimental research studies must be done to get reasonable results from numerical simulations with the help of results from those experimental works.

REFERENCES

Armour, T.A., J., Bickford, and T., Pfister, 2004, "Repair of Failing MSE Railroad Bridge Abutment", In: Geotechnical Special Publications GSP 136, *GeoSupport 2004: Drilled Shafts, Micropiling, Deep Mixing, Remedial Methods, and Specialty Foundation Systems*, Orlando, 2004, ASCE, Florida.

Beckham, W.K. and W.H., Mills, 1935, "Cotton-Fabric Reinforced Roads", *Engineering News Record*, pp. 453-455.

Brinkgreve, R.B.J. and M., Yogendrakumar, 1992, "Dynamic Response Analysis of Reinforced Soil Retaining Wall", *Journal of Geotechnical Engineering*, Vol. 118, No. 8, pp. 1158-1167.

Chalermyanont, T. and C.H., Benson, 2005, "Reliability-Baseed Design for External Stability of Mechanically Stabilized Earth Walls", *International Journal of Geomechanics*, Vol. 5, No. 3, pp. 196-205.

Chen, D.H., S., Nazarian, and J., Bilyeu, 2007, "Failure Analysis of a Bridge Embankment with Cracked Approach Slabs and Leaking Sand", *Journal of Performance of Constructed Facilities*, Vol. 21, No. 5, pp. 375-381.

Chen, W.F. and J.Y.R., Liew, 2003, *The Civil Engineeering Handbook*, Second Edition, CRC Press LLC, Danvers.

Choudhury, D. and S.S., Nimbalkar, 2006, "Pseudo-Dynamic Approach of Seismic Active Earth Pressure Behind Retaining Wall", *Geotechnical and Geological Engineering*, Vol. 24, No. 5, pp. 1103-1113.

Choudhury, D., S.S., Nimbalkar, and J.N., Mandal, 2006, "Comparison of Pseudo-Static and Pseudo-Dynamic Methods for Seismic Earth Pressure on Retaining Wall", Journal of Indian Geophysical Union, Vol. 10, pp. 263-271.

Das, B.M., 2007, *Principles of Foundation Engineering*, 6th Edition, Nelson, Toronto.

Das, B.M., 2007, *Fundamentals of Geotechnical Engineering*, 3rd Edition, CL Engineering, Madrid.

Day, R.W., 2002, *Geotechnical Earthquake Engineering Handbook*, McGraw-Hill, New York.

Elias, V., B.R., Christopher and R.R., Berg, 2001, *Mechanically Stabilized Earth Walls and Reinforced Soil Slopes Design and Construction Guidelines*, FHWA-NHI-00-043, Washington (DC).

Enünlü, A.K., 2007, *Investigation of Dynamic Behaviour of Geosynthetic Reinforced Soil Retaining Structures Under Earthquake Loads*, Ph.D. Thesis, Boğaziçi University.

Fenichell, S., 1996, *Plastic: The Making of a Synthetic Century*, HarperBusiness, New York City.

Filshill, A.S., 2010, *Long Term Structural Design of Geosynthetic Stormwater Chambers and the Use of Nanocomposites to Enhance Their Performance*, Ph.D. Thesis, Drexel University.

Giroud, J.P., 1992, "Geosynthetics in Dams: Two Decades of Experience", *Geotechnical Fabrics Report*, Vol. 10, No. 3, Number:5, Roseville, MN, USA, September, pp. 6-9, 22-28.

Hall, C., 1981, *Polymer Materials, Macmillan Publisher*, London.

Holtz, R.D., 1988, *Geosynthetics for Soil Improvement*, American Society of Civil Engineers, New York.

Leshchinsky, D. and J., Han, 2004, "Geosynthetic Reinforced Multitiered Walls", *Journal of Geotechnical and Geoenvironmental Engineering*, Vol. 130, No 12.

Kadayıfçı, A, 2005, *Influence of Various Parameters On Seismic Induced Permanent Displacement of Geosynthetic Reinforced Segmental Retaining Walls*, M.Sc. Thesis, Boğaziçi University.

Katz, D.A., 1998, "Polymers", http://www.chymist.com/Polymers.pdf, March 2013.

Kim, H.S. and O., Bilgin, 2007, "Studying the Effect of Concrete Key Size on Mechanically Stabilized Earth Wall Deformations using Finite Element Method", In: Geotechnical Special Publications GSP 157, *Computer Applications in Geotechnical Engineering*, Denver, 2007, ASCE, Colorado.

Koerner, R.M., 2005, *Designing With Geosynthetics*, 5th Edition, Pearson Prentice Hall, New Jersey.

Kramer, S.L., 1996, *Geotechnical Earthquake Engineering*, Prentice Hall, New Jersey.

Mahmood, T., 2009, *Failure Analysis of a Mechanically Stabilized Earth (MSE) Wall Using Finite Element Program*, M.Sc. Thesis, The University of Texas At Arlington.

Murthy, V.N.S., 2002, *Geotechnical Engineering: Principles and Practices of Soil Mechanics and Foundation Engineering*, Marcel Dekker, New York.

Narejo, D. and Ramsey, B., 2001, "MSE Wall Drainage Alternatives: Careful Drainage Design can Prevent Costly Retaining-Wall Failures", *GFR Magazine*, June/July 2001, Vol. 19, No 5.

Öztürk, T.E., 2005, *Influence of A Parametric Study of Seismic Response Analysis of Reinforced Soil Retaining Structures With Plaxis*, M.Sc. Thesis, Boğaziçi University.

Plaxis, 2012, *Safety Analysis and Displacements*, http://kb.plaxis.nl/tips-and-tricks/safety-analysis-and-displacements, May 2013.

Prasad, B.B., 2009, *Fundamentals of Soil Dynamics and Earthquake Engineering*, PHI Learning Private Limited, New Delhi.

San, K.C., Leshchinsky, D. and Matsui, T., 1994 "Geosynthetic Reinforced Slopes: Limit Equilibrium and Finite Element Analysis", *Soils and Foundations*, Vol. 34, No 2.

Seed, H.B. and R.V., Whitman, 1970, "Design of Earth Retaining Structures for Dynamic Loads", *Proceedings of the ASCE Specialty Conference on Lateral Stresses in the Ground and Design of Earth Retaining Structures*, pp. 103-147.

Shukla, S.K., J.H., Yin, 2006, *Fundamentals of Geosynthetic Engineering*, Taylor and Francis/A. A. Balkema, Leiden.

Staff, C.E., 1984, "The Foundation and Frowth of the Geomembrane Industry in the United States", *Proceedings of the International Conference on Geomembranes*, Denver, pp. 5-8.

Steedman, R.S. and X., Zeng, 1990, "The Influence of Phase on the Calculation of Pseudo-Static Earth Pressure on a Retaining Wall", *Geotechnique*, Vol. 40, pp. 103-112.

Taylor, D.W., 1948, *Fundamentals of Soil Mechanics*, Wiley, New York.

Tenax, 2006, *Reinforced Soil Slopes and Walls*, $http://www.polyfabrics.com.au/pdf/tenax_tt_slopes.pdf$, April 2013.

Terraforce, 2012, *Geosynthetic Reinforced Soil Segmental Retaining Walls*, http://www.terraforce.com/planning-design/design-alternatives/attachment/composite-retaining-wall/, April 2013.

Terzaghi, K., 1943, *Theoretical Soil Mechanics*, Wiley Inc., New York.

Towhata, I., 2008, *Geotechnical Earthquake Engineering*, Springer, Heidelberg.

Wood, J.H., 2008, "Design of Earth Retaining Walls for Outward Displacement in Earthquakes", *In: New Zealand Society for Earthquake Engineering Inc.*, 2008 NZSE Conference, 2008, New Zealand.

Yang, K.H. and C.N., Liu, 2007, "Finite Element Analysis of Earth Pressures for Narrow Retaining Walls", *Journal of Geo-Engineering*, Vol. 2, No. 2, pp.43-52.

Yoo, C., H.S., Jung, and I.J., Park, 2011, "Internal Stability of Geosynthetic-Reinforced Soil Walls In Tiered Configuration", *Geosynthetics International*, Vol. 18, No. 2, pp.74-83.

Yoo, C. and S.B., Kim, 2008, "Performance of a Two Tier Geosynthetic Reinforced Segmental Retaining Wall Under A Surcharge Load: Full-Scale Load Test and 3D Finite Element Analysis", *Geotextiles and Geomembranes*, Vol. 26, No. 6, pp. 460-472.

Zanten, R.V.V., 1986, *Geotextiles and Geomembranes in Civil Engineering*, A. A. Balkema, Rotterdam.

Zarabi-Kashani, K., 1979, S*Liding of Gravity Retaining Wall During Earthquakes Considering Vertical Accelerations and Changing Inclination of Failure Surface*, M.Sc. Thesis, Massachusetts Institute of Technology.